Biomass Conversion and Biorefinery (2024) 14:7401–7448
https://doi.org/10.1007/s13399-022-02905-3

REVIEW ARTICLE

# Modification of biomass-derived biochar: A practical approach towards development of sustainable $CO_2$ adsorbent

Nuradibah Mohd Amer[1,2] · Pooya Lahijani[3] · Maedeh Mohammadi[4] · Abdul Rahman Mohamed[1]

Received: 13 March 2022 / Revised: 28 May 2022 / Accepted: 1 June 2022 / Published online: 23 June 2022


## Abstract

The persistent increase in the atmospheric concentration of carbon dioxide ($CO_2$), the primary anthropogenic greenhouse gas contributing to global warming, makes research directed towards carbon capture and storage (CCS) imperative. In the past few years, among the available adsorbents, biochar has drawn significant interest as a promising carbon-based material for low-temperature $CO_2$ capture from flue/fuel gas (such as biogas or gasification-derived syngas) owing to its environmentally friendly nature, cost-effective and facile preparation method, and sustainable adsorption performance. This work provides a review of recent studies on the development of biochar from biomass feedstocks and its subsequent modification through various approaches, including physical, chemical and physicochemical activations for post-combustion $CO_2$ capture. An overview of the factors, including pyrolysis temperature, heating rate and time, and different modification methods, affecting the physicochemical attributes of biochar such as surface area, microporosity, surface properties and functional groups is presented. Biochar with a large micropore volume, a narrow microporosity (0.3–0.8 nm) and basic surface characteristics would be effective in adsorbing $CO_2$ molecules. In this regard, physical modification of biochar is closely related to pore formation, whereas chemical modification emphasizes the creation of oxygen and nitrogen-containing functional groups; hence, they contribute to the enhanced $CO_2$ capture through porosity development and surface chemistry alteration, respectively. Biochar has presented a strong selectivity towards $CO_2$ compared to other gasses and has revealed a sustainable performance in multi-cycles of $CO_2$ adsorption–desorption; these are crucial features to ensure the large-scale application of biochar for $CO_2$ capture.

**Keywords** $CO_2$ adsorption technologies · Biomass-derived biochar · Physical activation · Chemical activation · Physicochemical modification · $CO_2$ adsorption capacity

## 1 Introduction

Nowadays, the issues of global climate change have attracted worldwide attention. The pollutant gasses such as nitrogen oxides ($NO_x$), carbon monoxide (CO), carbon dioxide ($CO_2$), and sulphur dioxide ($SO_2$) are generated from energy sectors such as industrial plants, thermoelectric power plants, and combustion of fossil fuels [1]. In between, $CO_2$ emission from fossil fuel combustion is considered the main contributor to greenhouse gas (GHG) emissions. In addressing these environmental concerns, there is a continuous effort by the scientific community in proposing the priority actions and sectors that require a detailed look to fulfil net-zero emissions in 2050 [2]. The United Nations has taken the responsibility to manage a series of discussions at the international level to develop appropriate guidelines for accommodating the climate change impacts. As a result, the Kyoto Protocol was adopted on 11 December 1997 and enforced on 16 February 2005, focusing on the industrial countries to reduce GHG emissions. They have been recognized as the main contributor to the current high levels of GHG emissions in the atmosphere [3]. A decade after Kyoto Protocol, the Paris Agreement was adopted in Paris on 12 December

✉ Pooya Lahijani
pooya.lahijani@usm.my

1 Low Carbon Economy (LCE) Research Group, School of Chemical Engineering, Universiti Sains Malaysia, 14300 Nibong Tebal, Pulau Pinang, Malaysia

2 Faculty of Faculty of Chemical Engineering Technology, Kompleks Pusat Pengajian Jejawi 3, Universiti Malaysia Perlis, 02600 Arau, Perlis, Malaysia

3 School of Aerospace Engineering, Universiti Sains Malaysia, 14300 Nibong Tebal, Pulau Pinang, Malaysia

4 Faculty of Chemical Engineering, Babol Noshirvani University of Technology, Babol 47148, Iran

2015. The involved countries aimed to achieve a neutral climate by limiting global warming increase to 2 ℃ above the pre-industrial levels [4]. However, predictions on worldwide energy-related $CO_2$ emissions propose the $CO_2$ release from the energy sector will increase by 6%, from 33 Gt in 2015 to 35 Gt in 2050 [5]. Hence, to ensure the reduction of $CO_2$ concentration in the atmosphere, implementing efficient Carbon Capture and Storage (CCS) technologies, especially for large scale applications, are of great interest.

$CO_2$ capture technologies can be classified into three groups: pre-combustion, oxy-fuel combustion and post-combustion $CO_2$ capture. Interestingly, post-combustion $CO_2$ capture technologies are more favourable due to better compatibility with the existing gas emission control systems and low technological risk [6]. Solvent absorption, adsorption with solid adsorbents, cryogenic separation, and membrane separation are commonly well-known methods for post-combustion $CO_2$ capture [7]. Among these methods, adsorption with solid sorbents is preferred because of its ability to comply with a broad range of temperatures, low energy consumption, and ease of adsorbent regeneration [8]. Over the past few years, many types of adsorbents have been studied for $CO_2$ adsorption, including metal–organic frameworks (MOFs), zeolites, metal oxides, ion-exchange resins, layered double hydroxide, activated carbons, mesoporous carbon, and carbon nanomaterials [9–13]. Even though these materials exhibit excellent $CO_2$ adsorption performance, their use at a large scale has some drawbacks, such as high operational cost and adsorption competition issues [14]. In striving to find sustainable and cost-effective adsorbents, biochar has attracted considerable attention and has become a research hotspot as a valuable material to combat the global climate change problem. Biochar is a carbon-based solid product obtained from the thermal processing of biomass through various methods, including pyrolysis, gasification, torrefaction and hydrothermal carbonization [15, 16]. It has many multifunctional properties that are affected by the type of feedstock and production condition. Biochar can be generated from various biomass feedstocks such as wood and woody biomass [17–19], crop residues [20, 21], animal manure [22, 23], food waste [24, 25] and sewage sludge [26–28], as presented in Fig. 1.

Biochar has found numerous applications in the fields of environmental remediation (adsorption of different contaminants, heavy metals, nitrogen and phosphorous) [29–31], agriculture (improvement of soil fertility, stabilizing soil nutrients, and reduction of soil GHGs emission) [32, 33], climate change (adsorption of pollutant gases such as $NO_x$, $SO_x$, $H_2S$ and GHGs) [34, 35], and material science (development of catalyst, building materials and batteries) [36, 37]. Figure 2 visualizes the word cloud of the most frequently used keywords in journal articles in the field of biochar application in 2021(bibliographic data from Scopus).

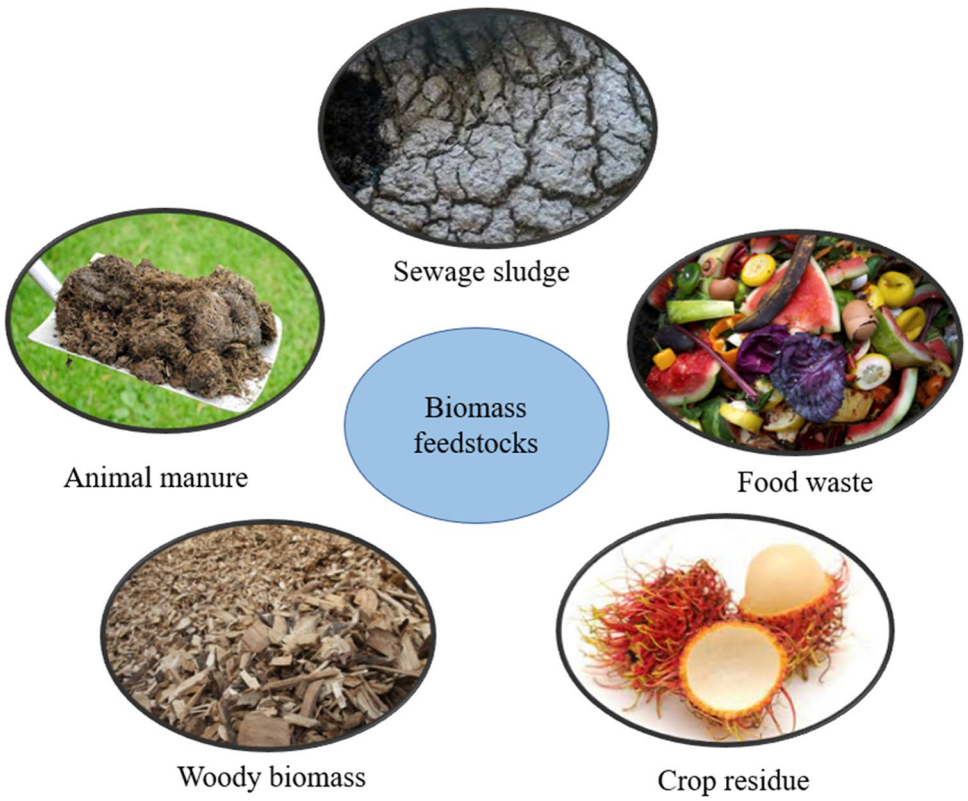


**Fig. 1** Different biomass feedstocks for the production of biochar

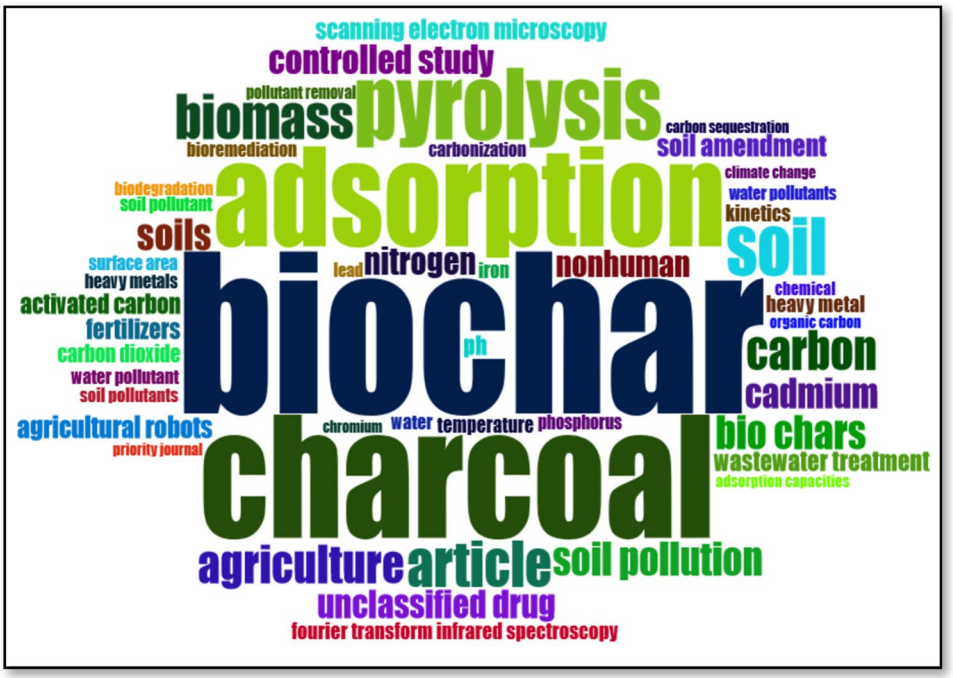


**Fig. 2** Visualized word cloud of the most frequently used keywords in journal articles in the field of biochar applications. Bibliographic data were extracted from the Scopus database, with a total of 1970 articles only in the year 2021

Recently biochar has emerged as a material of interest for carbon capture. To reflect this interest in research studies, the Scopus database was used to retrieve the number of articles per year from 1991 to March 13, 2022, with the keywords "char" AND "$CO_2$ adsorption" OR "$CO_2$ capture" OR "carbon capture". The results of this analysis are reflected in Fig. 3, which shows the growing scientific interest in using biochar-based adsorbents for $CO_2$ capture in recent years.

The type of sorbent used in $CO_2$ capture significantly impacts the $CO_2$ adsorption capacity [38]. In this regard, sorbents can be categorized into zeolites, MOFs, metal-oxide-based adsorbents and carbonaceous materials.

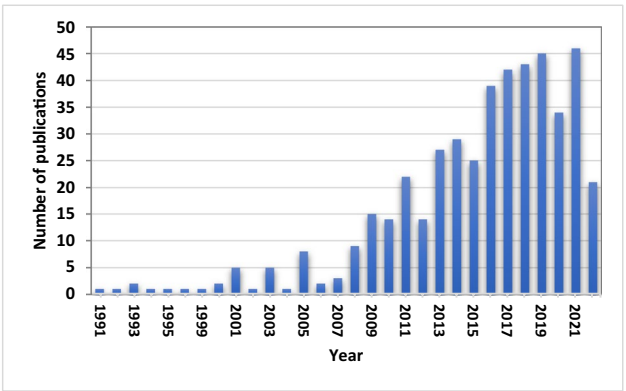


**Fig. 3** Annual scientific growth in the number of published articles containing the keywords "char" AND "$CO_2$ adsorption" OR "$CO_2$ capture" OR "carbon capture". The bibliographic data were obtained from Scopus from 1991 to March 13, 2022

Amongst all, activated carbons are promising carbonaceous materials that present good thermal, chemical and mechanical stability [39]. Despite their advantages, they have relatively low selectivity towards $CO_2$ over other gases such as $N_2$ and $CH_4$ [40]. Zeolites demonstrate an excellent selectivity to $CO_2$, yet they show a poor adsorption uptake and stability in the presence of moisture and impurities (such as $NO_x$, $SO_x$) [41]. MOFs present high $CO_2$ adsorption at elevated pressures; nevertheless, they have a lower $CO_2$ uptake than other adsorbents at low $CO_2$ partial pressures [42]. Even though MOFs possess high $CO_2$ adsorption capacity, their large-scale manufacturing cost should be considered due to the use of expensive precursors [43]. Metal-oxides, such as calcium oxide (CaO), are extensively used to capture $CO_2$ at a large scale. However, a major problem of CaO-based adsorbents is the sintering of adsorbent particles during the regeneration stage, which drastically reduces their adsorption capacity [44]. In striving to develop sustainable, low-cost $CO_2$ adsorbents, biochar has become a research hotspot. Biochar can be easily produced from various abundant and low-cost materials, such as woody and crop residues which also addresses the waste disposal problem in many agro and forestry-based industries. In comparison with activated carbon, the break-even price of biochar is about one-sixth of activated carbon [45]. Moreover, the average energy consumption for the production of biochar (6.1 MJ/kg) is significantly lower than that of activated carbon (97 MJ/kg) [46]. With all the facts from the economic points of view, biochar is one of the potential candidates for producing low-cost adsorbents

for $CO_2$ adsorption with the potential to be used in large-scale operations.

Biochar has shown promising potential as a $CO_2$ adsorbent, yet the adsorption uptake of pristine biochar is not very high as it does not have a well-developed porous structure and has poor surface chemistry. Therefore, physical and/or chemical modifications are usually implemented to enhance the $CO_2$ capture capacity of biochar [47–49]. In this context, this review demonstrates the potential of pristine and modified biochar derived from various biomass feedstocks for $CO_2$ capture based on the literature data. An outline of the parameters influencing the microstructure and surface chemistry of biochar, including pyrolysis conditions and the type of modification approaches, is provided. The performance of pristine and modified biochar in $CO_2$ adsorption is compared, and the mechanisms through which the $CO_2$ uptake capacity of modified biochar is enhanced are extensively discussed. Apart from that, the selectivity and reusability of the modified biochar are also elucidated. To the best of our knowledge, reviews covering such aspects of biomass-derived biochar for $CO_2$ capture are only a few. This review provides advanced access to emerging ideas on the current trends for the development and implementation of biochar to control $CO_2$ emissions from various emission sources. A complete overview starting from $CO_2$ capture technologies and ending with the challenges of using biochar as $CO_2$ adsorbent would provide insightful information that will be beneficial for the scientific community and those working on air pollution control and related biochar applications.

## 2 $CO_2$ capture technologies

The CCS technology captures and stores $CO_2$ before entering the atmosphere. CCS can be applied at large-scale emission sources, including natural gas processing, coal and gas-fired power generation, and manufacturing industries such as pulp, paper, cement, iron, and steel [50–52]. Figure 4 depicts a scheme of CCS technologies, including pre-combustion, oxy-fuel and post-combustion $CO_2$ capture processes.

The principle of pre-combustion technology is to capture $CO_2$ from the syngas after converting CO into $CO_2$ [53]. Initially, a fuel is reacted with air to produce a gas that is rich in CO and hydrogen ($H_2$). Then, the reaction of CO with the steam forms $CO_2$ and $H_2$ via water–gas shift (WGS) reaction, where $CO_2$ is then separated using chemical absorption processes such as those applied in Purisol, Fluor, Rectisol and Selexol, as presented in Table 1. Meanwhile, $H_2$ can be directly consumed as fuel. It is convenient to adsorb $CO_2$ since the $CO_2$ concentration is relatively high.

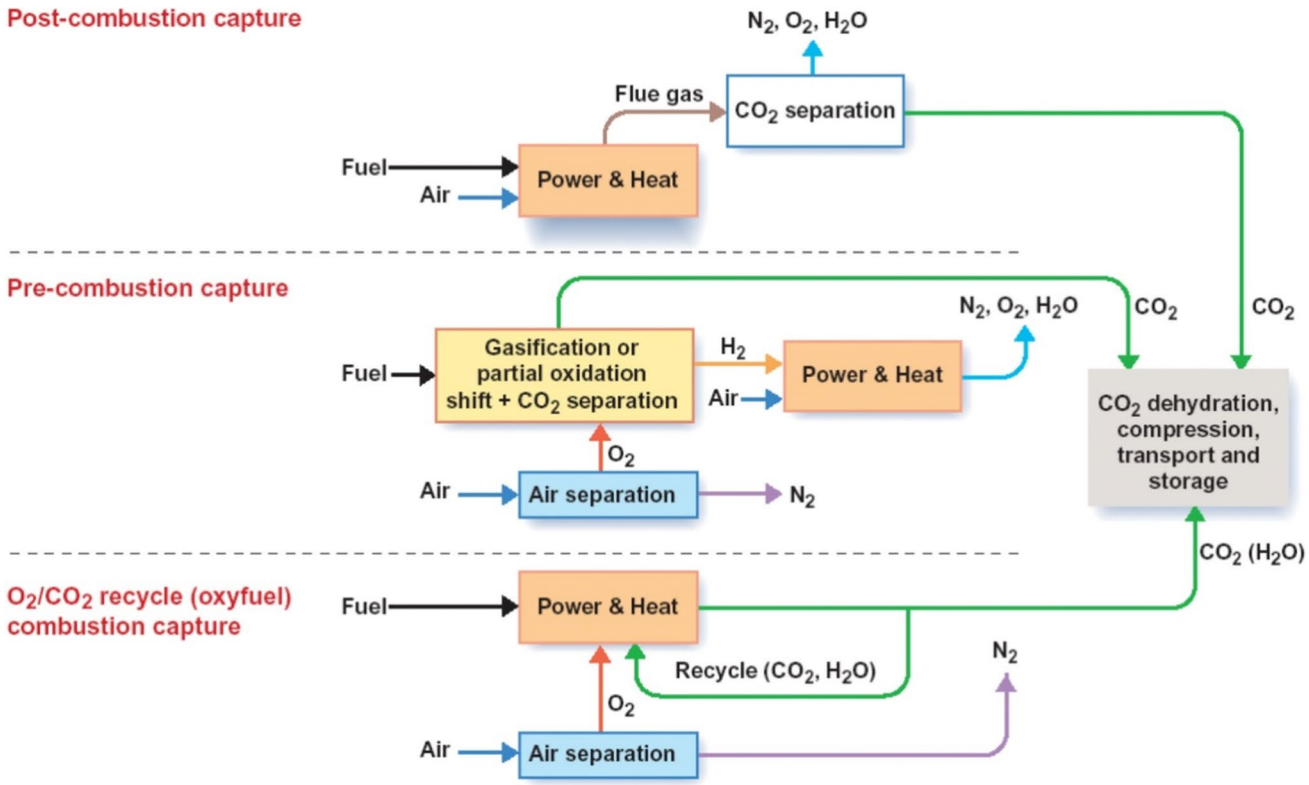


**Fig. 4** Diagram of $CO_2$ capture technologies, including pre-combustion, oxy-fuel combustion and post-combustion capture. Adapted with permission from [292]

The advantages of the pre-combustion technology include: the gas volume needed in the pre-combustion capture is significantly reduced because the processing takes place before the syngas is diluted with the combusted air [54], and the $CO_2$ is produced under pressure; therefore, less compression is required for $CO_2$ storage and transportation [55]. Even though this technology fulfils the industrial scale specification, retrofitting the existing plants is complicated and costly. Moreover, the syngas must be dried before the $CO_2$ separation can be performed [56].

In the second approach, oxy-fuel combustion, the fuel is burned in nearly pure oxygen instead of air, which induces a flue gas stream consisting of $CO_2$, water, and other trace impurities. Pure oxygen is obtained from an air separation unit that separates oxygen from nitrogen. The advantage of using this method is that it can be employed in the existing or new power plants along with the utilization of various biomass feedstocks [59]. In the oxy-fuel $CO_2$ capture process, cryogenic distillation is found to be the most suitable process for producing high purity oxygen for a large-scale operation [60]. However, the major drawback of this technology is that the supply of expensive pure oxygen and the high energy consumption for oxygen separation from the air would prevent the applicability of this method for $CO_2$ capture [59, 60].

As the third approach, $CO_2$ is directly captured from flue gas streams after combustion using wet or dry adsorbents in post-combustion technology. Generally, the fuel is combusted with air in a boiler to produce steam in a coal-fired power generation system. Then, electricity will be generated using a turbine [61]. The flue gas produced is mainly composed of $CO_2$ and $N_2$. At present, solvent scrubbing using amine solution is a promising method to react with $CO_2$ in the flue gas and produce purified $CO_2$ that can be compressed for storage [62]. The post-combustion technologies can be divided into (i) absorption-based, (ii) adsorption-based and (iii) membrane-based post-combustion processes. Table 2 represents the advantages and disadvantages of different methods for post-combustion technologies.

Chemical absorption is a favourable approach for absorbing $CO_2$ from the flue gas streams consisting of low to moderate $CO_2$ partial pressures in the range of 3–20% [56]. Absorption can be explained by the use of a liquid to separate the gaseous component from the flue gas, and this liquid is known as an absorbent or solvent for $CO_2$ capture. In this process, the gas phase is turned into a liquid phase as the gaseous components contact the absorbent. Various chemical absorption processes, including amine absorption, aqua ammonia absorption, dual alkali approach and sodium carbonate slurry, have been widely used for carbon capture and storage [63–68].

$CO_2$ adsorption using solid adsorbents is one of the well-known methods to reduce the $CO_2$ concentration in the atmosphere. The solid material is known as adsorbent, while the adsorbed $CO_2$ gas is referred to as adsorbate. During the adsorption process, the gaseous constituent comes into contact with a solid adsorbent, where $CO_2$ molecules are adsorbed onto the solid surface. Most adsorbents experience a severe reduction in sorption capacity at high adsorption temperatures [56]. The interaction of $CO_2$ with the biochar surface could be through weak physical adsorption (physisorption) or strong chemical reaction (chemisorption), or a combination of the both, depending on the structural features and surface chemistry of biochar, as well as the implemented adsorption condition (such as temperature and pressure) [47, 69, 70]. Physisorption is often associated with a lower heat of reaction compared to chemisorption [56]. After the adsorption process is completed, the desorption stage is conducted, where $CO_2$ is removed from the adsorbent, and the adsorbent is consequently regenerated. A number of techniques

**Table 1** Capturing solvent and disadvantages of different pre-combustion technologies

| Technology | Capturing solvent for $CO_2$ | Regeneration | Drawback | Reference |
|---|---|---|---|---|
| Purisol | N-methyl-2-pyrrolidone | Stripping $CO_2$ containing Purisol solvent with an inert gas | • Needs additional compression after the WGS reaction | [56, 57] |
| Fluor | Propylene carbonate | Flash desorption of $CO_2$ containing Fluor solvent | • High cost of solvent<br>• High circulation rates of solvent, thus increasing the operation costs | [56] |
| Rectisol | Chilled methanol | Flash desorption of $CO_2$ containing methanol solvent | • High operating and capital costs due to regeneration and complex operating systems<br>• Ability to absorb trace metals such as mercury that leads to the formation of amalgams | [56, 58] |
| Selexol | A mixture of dimethyl ether and polyethylene glycol | Stripping/flash desorption of $CO_2$ containing Selexol | • Only efficient at elevated pressures | [56, 57] |

**Table 2** Advantages, disadvantages and $CO_2$ capture performance of various post-combustion technologies

| Method | Advantages | Disadvantages | Remark | Reference |
|---|---|---|---|---|
| Absorption | | | | |
| Amine | Can be performed at a low $CO_2$ partial pressure gas stream when $CO_2$ reacts with the amine | High energy is required for stripping and regeneration process<br>The use of amine will cause corrosion to the equipment<br>Amine degradation due to heat, $SO_x$, $NO_x$ and $O_2$ | $CO_2$ capture capacity: 0.4 kg $CO_2$/kg monoethanol amine | [56, 63–65] |
| Aqua ammonia | Generates bio-products such as ammonium nitrate and sulphate, which can be used as fertilizer<br>Present higher adsorption capacity compared to amine and dual alkali absorption<br>No corrosion occurs in the equipment | Flue gas must be cooled to 15–27 ℃ before being contacted with ammonia solution due to the volatility of ammonia<br>High vaporization of ammonia during the stripping process | $CO_2$ capture capacity: 1.20 kg $CO_2$/kg ammonia | [56, 64, 66] |
| Dual alkali approach using methylaminoethanol (MAE) and activated carbon | Better modification of Solvay process using ammonia and lime | High energy required for the calcination process and $CO_2$ production hinders the large-scale $CO_2$ capture | $CO_2$ capture capacity: 0.54 kg $CO_2$/kg methylaminoethanol | [56, 67] |
| Sodium carbonate slurry | Solvent is non-volatile and non-hazardous<br>Low corrosion rate of equipment<br>Multi-system of pollutant capture | Rate of $CO_2$ absorption is slower than amine solutions, thus requiring a tall absorption column<br>High energy demand for regeneration in the stripping column | 90% $CO_2$ capture efficiency using 30 wt% sodium carbonates | [56, 65, 68] |
| Adsorption | | | | |
| Zeolites | Has a high surface area, regular porosity and interconnected pore channels<br>Presents high adsorption capacity at mild operating conditions (0–100 ℃, 0.1–1 bar of $CO_2$) | Impurities such as $SO_x$, $NO_x$, and $H_2O$ need to be removed because their presence could reduce the adsorption sites of $CO_2$ | $CO_2$ capture capacity: 0.004 to 0.216 g $CO_2$/g zeolite<br>(0.1–1 bar, 0–100 ℃) | [38, 56, 81, 82] |
| Activated carbon | Presents high adsorption capacity at elevated pressures<br>Good thermal stability at high temperature under inert atmospheres | Has a wide range of pore characteristics due to a variety of starting materials<br>Low $CO_2$ selectivity at low $CO_2$ partial pressure | $CO_2$ capture capacity: 0.003–0.154 g $CO_2$/g activated carbon<br>-1 bar, 25–75℃) | [38, 41, 56, 83, 84] |
| Biochar | Performs $CO_2$ adsorption at low temperatures<br>High $CO_2$ selectivity over air, $CH_4$ and $N_2$ at low temperature and ambient pressure | Has a wide range of pore characteristics due to a variety of starting materials<br>Present a low surface area and poor surface chemistry | $CO_2$ capture capacity: 0.02–0.12 g $CO_2$/g adsorbent<br>(1 bar, 30–70 ℃) | [85–87] |
| Metal–organic frameworks (MOFs) | Possibility to control the architecture and active functional groups of MOFs<br>Presents high adsorption capacity at elevated pressure (35 bar of $CO_2$<br>High thermal stability | Pre-treatment is required to remove the impurities such as $SO_x$, $NO_x$, and $H_2O$<br>Low $CO_2/N_2$ and $CO_2/CH_4$ selectivity at ambient pressure<br>Exhibits poor $CO_2$ capture at low $CO_2$ partial pressure | $CO_2$ capture capacity: 1.47 g $CO_2$/g adsorbent<br>(35 bar, room temperature) | [8, 56, 88–91] |
| Membrane separation | | | | |

**Table 2** (continued)

| Method | Advantages | Disadvantages | Remark | Reference |
|---|---|---|---|---|
| Organic membranes | No chemicals are added | Difficult commercial-scale manufacturer | Polyactive™ (organic membrane) | [13, 56, 92–94] |
| Inorganic membranes | No regeneration step is needed | A second stage membrane system is | $CO_2$ permeability (Barrer): 1100 | |
| Mixed matrix membranes | Avoidance of the operational problems associated with absorption, such as flooding, foaming and channelling | required, as the first stage is not capable of providing high $CO_2$ capture efficiency | $CO_2/N_2$ selectivity (α): 52 | |
| | | The membrane must be resistant to flue gas impurities, plasticization (hardening) and ageing | ZSM-5 zeolite (inorganic membrane) | |
| | | | $CO_2$ permeability (Barrer): 1140 | |
| | | | $CO_2/N_2$ selectivity (α): 54.3 | |
| | | Requires high-selectivity membranes due to the low $CO_2$ content in the feed stream | Polyvinyl acetate (mixed matrix membrane) | |
| | | | $CO_2$ permeability (Barrer): 3.1 | |
| | | | $CO_2/N_2$ selectivity (α): 34.7 | |

related to regeneration of the adsorbent can be enumerated [71, 72]: (1) PSA: pressure-swing adsorption [73], (2) TSA: temperature-swing adsorption [74], (3) PTSA: pressure and temperature-swing adsorption [69], (4) VPSA: vacuum pressure-swing adsorption [75], (5) ESA: electric-swing adsorption [76], (6) RPSA: rapid pressure-swing adsorption, and (7) URPSA: ultra-rapid pressure-swing adsorption [72]. Among the listed adsorption methods, TSA and PSA are the two most commonly applied techniques in the adsorption–desorption of biochar. In the TSA system, $CO_2$ is desorbed from the adsorbent as the temperature of the system is increased. Whereas in the PSA system, the adsorption is performed at elevated pressures; consequently, reducing pressure within the system releases $CO_2$ from the solid material. The benefit of a PSA system is that the regeneration can be accomplished in a few seconds compared to hours in the TSA system [77]. However, in the TSA system, the solid adsorbent can still be regenerated while preserving a high $CO_2$ partial pressure [56].

Recently, membrane separation processes have been commercially used to remove $CO_2$ from the natural gas streams [78], consisting of $CH_4$ and $CO_2$, where the $CO_2$ concentration and the overall pressure are relatively high. The membrane separation strongly relies on selectivity and permeability. Here, $CO_2$ is selectively separated from the other gas components and transported to the other side of the membrane by the use of a permeable or semi-permeable membrane [56]. For efficient separation, it is suggested that the flue gas must be pre-treated to avoid any impurities such as $NO_x$ and $SO_x$, which can cause an adverse effect during the separation process [56].

From the economic perspective, pre-combustion technology could offer a lower cost than oxy-fuel and post-combustion technologies by approximately 21–24 and 38–45%, respectively [59]. However, the additional cost and the complexity of setting up the process due to the retrofitting of current equipment may limit its commercialization. Among the CCS technologies, post-combustion $CO_2$ capture is a widely used technique to tackle escalating $CO_2$ concentrations [59]. Most power plants favour the adsorption of $CO_2$ after a complete occurrence of the reaction [79]. Ideally, an efficient adsorbent for post-combustion $CO_2$ capture must present a high $CO_2$ capture capacity and stability, high selectivity and low manufacturing cost for large-scale operations. In addition, a detailed design of the process in the adsorption/desorption cycles is essential to minimize the energy consumption in the post-combustion operating conditions [80].

## 3 Biochar production

Biochar could be developed through conventional pyrolysis, flash carbonization, gasification, torrefaction and hydrothermal carbonization, as illustrated in Fig. 5.

Conventional pyrolysis under continuous inert gas flow can be categorized into slow, fast, and flash pyrolysis. This thermal process produces three main products; biochar, bio-oil and non-condensable gaseous such as carbon monoxide, hydrogen, methane and carbon dioxide [95]. In fast pyrolysis, the primary product is bio-oil, which constitutes 50–75% of the feedstock mass. The reaction normally occurs at 450–600 ℃ for less than 10 min at a heating rate of 16–150 ℃/min [96–98]. An improved form of fast pyrolysis is flash pyrolysis which operates at a temperature ranging from 600–1300 ℃, which can be attained within 3 min. Conversely, lower pyrolysis temperature and slow heating rates contribute to higher char yield, as represented by slow pyrolysis. The process is performed at the temperature range of 300–900 ℃ for about 1.5 h, depending on the process condition. The primary product is biochar, which relatively accounts for 25–35% of the feedstock mass [99]. Apart from conventional pyrolysis, an advanced pyrolysis technique known as microwave-assisted pyrolysis is applied, which is a rapid, efficient, selective and controllable technique to obtain solid, liquid and gaseous products from biomass. Microwave-assisted pyrolysis has manifold benefits compared to conventional pyrolysis, such as volumetric heating, energy transfer rather than heat transfer, non-contacting heating and heating from the inside material body [100]. In flash carbonization, biochar is produced from biomass feedstock at the following conditions: (1) temperature: 300–600 ℃, pressure: 1–2 MPa, and residence time: 30 min [101, 102]. In this process, biomass is efficiently converted into biochar with 70–80% fixed carbon content, and biochar yield is approximately 40–50% [103].

Gasification is performed at high temperatures in the range of 600–1000 ℃ for 2–3 h using a gasifying agent such as steam, air and oxygen. This process involves two steps: (1) production of biochar and volatile matter through pyrolysis and (2) syngas production by gasification of biochar and secondary cracking of volatile matters [104]. The main product generated is a non-condensable gas rich in carbon dioxide and hydrogen. However, the biochar yield is relatively low (5–10% of the feedstock mass) as most organic compounds are gasified into gas [105].

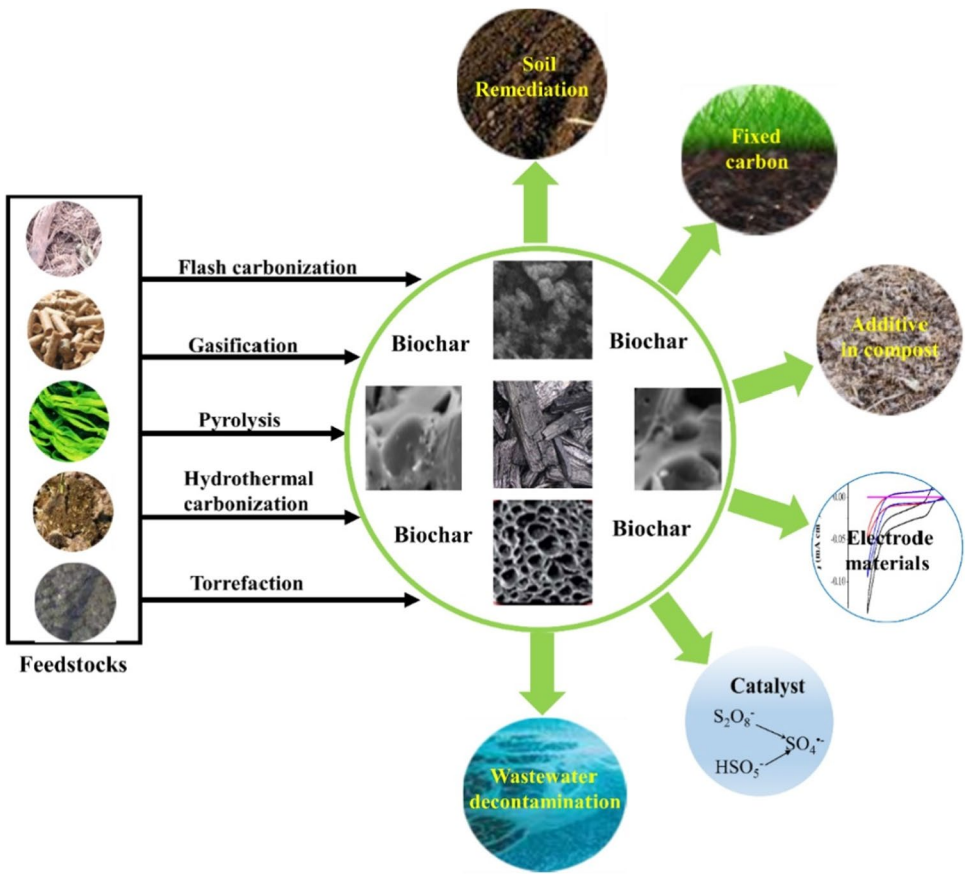


**Fig. 5** Production of biochar through various thermochemical processes. Adapted with permission from [101]

Torrefaction is a thermochemical treatment process conducted at a lower temperature, around 200–300 ℃ for 15–120 min [106], where the biomass is subjected to slow heating in an inert condition. It is also referred to as mild pyrolysis, as the heating condition is similar to pyrolysis, generally performed at a temperature of 350 to 650 ℃ [107]. During torrefaction, the biomass decomposes slowly and emits $H_2O$ and $CO_2$. With increasing torrefaction temperature, the elemental compositions (carbon, hydrogen, nitrogen, oxygen), the biochar's yield and volatile matter decrease, while higher heating value (HHV), fixed carbon and ash content increase [108].

The hydrothermal carbonization (HTC) process, also known as wet torrefaction, is carried out in subcritical water [109] under autogenous pressure (0.3–4.0 MPa) [110], where the raw material is heated in the hydrothermal reactor at a temperature between 170 and 260 ℃ for 15–90 min. This process generates three main products, namely: solid products (hydrochar), aqueous compounds and small fractions of gases (major gas: $CO_2$) [111]. Interestingly, a carbonization reaction is performed in water at a temperature lower than that of pyrolysis. Moreover, during the HTC process, the ash content could be reduced as the inorganic compound can be washed away into the liquid phase [112]. Among all the biochar production methods, slow pyrolysis has a higher production yield (25–35%). Although the hydrothermal process operates at temperatures less than 300 ℃, which is lower than that of pyrolysis temperature, the hydrochar needs to undergo the drying process for 24 h before being subjected to any modification techniques [113, 114]. Additionally, no "high-end equipment" is required to synthesise the biochar in slow pyrolysis. Table 3 summarizes the thermochemical processes for biochar production.

## 4 Physicochemical characteristics of biochar for $CO_2$ capture

### 4.1 Surface area and porosity

The physicochemical characteristics of biochar are crucial for $CO_2$ uptake and depend on various factors. These parameters include feedstock properties, pyrolysis temperature, residence time and heating rate, and the implemented modification technique (physical, chemical or physicochemical treatment) [124–127]. In the case of gas adsorption, the development of highly microporous biochar with a large specific surface area is desired [47]. The porous structure of biochar is created during the pyrolysis of feedstock due to the volatilization of organic matters [128]. According to the International Union of Pure and Applied Chemistry (IUPAC), the distribution of pore size is as follows: micropores (< 2 nm), mesopores (2–50 nm) and macropores (> 50 nm) [129]. Figure 6 shows the porosity type and the possible functional groups on the carbon structure of biochar.

Studies have indicated that for efficient $CO_2$ capture at 1 bar, it is necessary to generate a high volume of micropores with pore size in the range of 0.5–0.7 nm [130]. For example, Dang et al. [131] who obtained biochar from pine nut shell modified by KOH that had a pore size between 0.33 and 0.63 nm, reported an excellent $CO_2$ capture of 220 mg/g at 25 ℃ and 1 bar. Studies have also reported that the development of micropores has a greater impact on $CO_2$ capture compared to total pore volume and surface area development [131, 132]. Notably, pores less than 0.8 nm significantly contribute to $CO_2$ uptake at 1 bar, while pores with a diameter smaller than 0.5 nm capture $CO_2$ molecules at low partial pressure (0.1 bar) [130]. This is consistent with the previous finding that the maximum $CO_2$ adsorption (145.20 mg/g) at 0 ℃ and 0.15 bar was observed for the biochar with micropores in the range of 0.33–0.50 nm [131]. The kinetic diameter of $CO_2$ (0.33 nm) is relatively smaller than methane (0.38 nm) and nitrogen (0.364 nm) [133]. Therefore, the $CO_2$ adsorption will be facilitated if the adsorbent has a pore size close to the $CO_2$ diameter.

#### 4.1.1 Effects of pyrolysis temperature

The structural properties and surface chemistry of biochar determine its performance in $CO_2$ adsorption. Apart from the properties of biomass feedstock, pyrolysis conditions,

**Table 3** Thermochemical conversion techniques for biochar production and their process conditions

| Processes | Condition | | | Reference |
|---|---|---|---|---|
| | Temperature | Residence time | Heating rate | |
| Slow pyrolysis | 300–900 ℃ | 1–1.5 h | 5–20 ℃/min | [115–118] |
| Fast pyrolysis | 450–600℃ | < 1 -10 min | 16–150 ℃/min | [96–98] |
| Flash pyrolysis | 600–1300 ℃ | < 10 s -3 min | 300 ℃/min | [96, 119] |
| Microwave-assisted pyrolysis | na | 15–30 min | | [100, 120] |
| Gasification | 600–1000 ℃ | 2–3 h | | [25, 104, 121] |
| Torrefaction | 200–300℃ | 15–120 min | | [111, 122] |
| Hydrothermal carbonization | 170–260 ℃ | 15–90 min | | [87, 114, 123] |

na: not available

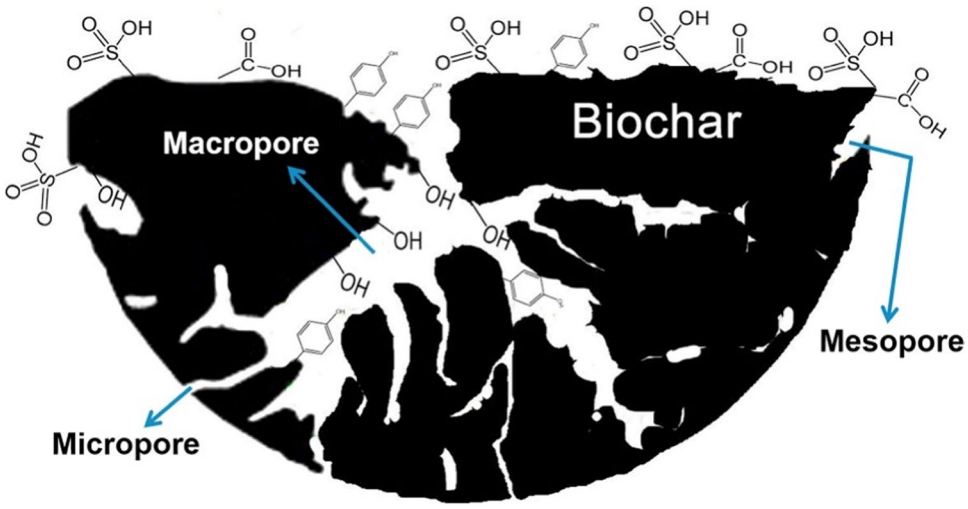


**Fig. 6** Morphology and the presence of surface functional groups on biochar. Adapted with permission from [37]

especially pyrolysis temperatures, have considerable impacts on biochar characteristics [134, 135]. Previous studies demonstrated that pyrolysis temperature plays a crucial role in producing biochar which presents high surface area and micropore volume with superior $CO_2$ adsorption capacity [20, 117, 136].

When biomass undergoes pyrolysis, pore development occurs due to the loss of water molecules in the dehydration process and the release of volatile matters from the carbon structure of biochar. At low pyrolysis temperature (< 400 ℃), this condition is not adequate to complete the devolatilization of volatile matters; thus, the creation of new pores is hindered [137, 138]. As the temperature goes up to 500 ℃, more volatiles are released, creating sparse regions, leading to cracks in the material and, consequently, developing more pores [139, 140]. At high pyrolysis temperatures (500–900 ℃), the generated energy could be used to develop microporosity and boost the evolution of pore structure [49]. Table 4 displays the effects of different pyrolysis temperatures on the pristine biochar properties derived from various biomass feedstocks. The generally observed trend is that surface area and micropores volume/total pore volume increase as the pyrolysis temperature is increased. It should be noted that at high pyrolysis temperatures (> 900 ℃), softening and sintering of the high molecular weight volatiles may occur, resulting in the shrinkage of the total pore volume of biochar. As such, the extreme pyrolysis temperature reduces the micropore volume and surface area [141]. Hence, the pyrolysis temperature should be carefully controlled to obtain a suitable microporosity and surface area for a high $CO_2$ uptake. A literature survey suggests that the pyrolysis temperature of 400–900 ℃ is suitable for converting biomass feedstocks to biochar [20, 142, 143].

In general, biochar yield decreased over the temperature of 300–900 ℃ [144–146]. At higher temperatures, the rapid decomposition of lignocellulosic components reduces biochar yield [144]. Moreover, more volatile matters are released as the biomass is heated up [145]. Lahijani et al. [117] pyrolyzed walnut shells at three different temperatures (500, 700 and 900 ℃) under $N_2$ gas for 90 min. The obtained char yields were 31.7, 28.4 and 23.8% with the respective temperatures. Even though the biochar yield decreased at 900 ℃, the highest micropore volume of 0.159 $cm^3/g$ was obtained for this sample. In this context, the development of micropores should be taken into account when considering the optimum pyrolysis temperature in producing biochar as $CO_2$ capturing medium. Pyrolysis has been carried out under different gas environments such as nitrogen ($N_2$), carbon dioxide ($CO_2$), helium (He), argon (Ar), and steam ($H_2O$) [147–151]. Among all, nitrogen is the most popular and extensively used gas due to its availability, cost-effectiveness and inert behaviour [54]. Guizani et al. [152] reported that the char yield produced under $N_2$ gas (13.10%) was higher than that obtained in the $CO_2$ atmosphere (11.32%). According to them, the additional mass decay in the char pyrolyzed under $CO_2$ could be explained by $CO_2$ gasification of char, which occurred concurrently with biomass pyrolysis. Gas flow rate is also an important parameter during the pyrolysis, which may affect the char yield. A high gas flow rate removes volatile matters faster from the hot zone, reducing secondary exothermic reactions such as thermal cracking, partial oxidation, repolymerization and recondensation, leading to the reduction of char formation [153]. In a study by Liu et al. [153], peanut shells were carbonized at 500 ℃ for 60 min. $N_2$ gas at various flow rates (20, 50, 100, and 200 ml/min) was used for carbonization. They found that the obtained biochar yield reduced approximately from 35 to 28%, as the gas flow increased from 20 to 200 ml/min. Similar results were reported in the production of laurel residue-derived biochar; when the nitrogen flow rate was increased from 50 to 400 ml/min, the biochar yield

**Table 4** Effect of pyrolysis temperature on pristine biochar properties derived from various biomass feedstocks

| Feedstock | Pyrolysis temperature (℃) | C (%) | H (%) | N (%) | O (%) | BET surface area ($m^2/g$) | Total pore volume ($cm^3/g$) | Micropores volume ($cm^3/g$) | Ash (%) | pH | Reference |
|---|---|---|---|---|---|---|---|---|---|---|---|
| Rambutan peel | 500 | 76.36 | 2.90 | 1.35 | 19.22 | 7.80 | 0.011 | 0.002 | - | - | [87] |
| | 700 | 81.64 | 1.37 | 1.00 | 15.93 | 175.84 | 0.111 | 0.066 | - | - | |
| | 900 | 83.38 | 0.90 | 0.77 | 14.71 | 569.64 | 0.313 | 0.201 | - | - | |
| Walnut shell | 500 | 69.42 | 3.85 | 1.54 | 25.07 | 94.509 | 0.054 | 0.021 | - | - | [117] |
| | 700 | 80.35 | 1.61 | 0.41 | 17.54 | 264.991 | 0.141 | 0.104 | - | - | |
| | 900 | 84.86 | 1.16 | 0.34 | 13.63 | 397.015 | 0.198 | 0.159 | - | - | |
| Date palms | 300 | 63.65 | 3.82 | 1.01 | 18.78 | 2.040 | 0.0057 | - | 12.74 | - | [142] |
| | 400 | 64.95 | 2.96 | 0.89 | 17.04 | 5.535 | 0.0055 | - | 14.16 | - | |
| | 500 | 70.75 | 2.33 | 0.86 | 9.85 | 123.625 | 0.0209 | - | 16.21 | - | |
| | 600 | 74.76 | 1.60 | 0.71 | 7.31 | 221.230 | 0.0317 | - | 17.8 | - | |
| | 700 | 72.76 | 0.9 | 0.61 | 5.32 | 249.130 | 0.0308 | - | 18.37 | - | |
| Peanut shell | 400 | 58.4 | 1.5 | 1.8 | 21.0 | 3.0 | 0.007 | - | 9 | 9.3 | [143] |
| | 500 | 64.5 | 3.5 | 1.7 | 18.5 | 5.0 | 0.022 | - | 10 | 9.4 | |
| | 600 | 71.9 | 2.8 | 1.6 | 15.0 | 28.0 | 0.11 | - | 11 | 9.6 | |
| | 700 | 74.4 | 2 | 1.4 | 14.2 | 195.0 | 0.033 | - | 12 | 9.9 | |
| Vegetable waste | 200 | 52.89 | 6.9 | 4.2 | 36.02 | 0.36 | 0.00259 | - | 16.59 | 5.95 | [155] |
| | 500 | 74.71 | 3.08 | 5.41 | 16.81 | 1.16 | 0.00242 | - | 36.67 | 11.23 | |
| Pine cone | 200 | 69.74 | 2.13 | 1.03 | 27.09 | 0.47 | 0.00238 | - | 0.77 | 4.15 | [143] |
| | 500 | 74.64 | 2.62 | 1.81 | 20.94 | 192.97 | 0.0102 | - | 8.96 | 6.77 | |
| Wheat straw | 400 | 57.8 | 3.2 | 1.5 | 21.6 | 5.5 | 0.012 | - | 11 | 8.2 | [143] |
| | 500 | 70.3 | 2.9 | 1.4 | 17.7 | 10.0 | 0.09 | - | 11 | 8.3 | |
| | 600 | 73.4 | 2.1 | 1.4 | 14.9 | 111.0 | 0.11 | - | 12 | 9.2 | |
| | 700 | 73.9 | 1.3 | 1.2 | 14.6 | 177.0 | 0.058 | - | 15 | 9.2 | |
| Corn straw | 400 | 56.1 | 4.3 | 2.4 | 22.0 | 4.0 | 0.008 | - | 14 | 10.2 | [143] |
| | 500 | 58.0 | 2.7 | 2.3 | 21.5 | 6.0 | 0.012 | - | 17 | 10.4 | |
| | 600 | 58.6 | 2.0 | 2.0 | 18.7 | 7.0 | 0.012 | - | 18 | 10.4 | |
| | 700 | 59.5 | 1.5 | 1.6 | 16.6 | 3.0 | 0.006 | - | 18 | 10.4 | |
| Miscanthus | 500 | 74.60 | 3.38 | 0.45 | 17.42 | 168 | 0.08 | - | 3.41 | - | [136] |
| | 600 | 82.35 | 2.32 | 0.28 | 11.22 | 345 | 0.18 | - | 4.35 | - | |
| | 700 | 83.69 | 2.40 | 0.39 | 8.20 | 368 | 0.18 | - | 4.87 | - | |
| | 800 | 84.47 | 2.28 | 0.30 | 7.61 | 390 | 0.20 | - | 5.02 | - | |
| Switchgrass | 500 | 67.83 | 3.28 | 1.01 | 16.32 | 162 | 0.08 | - | 10.76 | - | [136] |
| | 600 | 77.00 | 2.04 | 0.57 | 9.68 | 325 | 0.15 | - | 12.78 | - | |
| | 700 | 76.98 | 2.25 | 0.91 | 11.00 | 344 | 0.18 | - | 8.39 | - | |
| | 800 | 78.64 | 1.46 | 0.79 | 4.88 | 351 | 0.18 | - | 13.94 | - | |
| Corn stover | 500 | 71.47 | 3.28 | 0.85 | 13.44 | 149 | 0.08 | - | 10.20 | - | [136] |

**Table 4** (continued)

| Feedstock | Pyrolysis temperature (℃) | C (%) | H (%) | N (%) | O (%) | BET surface area ($m^2/g$) | Total pore volume ($cm^3/g$) | Micropores volume ($cm^3/g$) | Ash (%) | pH | Reference |
|---|---|---|---|---|---|---|---|---|---|---|---|
| | 600 | 74.47 | 2.24 | 0.81 | 11.82 | 293 | 0.14 | - | 12.00 | - | |
| | 700 | 76.23 | 1.92 | 0.68 | 5.83 | 308 | 0.14 | - | 15.00 | - | |
| | 800 | 73.50 | 2.12 | 0.69 | 10.92 | 357 | 0.18 | - | 12.30 | - | |
| Sugarcane bagasse | 500 | 65.12 | 2.13 | 0.62 | 15.80 | 138 | 0.08 | - | 15.74 | - | [136] |
| | 600 | 68.10 | 1.90 | 0.49 | 10.08 | 273 | 0.14 | - | 19.78 | - | |
| | 700 | 73.58 | 2.40 | 0.61 | 3.09 | 289 | 0.14 | - | 19.80 | - | |
| | 800 | 72.73 | 1.66 | 0.49 | 4.67 | 290 | 0.14 | - | 20.12 | - | |
| Apple tree ranches | 300 | 62.20 | 5.18 | 1.69 | 24.21 | 2.39 | 0.00256 | 0.00013 | 6.72 | - | [156] |
| | 400 | 71.13 | 4.03 | 1.94 | 15.05 | 7.00 | 0.00652 | 0.00052 | 7.85 | | |
| | 500 | 74.88 | 2.88 | 1.77 | 10.41 | 37.24 | 0.01241 | 0.00158 | 10.06 | - | |
| | 600 | 80.01 | 2.72 | 1.28 | 6.59 | 108.59 | 0.05884 | 0.03787 | 9.40 | - | |
| Swine manure | Raw | 47.42 | 6.01 | 4.11 | 26.07 | 0.53 | - | - | 20.9 | 7.8 | [157] |
| | 350 | 51.51 | 4.91 | 3.54 | 11.10 | 0.92 | - | - | 32.5 | 8.4 | |
| | 700 | 44.06 | 0.74 | 2.61 | 4.03 | 4.11 | - | - | 52.9 | 9.5 | |
| Paved feedlot manure | Raw | 45.05 | 5.47 | 2.37 | 32.47 | 1.02 | - | - | 15.4 | 7.3 | [157] |
| | 350 | 53.32 | 4.05 | 3.64 | 15.70 | 1.34 | - | - | 28.7 | 9.1 | |
| | 700 | 52.41 | 0.91 | 1.70 | 7.20 | 145.2 | - | - | 44.0 | 10.3 | |
| Poultry litter | Raw | 42.15 | 5.23 | 3.67 | 34.80 | 0.57 | - | - | 16.9 | 8.2 | [157] |
| | 350 | 51.07 | 3.79 | 4.45 | 15.63 | 3.93 | - | - | 30.7 | 8.7 | |
| | 700 | 45.91 | 1.98 | 2.07 | 10.53 | 50.9 | - | - | 46.2 | 10.3 | |
| Turkey litter | Raw | 40.45 | 5.04 | 3.43 | 30.23 | 1.45 | - | - | 20.3 | 7.0 | [157] |
| | 350 | 49.28 | 3.60 | 4.07 | 15.40 | 2.60 | - | - | 34.8 | 8.0 | |
| | 700 | 44.77 | 0.91 | 1.94 | 5.80 | 66.7 | - | - | 49.9 | 9.9 | |
| Dairy manure | Raw | 46.52 | 5.49 | 2.29 | 33.20 | 1.32 | - | - | 14.8 | 8.3 | [157] |
| | 350 | 55.80 | 4.29 | 2.60 | 18.73 | 1.64 | - | - | 24.2 | 9.2 | |
| | 700 | 56.67 | 0.94 | 1.51 | 4.13 | 186.5 | - | - | 39.5 | 9.9 | |
| Pig manure | 350 | 31.58 | 2.36 | 3.80 | 16.93 | 23.80 | 0.053 | - | 45.33 | 8.3 | [138] |
| | 700 | 25.16 | 1.12 | 2.05 | 4.83 | 32.60 | 0.035 | - | 66.84 | 9.5 | |

reduced from 28.48 to 27.2% [154]. Therefore, the selection of the appropriate carbonization gas and its flow rate is important to obtain a high yield of biochar.

#### 4.1.2 Effect of pyrolysis holding time and heating rate

Apart from pyrolysis temperature, holding time and heating rate are other two factors that influence the development of micropores and surface area. Increasing the pyrolysis time boosts the rudimentary pore generation as the carbon surface releases the volatile matter [49]. However, prolonged pyrolysis time at high temperatures may lead to an intermediate melt formation due to progressively softening and sintering of the low molecular weight volatiles [141]. Here, the intermediate melt could partially block the pores, thus reducing the surface area. Lua et al. [141] observed that a maximum surface area of 519 $m^2$/g and micropore volume of 0.215 $cm^3$/g was achieved at 120 min of residence time for oil palm shells. While prolonging the residence time to 180 min reduced the surface area and micropores volume to 380 $m^2$/g and 0.155 $cm^3$/g, respectively. On the other hand, insufficient holding time to release the volatiles would result in the accumulation of these matters between and within the particles, and thus the deposition of these matters causes pore entrance blocking. In terms of biochar yield and fixed carbon content, Yang et al. [158] found that a holding time of 120 min produced a high yield and fixed carbon content of 32.67% and 79.38%, respectively, using pruned apple tree branches. Generally, the literature survey shows that a holding time between 60 and 120 min is suitable to improve the surface area and porosity of biochar for $CO_2$ uptake [141, 158, 159].

The heating rate is strongly associated with heat and mass transfer inside the particles. At a low heating rate, the reaction is relatively slow, while, at a high heating rate, the reaction rate is more pronounced due to progressive heat and mass transfer [49]. For example, increasing the heating rate from 1 to 20 ℃/min increased the surface area of rapeseed stem-derived biochar from 259.9 to 384.1 $m^2$/g and micropores volume from 0.097 to 0.116 $cm^3$/g [159]. However, an excessive heating rate also melts the biochar particles and likely smooths the biochar surface [126]. In a study carried out by Angin et al. [160], a reduction in the surface area and micropores volume from 4.23 to 3.64 $m^2$/g and 0.0067 to 0.0057 $cm^3$/g, respectively, was experienced with an increase of the heating from 10 to 50 ℃/min. Chen et al. [127] reported that increasing the heating rate from 5 to 30 ℃/min increased the surface area and micropores volume of biochar from ~ 400 to 411.06 $m^2$/g and ~ 0.120 to ~ 0.125 $cm^3$/g, respectively. Further increasing the heating rate to 50 ℃/min reduced the surface area and micropores volume to 385.38 $m^2$/g and ~ 0.10 $cm^3$/g, respectively. In conclusion, the available literature suggests that a heating rate in the range of 5 to 30 ℃ is preferable for promoting the evolution of biochar porosity and its surface area development for $CO_2$ adsorption application [127, 159].

### 4.2 Biochar pH

Generally, biochar is alkaline, and its pH is around 8.0 to 11.0 (Table 4). Studies have indicated that pyrolysis temperature influences the biochar pH [161]. The relevance of pyrolysis temperature and pH of several biochar samples derived from various biomass feedstocks, such as animal manure, woody biomass, and agricultural residues, is shown in Table 4. The data demonstrate a positive correlation, where the biochar pH increases as the pyrolysis temperature is increased. It should be highlighted that increasing the pyrolysis temperature results in higher pH of biochar due to the disappearance of the acidic group at higher temperatures [162]. Conversely, at low temperature (< 300℃), the acidic value could be attributed to the remaining organic acids and phenolic constituents resulting from the decomposition of cellulose and hemicellulose on biochar surface [163]. For example, Al-wabel et al. [164] showed that with the increase of the temperature from 200 to 800 ℃, the pH of the biochar derived from Conocarpus wastes increased from 7.37 to 12.38, corresponding to the decrease of acidic surface groups from 4.17 to 0.22 mmol/g biochar, which was determined by Boehm's titration. Yuan et al. [165] reported that pyrolysis temperature above 300 ℃ for canola straw, corn straw, peanut straw and soybean biochar might lead to the formation of carbonates (i.e. $MgCO_3$, $CaCO_3$), thus resulting in pH increment up to 10.76, 11.32, 11.15 and 11.10, respectively. However, at lower pyrolysis temperature (200 ℃), Zhang et al. [163] showed that the biochar derived from wheat straw and lignosulfonate had acidic pH ranging from 4.87–6.11. Similar to this study, vegetable waste and pine cone-derived biochar also exhibited acidic pH of 5.95 and 4.15, at the same pyrolysis temperature of 200 ℃ [155]. The acidic condition is due to the decomposition of cellulose and hemicelluloses at temperatures around 180–250 ℃, which produce organic acid and phenolic compounds that remain on the biochar surface and lower the pH of the biochar.

Ash content also has a significant effect on the pH of biochar. An increase in the pyrolysis temperature results in higher ash content of biochar, thus affecting its pH. In a study by Ghaffar et al. [166], as the pyrolysis temperature increased from 350 to 500℃, the higher ash content and the removal of acid functional groups (such as carboxylic (-COOH), phenolic (-$C_6H_5$) and carbonyl (-C = O) groups) from the Brazilian pepper-derived biochar surface contributed to the increment of pH from 7.72 to 9.65. This is a generally observed trend, but the observed results are not the same in some cases, probably depending on biomass feedstock. Therefore, pyrolysis temperatures above 400 ℃

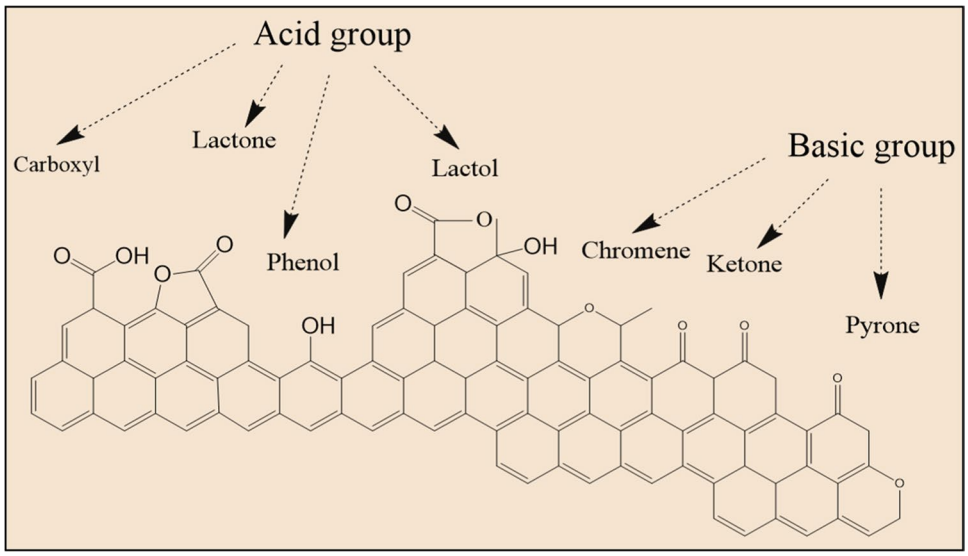


**Fig. 7** Acidic and basic oxygen functionalities on biochar surface. Adapted with permission from [171]

are appropriate to develop biochar with basic characteristics. Due to the acidic character of $CO_2$ gas, the interaction with basic biochar would be feasible for $CO_2$ adsorption. According to the literature, it can be concluded that higher pyrolysis temperatures lead to increased biochar surface area and microporosity with a higher concentration of basic functional groups, which are beneficial attributes for $CO_2$ capture [134, 156, 163, 166, 167].

## 4.3 Surface functional groups

Besides the surface area and microporosity of biochar, surface functional groups on biochar also play a significant role in determining the surface chemistry of biochar and thus its $CO_2$ adsorption performance [168, 169]. At low adsorption pressures, the surface functional groups contribute to the enhanced $CO_2$ capture performance, regardless of the porosity of biochar. While, at high pressures, for the pores larger than 1.0 nm, the surface functional groups play an important role in giving a higher $CO_2$ adsorption capacity [168]. Here, basic surface characteristics and high aromaticity are desirable to ensure the high $CO_2$ capture capacity of the biochar, which are discussed in the following.

### 4.3.1 Surface basicity

Basically, the $CO_2$ adsorption can be improved by increasing the biochar surface alkalinity [117]. Here, the oxygen and nitrogen surface functional groups have been recognized as the main contributors to carbon's surface acidity and alkalinity [170, 171]. According to Boehm et al. [170], surface functional groups can be categorized into acidic, basic, and neutral types. Oxygen-containing functional groups are mainly acidic, as shown in Fig. 7. Specifically, lactol, phenols, lactones and carboxylic acid have been postulated as the sources of surface acidity [172]. However, not all the oxygen-containing groups tend to show acidic characteristics. For instance, chromene, ketone and pyrone are more likely to be basic groups and contribute to surface basicity [125].

In the case of $CO_2$ gas adsorption with an acidic character, biochar with basic surface functional groups is much favoured. In this regard, acidic oxygen functionalities are not beneficial for $CO_2$ adsorption. The relationship between thermal desorption temperature and related desorption products during temperature-programmed desorption (TPD), as illustrated in Fig. 8, indicates that acidic oxygen functional groups such as phenol, lactone and carboxyl dissociate to CO and $CO_2$ at the temperature range of 100–700℃ (373-973 K). Most basic functional groups decompose to $CO_2$ and CO above 600 ℃ (873 K) except anhydride, which starts to decompose at 350 ℃ (623 K). It can be concluded that most oxygen-containing acidic groups could be removed from the biochar surface at high temperatures, thus producing biochar favourable for adsorption of $CO_2$ acidic gas.

On the other hand, the presence of nitrogen-containing groups such as pyrrolic, pyridinic, lactam, imide, and amide enhance biochar's surface basicity [48]. These functional groups can be incorporated into the biochar surface using different nitrogen-containing reagents such as ammonia, amines, nitric acid, and other nitrogen-containing precursors (i.e. melamine, polyacrylonitrile) through biochar activation [173, 174]. In an attempt to increase the surface basicity of biochar for enhancing the $CO_2$ uptake, Yaumi et al. [175] impregnated rice husk with melamine, and by introducing the N-containing group onto the biochar surface, the concentration of basic surface groups increased

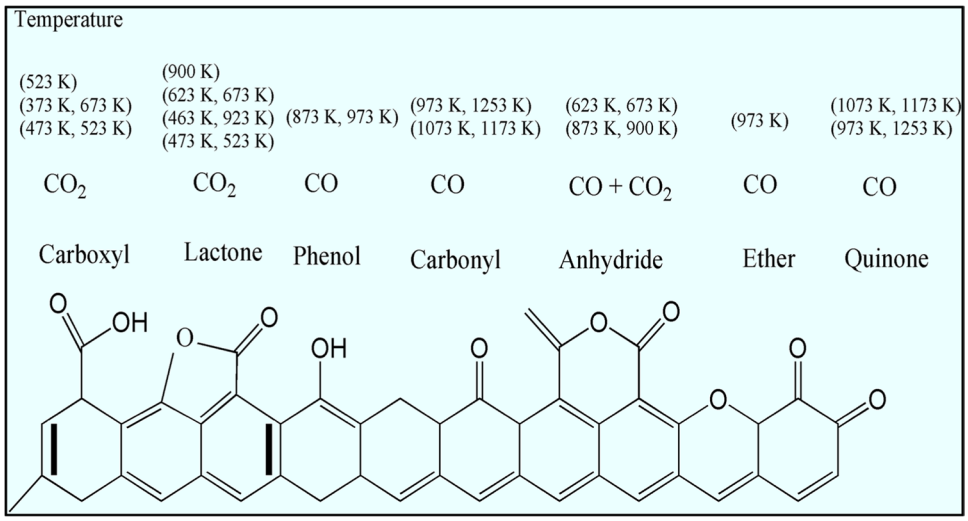


**Fig. 8** Surface oxygen-containing groups and their decomposition by TPD. Adapted with permission from [293]

from 1.43 to 4.10 mmol/g, corresponding to improved surface alkalinity.

#### 4.3.2 Aromaticity

Aromaticity is a chemical property that facilitates $CO_2$ adsorption on the biochar surface. Fixed carbon fraction is strongly related to biochar's aromaticity produced from the pyrolysis and gasification [176]. High aromaticity can indicate the carbon stability and its resistance to biodegradation [177], and van Krevelen diagram is used to determine the degree of aromaticity and maturation of char based on atomic H/C and O/C ratios. A low ratio of H/C and O/C (< 0.2) indicates that the biochar is chemically stable [178, 179]. Aromaticity and hydrophobicity are interrelated properties; when the aromaticity of biochar increases, consequently its hydrophobicity enhances [47]. Biochar with non-polar and hydrophobic characteristics may favour the sorption of $CO_2$ molecules by limiting the accessibility of $H_2O$ molecules on the biochar surface [48]. It was reported that biochar derived from white oak possessed an extremely low O/C ratio of 0.051, implying low polarity and high hydrophobicity [180, 181], which both factors contribute to the enhancement of $CO_2$ sequestration.

### 4.4 Elemental composition of biochar

In general, the elemental composition of biochar is highly affected by pyrolysis temperature. The carbon content increases as a function of pyrolysis temperature. By increasing the pyrolysis temperature, the heat treatment-driven loss of the OH functional group from the lignocellulosic biomass occurs due to dehydration, resulting in the disappearance of H and O atoms [182]. Additionally, the elimination of water, $CO_2$, CO, hydrocarbons, and tarry vapours during the carbonization contributes to the decrement of H, O and N contents as the biomass is heated up [183]. Moreover, the losses of H and C at the elevated temperature may result from the breakage and cleavage of the weak bonds in the carbon structure [184, 185]. Accordingly and as the data in Table 4 show, the H, O and N contents reduce when the pyrolysis temperature increases.

The elemental contents data obtained from CHNS analysis provides insightful information about the chemistry of biochar. For example, the O/C, H/C and (O + N)/C values are known as hydrophobicity, aromaticity and polarity indexes, respectively [186–188]. A high H/C ratio suggests a low degree of aromaticity and carbonization, while high O/C and (O + N)/C ratios indicate low hydrophobicity and high polarity, respectively [186]. In the case of $CO_2$ adsorption, biochar with lower H/C and O/C presents better efficiency in the adsorption. Zubbri et al. [87] investigated the effect of various thermochemical treatments on the $CO_2$ adsorption capacity of the biomass-derived adsorbents. The implemented treatments included hydrothermal carbonization (at 170 °C) to obtain hydrochar, pyrolysis (850 °C) to obtain biochar, and KOH impregnation of hydrochar followed by activation (850 °C); the samples were designated as HC $_{170–90}$, biochar $_{850–120}$ and HC-2KOH $_{850–120}$, respectively. They observed that the value of O/C reduced along with increasing the severity of thermal treatment in the following order HC $_{170–90}$ (1.51) > HC-2KOH $_{850–120}$ (1.18) > biochar $_{850–120}$ (0.86). At high temperatures, the reduction of the hydrophilic sites may be attributed to the dehydration process (loss of O- and H- functional groups), making the char surface more hydrophobic. Similarly, the H/C ratio reduced with the thermal treatment processes in the following order HC $_{170–90}$ (0.38) > HC-2KOH $_{850–120}$ (0.34) > biochar $_{850–120}$ (0.18), indicating higher aromaticity. Other than that, the polarity index, represented by the ratio of (O + N)/C decreased with heat treatment. Among all samples, the KOH activated hydrochar (HC-2KOH $_{850–120}$) possessed the

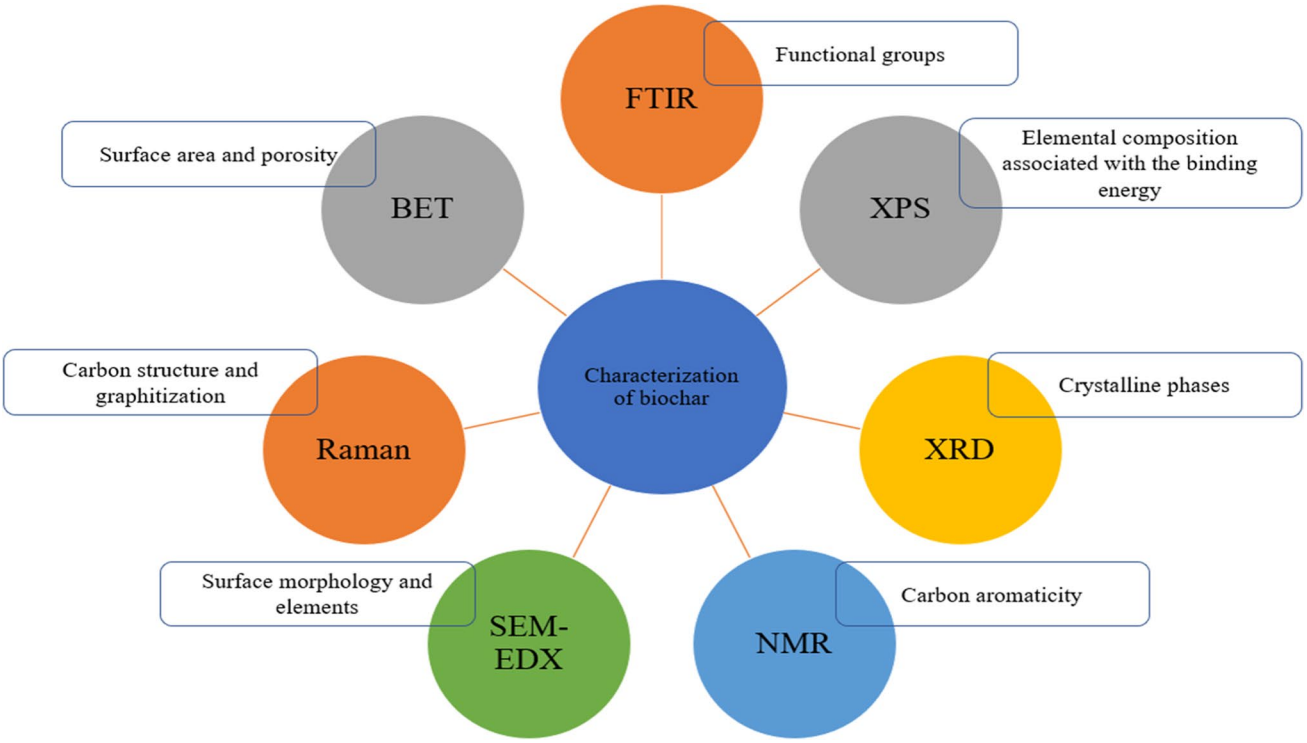


**Fig. 9** Characterization methods used to analyse the physicochemical properties of biochar. Adapted with permission from [47]

highest adsorption capacity of 122.37 mg/g at 30 ℃ and 1 bar. In another study by Gargiulo et al. [86], the authors obtained cellulose fibres-derived biochar by employing steam-assisted slow pyrolysis at various temperatures (600, 650 and 700 ℃). The biochar pyrolyzed at 700 ℃ exhibited the lowest H/C ratio of 0.09 among the prepared biochars. In this case, high aromaticity was closely related to the stability of biochar which enhanced $CO_2$ sorption capacity to 102.52 mg/g at 25 ℃ and 1 bar. In another attempt to investigate the performance of different biomass feedstocks towards $CO_2$ adsorption, Bamdad et al. [189] pyrolyzed softwood bark, softwood sawdust, hardwood and a mixture of softwood bark and sawdust at a temperature between 400 and 500 ℃. They found softwood sawdust pyrolyzed at 500 ℃ with the lowest H/C ratio of 0.03 showed the maximum $CO_2$ adsorption capacity of 105.60 mg/g at 20 ℃ and 1 bar compared to the other resultant biochars.

### 4.5 Analytical techniques to determine the physicochemical properties of biochar

After preparing pristine and modified biochar, it is important to carry out some characterization analyses on the biochar to gain some insights into the structural features of biochar and its surface chemistry. The common methods used to characterize the physicochemical properties of biochar include Raman spectroscopy, surface area and porosity analysis using Brunauer–Emmett–Teller (BET), Fourier transform infrared spectrometry (FTIR), X-ray photoelectron spectroscopy (XPS), X-ray diffraction (XRD), solid-state $^{13}C$ nuclear magnetic resonance (NMR), and scanning electron microscopy-energy dispersive X-ray spectroscopy (SEM–EDX), as shown in Fig. 9.

Raman spectroscopy is normally used to determine the carbon structural characteristic of the biochar, where the two prominent peaks, which respectively represent the amorphous (*D*-band) and crystalline (*G*-band) region formed during the pyrolysis of biochar [190]. The surface area and porosity of biochar are measured via nitrogen adsorption at 77 K. The assessment of the micropore volume is usually accomplished by the Dubinin–Radushkevich (DR) method or the t-plot method [191]. Mesopore volume can be calculated by the difference between the total pore volume and micropore volume [49]. For pore size distribution, the Barrett-Joyner-Halenda (BJH) method is only suitable for calculating mesopores [192], while the density functional theory (DFT) is applicable for micropores and mesopores determination [49]. FTIR can be used to analyse the presence of the related functional groups within the wavelength between 4000 and 400 $cm^{-1}$, while XPS is used to determine the chemical state and the concentration of elements on the adsorbent surface. Specifically, the FTIR absorption peak and XPS binding energy for fresh and spent (after adsorption) adsorbent, which provide insightful information

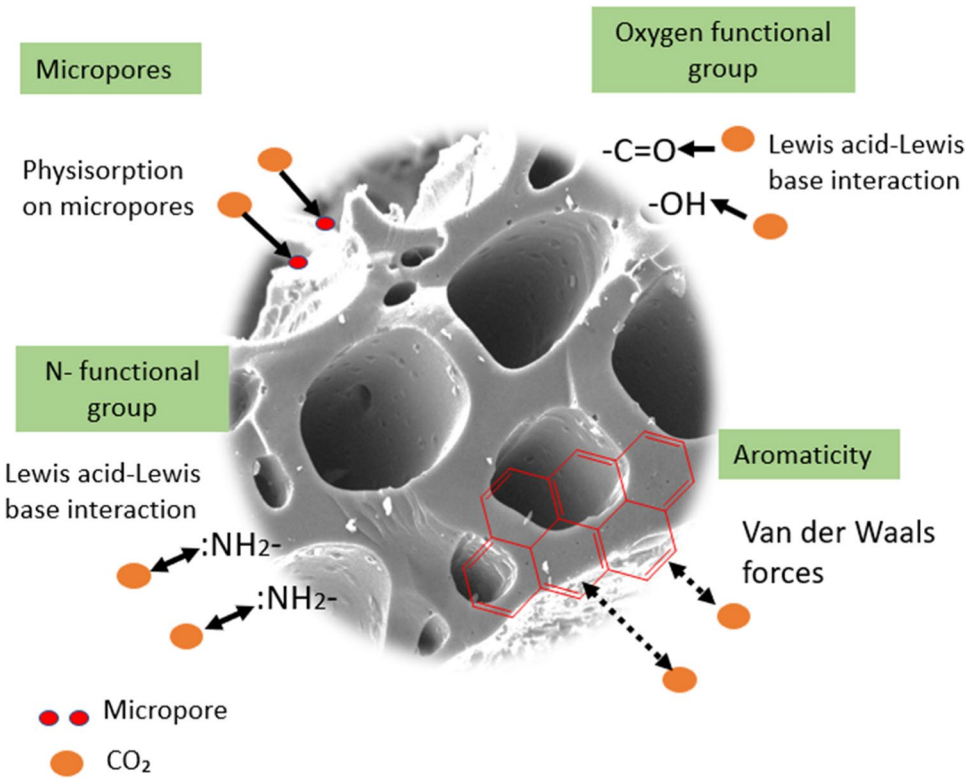


**Fig. 10** Possible mechanisms involved in $CO_2$ adsorption of biochar. Adapted with permission from [195]

regarding the various surface functionalities, such as O and N-containing functional groups are crucial to interpret the $CO_2$ adsorption mechanism, which is highly influenced by the basic or acidic characteristic of the biochar surface [34, 190]. To examine the carbon structure and the mineralogical analysis of biochar, XRD could be performed [117]. NMR is commonly used to investigate the quantitative aromaticity and non-protonated aromatic fraction of the biochar [193]. SEM analysis is conducted to observe the changes in the surface morphology of biochar. Here, porosity development, pore widening and pore-clogging could be observed after the implementation of various modification techniques. Additionally, EDX is used to determine the elemental composition of the biochar surface [20].

## 5 $CO_2$ capture mechanisms by biochar

Various interactions can contribute to the adsorption of $CO_2$ on the biochar surface, but the most perceived ones include physisorption on micropores, van der Waals attractions and Lewis-acid base interactions by O and N containing-functional groups, as demonstrated in Fig. 10.

The adsorption performance of biochar greatly depends on its pore structure. Here, pore size distribution will dictate the diffusion rate of $CO_2$ molecules onto the biochar surface, where the surface area determines the number of active sites for adsorption to occur [194]. The micropore filling effect contributes to the physisorption of $CO_2$ [117, 195]. Biochars having micropores in the range of 0.3–0.8 nm are effective for $CO_2$ capture; specifically, those with pores below 0.5 nm are the most desirable ones [195]. In addition to this, the highly aromatic structure of biochar could enhance the physical adsorption of $CO_2$ via van der Waals attractions [195, 196]. Moreover, various functional groups, especially O and N-containing functional groups on biochar surface, contribute to the $CO_2$ adsorption either via hydrogen bonding and/or Lewis aid-base interactions [197, 198]. In general, the majority of O-containing functional groups are acidic, and hence would inhibit the adsorption of acidic $CO_2$. According to the acid–base interacting mechanism, the presence of acidic groups on the biochar surface would lead to a negative effect on $CO_2$ adsorption capacity. However, the inclusion of hydroxyl (-OH) and carboxyl (-COOH) in the biochar matrix may improve the hydrogen bonding interaction with $CO_2$ molecules [198, 199]. Here, the strongly electropositive H atom in hydroxyl and carboxyl groups interacts with the electronegative O atom in $CO_2$ to produce a hydrogen bond (O–H···O=C= O) due to the considerable electronegativity difference between O atom (3.5) and H atom (2.1) [200, 201]. This interaction is considered a weak hydrogen bonding compared to the other hydrogen bonding between O–H···O, and N–H···O, where H atom is covalently bonded to strong electronegative atoms (O and N atoms). Another mechanism that contributes to $CO_2$ adsorption is the interaction of basic N-containing functional groups with acidic $CO_2$

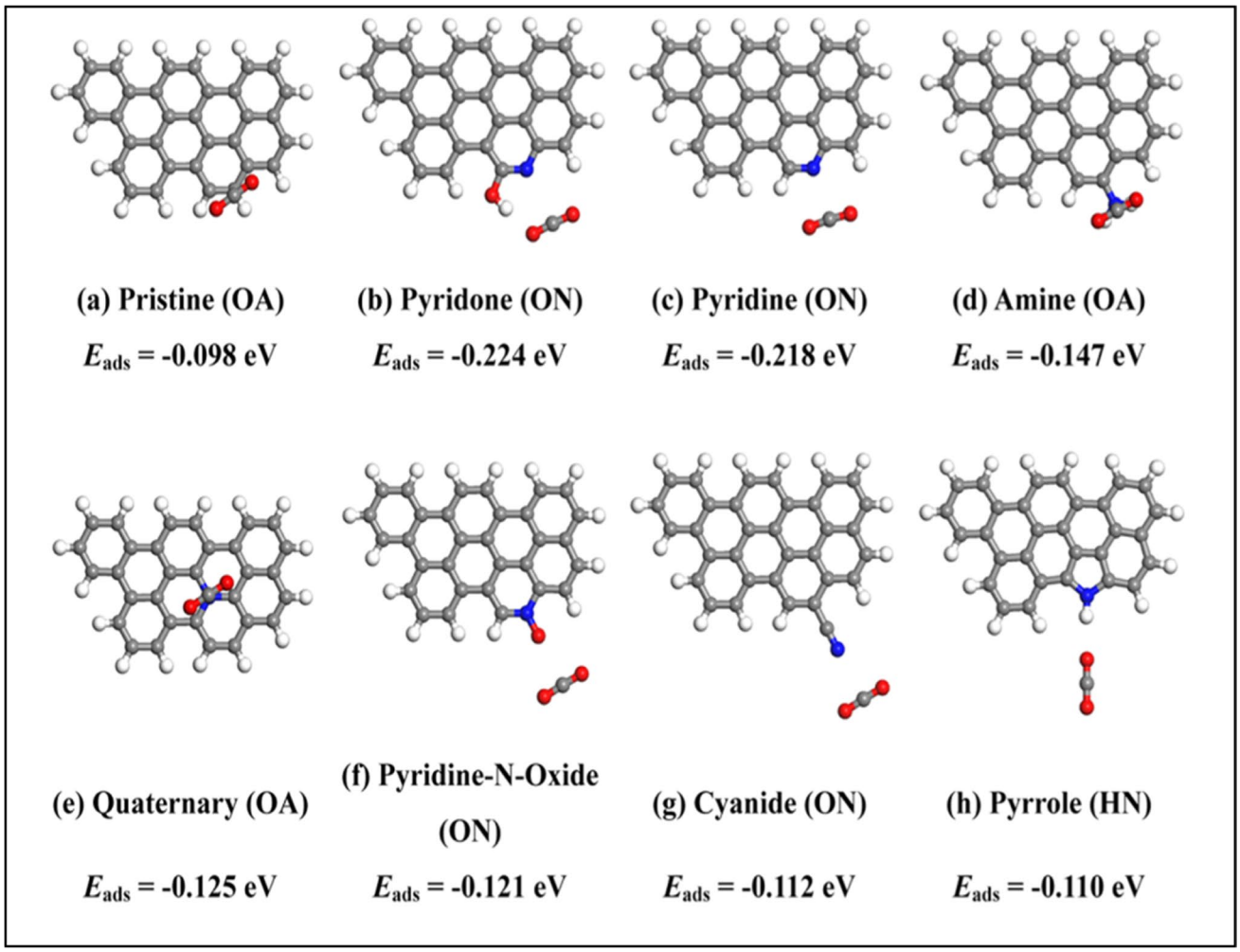


**Fig. 11** Optimized geometry after $CO_2$ adsorption and the binding energy ($E_{ads}$) values for the different N-containing functional groups. Atom colours: C = grey, H = white, O = red and N = blue. Adapted with permission from [197]

molecules, known as a Lewis acid–base reaction [201–203]. In general, pyridone, pyridine, amine, quaternary-N, pyridine-N-oxide, cyanide, and pyrrole groups are the most common types of N-containing functional groups with different basic strengths. Among the N-containing functional groups, pyridone, pyridine and pyrrole significantly affect the $CO_2$ adsorption [47]. Lim et al. [197] used density functional theories (DFT) to investigate the interaction of various N-containing functional groups with $CO_2$. They found that the binding energies ($E_{ads}$) estimated from various beginning configurations reveal how the functional groups interact with the $CO_2$ atom to determine which configuration is most beneficial for adsorption. $CO_2$ configurations with related N-functional group binding energies are shown in Fig. 11.

In Fig. 11 (a), the $E_{ads}$ value is less than -0.10 eV indicating weak van der Waals interactions. Pyridone possesses the highest binding energy of $CO_2$ (-0.224 eV) compared to the other N-containing functional groups. The adsorption behaviour of a pyridone with $CO_2$ is mostly determined by two types of interactions: Lewis acid–base and hydrogen-bonding interactions. For pyridine, the $E_{ads}$ value is almost near to that of pyridine, which explains pyridinic-N is more favourable for adsorption of $CO_2$ due to its stronger electronegativity. In addition to this, it is possible that pyridinic-N prefers the electron-deficient C atom over the O atom in $CO_2$ molecules. Pyrrole interacts with $CO_2$ through hydrogen bonding, whereas the $CO_2$ interactions occur in pyridine-N-oxide group involving the reaction between the carbon atom of $CO_2$ with the oxygen atom of the functional group (-NO···C and -NH···O). The lowest $E_{ads}$ value of -0.110 eV may be attributed to a weaker Lewis acid-basic interaction than that of pyridine group and the hydrogen bonding of pyridone group. Other N-functional groups, including cyanide, quaternary and amines, formed weak Lewis acid–base reaction with $CO_2$;

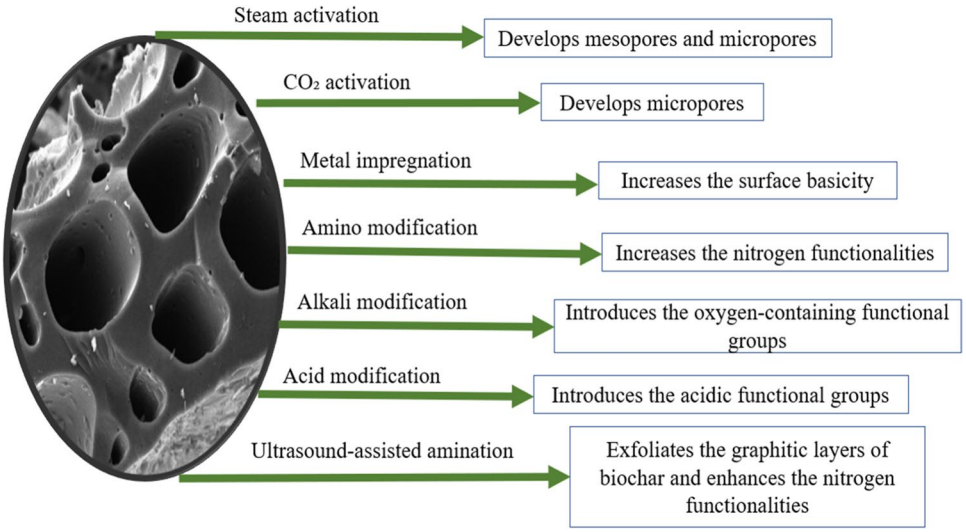


**Fig. 12** Different modification methods implemented on the biochar surface

hence, the presence of these three groups was less significant for adsorption of $CO_2$.

## 6 Modified biochar for $CO_2$ adsorption

Biochar has multifunctional properties that make it a promising adsorbent. The high availability of biomass feedstock is the key parameter for its cost-effectiveness, making it much cheaper than other available $CO_2$ adsorbents [48]. However, pristine biochar exhibits low $CO_2$ uptake due to its low microporosity and lack of enriched surface chemistry. Thus, the adsorption of $CO_2$ molecules on biochar should be enhanced through various modification techniques. From the surface chemistry perspective, the adsorption of $CO_2$ on pristine biochar is not very efficient as $CO_2$ is a weak Lewis acidic gas (electron acceptor) [204]. Strong acid–base interaction with the Lewis basic sites (electron donor) will promote the surface affinity and selectivity towards $CO_2$ molecules [205]. In this regard, biochar modification can be implemented through various methods using different activating agents and activation conditions [206] to produce biochar with desirable surface properties, thus enhancing the adsorption capacity. To obtain biochar with desired properties, the biomass feedstock is normally subjected to treatment before or after the carbonization. The following sub-sections highlight the modification of biochar through physical activations ($CO_2$ activation and steam activation), chemical activations (metalized-biochar, amino-modified biochar, alkali-modified biochar) and physicochemical activation (ultrasound-assisted amination). A scheme of the implemented modification methods and the routes through which each method affects the physicochemical characteristics of biochar is presented in Fig. 12.

### 6.1 Physical activation

Physical activation uses several oxidising agents such as steam, $CO_2$, and air at temperatures above 700 ℃ to increase the porosity of biochar [207]. The penetration of these oxidising agents into the internal surfaces followed by the carbon atom gasification results in the opening and widening of the inaccessible pores [208]. Here, the selection of oxidising agents plays a crucial role in creating microporous biochar [209]. Oxidation with $CO_2$ is favourable for generating and widening the existing micropores, while steam activation creates micropores and mesopores [207]. These activations can be performed either during pyrolysis or after pyrolysis. Table 5 summarises the related literature on the physical activation of biochar for $CO_2$ adsorption.

#### 6.1.1 Steam activation

Steam activation is utilized to develop the porous structure and introduce oxygen-containing functional groups (i.e., carbonyl, carboxylic, hydroxyl, ether and phenolic groups) onto the carbon surface [169]. For this purpose, steam activation is normally performed at a temperature between 800 and 900 °C for 30 min until 3 h [210] with a steam flow rate of 120 to 300 ml/min [211, 212]. Theoretically, the porous structure of biochar can be improved by devolatilization of trapped products such as aldehydes, ketones, and some acids [213] that result from incomplete combustion during pyrolysis. Pore development in steam activation is related to carbon depletion and the water–gas shift reaction [214]. Therefore, steam activation could develop a variety of pore size distributions and produce micropore and mesopore [208, 215, 216].

The reactions involved in steam activation are explained in Eqs. (1)-(8) [207, 217]. The development of the surface oxide

**Table 5** Effect of physical activation and operating conditions on the $CO_2$ adsorption capacity of biochar

| Feedstock | Pyrolysis temperature (℃) | Activating agent | Activation temperature (℃) | Activation time (min) | Adsorption condition | | $CO_2$ concentration (%) | $CO_2$ adsorption capacity (mg/g) | Reference |
|---|---|---|---|---|---|---|---|---|---|
| | | | | | Temperature (℃) | Pressure (bar) | | | |
| Soybean straw | 500 | $CO_2$ | Pristine | 0 | 30 | 1 | 10 | 45 | [200] |
| | | | Pristine | 0 | 120 | 1 | 10 | 24 | |
| | | | 500 | 30 | 30 | 1 | 10 | 46 | |
| | | | 500 | 30 | 120 | 1 | 10 | 27 | |
| | | | 600 | 30 | 30 | 1 | 10 | 58 | |
| | | | 600 | 30 | 120 | 1 | 10 | 26 | |
| | | | 700 | 30 | 30 | 1 | 10 | 60 | |
| | | | 700 | 30 | 120 | 1 | 10 | 27 | |
| | | | 800 | 30 | 30 | 1 | 10 | 76 | |
| | | | 800 | 30 | 120 | 1 | 10 | 32 | |
| | | | 900 | 30 | 30 | 1 | 10 | 70 | |
| | | | 900 | 30 | 120 | 1 | 10 | 31 | |
| Whitewood | 500 | $CO_2$ | 890 | 100 | 25 | 1 | 10 | 28 | [226] |
| | | | 890 | 100 | 25 | 1 | 30 | 63 | |
| | | | 890 | 100 | 45 | 1 | 20 | 36 | |
| | | | 890 | 100 | 65 | 1 | 10 | 12 | |
| | | | 890 | 100 | 65 | 1 | 30 | 29 | |
| Vine shoots | 600 | $CO_2$ | 890 | 60 | 25 | 0.15 | 100 | 66.18 | [19] |
| | | | 890 | 60 | 75 | 0.15 | 100 | 13.16 | |
| | | | 890 | 180 | 25 | 0.15 | 100 | 69.52 | |
| | | | 890 | 180 | 75 | 0.15 | 100 | 13.16 | |
| Pine sawdust | 550 | $CO_2$ | 550 | 45 | 25 | 1 | 15 | 32.12 | [195] |
| Whitewood | 500 | Steam | 700 | 84 | 25 | 1 | 10 | 26 | [226] |
| | | | 700 | 84 | 25 | 1 | 30 | 59 | |
| | | | 700 | 84 | 15 | 1 | 20 | 35 | |
| | | | 700 | 84 | 45 | 1 | 10 | 15 | |
| | | | 700 | 84 | 75 | 1 | 30 | 35 | |
| Cellulose fibres | 650 | Steam | Steam-assisted slow pyrolysis at 650 ℃ | - | 25 | 1 | 100 | 75.68 | [86] |
| Cellulose fibers | 700 | | Steam-assisted slow pyrolysis at 700 ℃ | - | 2 | 1 | 100 | 102.52 | |
| *Pinus nigra* wood | 600 | | Steam-assisted slow pyrolysis at 600 ℃ | - | 2 | 1 | 100 | 49.28 | |

(C(O)) in Eq. (1) comes from the oxygen exchange from the water molecule ($H_2O$) to the vacant carbon site ($C_f$) on the surface, which may be devolved as carbon monoxide (CO) (Eq. (2)). The production of $CO_2$ in Eq. (3) due to the formation of CO increases the rate of carbon gasification by scavenging the C(O). The water–gas shift reaction occurs where CO and $H_2O$ are dissociated to $CO_2$ and hydrogen ($H_2$) (Eq. (4)). Simultaneously, carbon gasification occurs where the $C_f$ reacts with $H_2O$ to produce $CO_2$ and $H_2$ (Eq. (5)). The presence of $CO_2$ and $H_2$ actives $C_f$ and carbon gasification occurs to form CO (Eq. (6)) and $CH_4$ (Eq. (7)). Further reaction of $CH_4$ and $H_2O$ produces CO and $H_2$ (Eq. (8)).

$$C_f + H_2O \rightarrow C(O) + H_2 \quad (1)$$

$$C(O) \rightarrow CO + C_f \quad (2)$$

$$CO_{(g)} + C(O) \rightarrow CO_{2(g)} + C_f \quad (3)$$

$$CO + H_2O \rightarrow CO_2 + H_2 \quad (4)$$

$$C_f + 2H_2O \rightarrow CO_2 + 2H_2 \quad (5)$$

$$C_f + CO_2 \rightarrow 2CO \quad (6)$$

$$C_f + 2H_2 \rightarrow CH_4 \quad (7)$$

$$CH_4 + H_2O \rightarrow CO + 3H_2 \quad (8)$$

The overall reaction is presented in Eq. (9) [218].

$$C_{(s)} + H_2O_{(g)} \rightarrow CO_{(g)} + H_{2(g)}\Delta H = 117kJ/mol \quad (9)$$

In general, the volume/radius of pore and surface area are positively correlated with steam activation temperature and time due to the continuous removal of carbon atoms from the carbon surface [207]. At high activating temperatures, i.e. around 700–800 ℃, the changes in the surface oxygen-containing groups, aromatic structure, and alkali and alkaline earth metal (AAEM) species contribute to the reactivity of steam activated biochar. Here, at the temperature of 700–800 ℃, the agglomeration of AAEM species increases their particle size and penetration of H radical into the carbon surface leads to changes in the ring condensation reactions, which increases the biochar reactivity. However, raising the temperature to above 800 ℃ makes the biochar more ordered due to the consumption of small aromatic ring structures and reduces its reactivity. Conversely, steam activation below 300 ℃ is not suggested as this low activation temperature cannot remove the strong hydroxyl binding groups [219]. It should be highlighted that the reactivity of biochar depends on the AAEM species, which improve the oxygen-containing groups at the initial gasification process. These AAEM species are further consumed as the activation temperature increases. Generally, a long activation time (> 45–60 min) at a high temperature allows the overactivation phenomenon. Here, more gasification at a faster rate will collapse the wall structure and negatively affect the biochar surface [207]. In this case, pores are still developed, but some pores may exceed the desirable size for $CO_2$ capture. Here, micropores can be converted to mesopores and macropores, decreasing the volume fraction of micropores [220]. In short, the optimum steam activation temperature and time should be strictly determined to avoid the overactivation phenomenon, which might lead to developing biochar with low surface area and pore volume.

From the previous studies, it should be highlighted that the activation temperature plays an important role in improving the surface area and total pore volume of the modified biochar [137, 221]. The porosity type is greatly influenced by the activating temperature, where steam activation below 750 ℃ generates micropores, while increasing the steam activation temperature up to 750 ℃ may lead to the development of pores distribution consisting of micropores and mesopores [221]. To increase the microporosity and surface area of barley straw-derived biochar, Pallarés et al. [137] used different steam activation temperatures (600, 700 and 800 ℃) for 1 h. Among the activated biochar samples, the one activated at 700 ℃ possessed the higher micropores surface area of 540 $m^2$/g followed by the biochar activated at 800 ℃ (500 $m^3$/g). At the lowest activation temperature of 600 ℃, the micropore surface area could not be detected, as the formation of new pores was not completed due to insufficient activation temperature. Therefore, the employment of suitable activation temperature is critical in producing biochar with high microporosity which is favoured for a high $CO_2$ uptake.

#### 6.1.2 $CO_2$ activation

Unlike steam activation, which yields in a pore distribution consisting of micropores and mesopores, $CO_2$ activation tends to develop micropores. In gas adsorption, where the small molecules, such as $CO_2$, need to be adsorbed, the occurrence of micropores is more important than mesopores and macropores [222]. Advantageously, the development of highly microporous biochar by $CO_2$ activation facilitates the adsorption of $CO_2$ under ambient conditions [200]. As mentioned previously, $CO_2$ can be used either during the pyrolysis of biomass feedstock, which is referred to as direct activation or after it. The Boudouard reaction explains the mechanism of biochar activation with $CO_2$ [207, 209]. In this reaction, vacant active sites, denoted as $C_f$, on the carbon surface undergo dissociative chemisorption of $CO_2$ to form C(O) and CO, as shown in (Eq. (10)). Next, the pore structure is developed as the surface oxide is desorbed from the surface (Eq. (11)). Finally, CO in the gaseous product is adsorbed on the active carbon site of the char and retards the gasification (Eq. (12)).

$$C_f + CO_2 \rightarrow C(O) + CO \quad (10)$$

$$C(O) \rightarrow CO \quad (11)$$

$$C_f + CO \rightarrow C(CO) \quad (12)$$

Among the operating parameters for $CO_2$ activation, which are activation temperature, $CO_2$ flowrate, and holding time, most studies reported that activation temperature is the critical parameter in controlling biochar's textural properties [137, 223]. Zhang et al. [200] employed direct $CO_2$ activation to develop microporous biochar. They used soya bean straw as a precursor and pyrolyzed it under $N_2$ gas, and then switched to $CO_2$ gas after the pre-set temperatures (500, 600,

700, 800 and 900 ℃) were achieved for 30 min. Initially, the micropore surface area for pristine biochar was 250 $m^2$/g. After $CO_2$ activation at 800 ℃, the micropore surface area increased almost 2 times to 473 $m^2$/g. Here, the hot corrosion on the biochar surface created narrow micropores and weakly improved the mesopores and macropores. Using this activated biochar, a $CO_2$ uptake of 76 mg/g was obtained. However, an increase in the activation temperature to 900 ℃ reduced the micropore surface area to 455 $m^2$/g. It was discussed that at high temperatures, the hot corrosion became more intense and led to the disruption of coalescence of micropores to mesopores and macropore. As a result, his phenomenon reduced the micropore surface area. Ogungbenro et al. [223] performed $CO_2$ activation at three different temperatures (600, 700 and 900 ℃) after pyrolysis of date fruit seeds at 800 ℃. Initially, the $CO_2$ adsorption capacity for pristine biochar was 91.12 mg/g at 20 ℃ and 1 bar. While the biochar activated under $CO_2$ at 900 ℃ for 1 h, exhibited the highest $CO_2$ sorption of 141.14 mg/g followed by the ones activated at 700 ℃ (126.21 mg/g) and 600 ℃ (119.11 mg/g) at 20 ℃ and 1 bar. Enhancement of $CO_2$ adsorption capacity was confidently related to the increment of surface area from 531.33 to 798.38 $m^2$/g and micropore volume from 0.19 to 0.28 $cm^3$/g after $CO_2$ activation. Apart from activation temperature, holding time also significantly affects the microporosity and surface area of biochar. Studies indicate prolonging the activation time to over 2 h may collapse the pores, and the widening of the micropores is continuously developed, reducing the surface area and micropores volume [137, 223]. Ogungbenro et al. [223] reported that the biochar activated using $CO_2$ at 800 ℃ for 3 h revealed the lowest surface area and micropore volume of 192.65 $m^2$/g and 0.07 $cm^3$/g, respectively, among the activated biochar samples at different activation times (1, 2 and 3 h). In another investigation, Pallarés et al. [137], carbonized barley straw at 500 ℃ and further activated it using $CO_2$ at 800 ℃. It was reported that the surface area and micropores volume of barley straw activated for 2 h (769 $m^2$/g and 0.3252 $cm^3$/g, respectively), were lower than those obtained from 1 h activation with values of 789 $m^2$/g and 0.3495 $cm^3$/g, respectively.

It should be highlighted that at high temperatures, a shorter holding time is sufficient to prevent the excessive burn-off of biochar and pores widening. Otherwise, a longer holding time is required at lower activation temperatures so that the $CO_2$ molecules could penetrate into the carbon matrix to generate more micropores. In studying the effect of $CO_2$ flow rate, an extreme reduction in surface area and micropore volume from 789 to 160 $m^2$/g and 0.3268 to 0.0657 $cm^3$/g, respectively, was reported when $CO_2$ flow rate was increased from 2500 to 4000 $cm^3$/min [137]. Here, the insufficient contact of $CO_2$ molecules with carbon and the shorter residence time reduced the chance for pore development. In summary, in physical activation, $CO_2$ activation is preferred as steam activation is difficult to control due to the high reactivity of steam [224]. Furthermore, the diffusion rate in steam activation is lower than the reaction rate; hence, carbon atoms and steam can only react on the carbon surface, while $CO_2$ activation can overcome these limitations [225]. As a result, $CO_2$ activation produces biochar with higher micropores volume and surface area than steam activation. In a study conducted by Pallarés et al. [137], barley straw was carbonized under nitrogen and activated using $CO_2$ and steam (in separate experiments) at activation temperatures of 700–900 ℃ for 1–2 h. The authors confirmed that $CO_2$-activated biochar had higher micropores volume and BET surface area of 0.3268 $cm^3$/g and 789 $m^2$/g, respectively, at the activation temperature of 800 ℃ for 1 h. While, steam-activated biochar produced the maximum micropores volume of 0.2304 $cm^3$/g and the BET surface area of 552 $m^2$/g (700 ℃, 1 h). Notably, the biochar activated with $CO_2$ showed a 41.84% increment in microporosity than that activated by steam.

## 6.2 Chemical activation

Chemical activation is applied to pristine biochar to improve its surface chemical properties, mainly surface basicity and surface functional groups. Chemical activation can be implemented via two routes; direct impregnation of biomass feedstock with a chemical agent followed by thermal treatment and activation of synthesized biochar with a chemical agent, which further undergoes heat treatment [207]. The use of different chemical agents will generate various surface functionalities. Specifically, the implementation of chemical activation enhances the surface basicity, which is beneficial for acidic $CO_2$ adsorption. The following chemical activation section highlights three types of modification as a research hotspot, including metalized-biochar, alkali-modified biochar, and amino-modified biochar, as summarized in Table 6.

### 6.2.1 Metalized-biochar

Studies have indicated that impregnating pristine biochar with metal or metal oxide can increase its $CO_2$ capture capacity. According to the reports, impregnation of biochar with metal salt solutions with basic properties such as magnesium, aluminium, iron (III) and calcium resulted in the enhancement of acidic $CO_2$ gas adsorption by an increment of surface basicity [227, 228]. In a study performed by Zubbri et al. [20], impregnation of biochar by several magnesium salts such as magnesium nitrate, magnesium sulphate, magnesium chloride and magnesium acetate and their effect on the $CO_2$ adsorption capacity were examined. Firstly, rambutan peel was pyrolyzed at various temperatures (500, 700

**Table 6** Effect of chemical activation and operating conditions on the $CO_2$ adsorption capacity of biochar

| Feedstock | Pyrolysis temperature (℃) | Type of modification | Activation condition | Adsorption condition | | $CO_2$ concentration (%) | $CO_2$ adsorption capacity (mg/g) | Reference |
|---|---|---|---|---|---|---|---|---|
| | | | | Temperature (℃) | Pressure (bar) | | | |
| Whitewood | 500 | Alkali modification | Impregnation of biochar with KOH at a weight ratio of 1:0.81 for 4 h followed by activation at 775 ℃ for 2 h | 25 | 1 | 10 | 27 | [226] |
| | | | | 25 | 1 | 30 | 78 | |
| | | | | 45 | 1 | 20 | 37 | |
| | | | | 65 | 1 | 10 | 14 | |
| | | | | 65 | 1 | 30 | 40 | |
| Sargassum seaweed | 800 | Alkali modification | Impregnation of biomass with KOH at a weight ratio of 1:1 followed by calcination at 800 ℃ for 2 h | 25 | 1 | 12 | 46.20 | [262] |
| | | | | 50 | 1 | 12 | 30.80 | |
| | | | | 7 | 1 | 12 | 22.44 | |
| | | | | 100 | 1 | 12 | 19.80 | |
| Enteromorpha seaweed | 800 | Alkali modification | Impregnation of biomass with KOH at a weight ratio of 1:1 followed by calcination at 800 ℃ for 2 h | 25 | 1 | 12 | 22.80 | [262] |
| | | | | 50 | 1 | 12 | 20.68 | |
| | | | | 75 | 1 | 12 | 18.48 | |
| | | | | 100 | 1 | 12 | 16.28 | |
| 40% Food waste + 80% Wood waste | Gasification | Alkali modification | Gasification in 10 kW fixed-bed gasifier | 25 | 1 | 100 | ~39.60 | [25] |
| | | | Gasification in 10 kW fixed-bed gasifier followed by impregnation of biochar with KOH at a ratio of 1:1, followed by activation at 850 ℃ for 2 h | 25 | 1 | 100 | ~57.20 | |
| Coconut shell | - | Alkali modification | Impregnation of commercial coconut shell with 32% NaOH followed by shaken in the water bath shaker for 3 h | 35 | 1 | 10 | 27.10 | [243] |
| | | | | 45 | 1 | 10 | 24.30 | |
| | | | | 55 | 1 | 10 | 16.62 | |
| | | | | 35 | 1 | 15 | 29.62 | |
| | | | | 35 | 1 | 20 | 34.18 | |
| Soybean | 600 | Acid modification | Impregnation of biomass with $ZnCl_2$ at a ratio of 1:1 followed by carbonization at 600 ℃ for 2 h | 40 | 1 | 15 | 41.00 | [270] |
| | | | | 75 | 1 | 15 | 22.40 | |
| Slash pine wood | 580 | Acid modification | Impregnation of biomass with $ZnCl_2$ at a ratio of 1:1 followed by carbonization at 580 ℃ for 2 h (pre-impregnation) | 0 | 1 | 100 | 190.08 | [271] |
| | 360 | | Pyrolysis of biomass at 360 ℃ for 2 h followed by impregnation of biochar with $ZnCl_2$ at a ratio of 1:1 (post-impregnation) and activation at 580 ℃ for 2 h | 0 | 1 | 100 | 196.24 | |
| Eucalyptus wood | 450 | | Impregnation of biomass with different $H_3PO_4$ /$ZnCl_2$ amounts followed by carbonization under $N_2$ at 450/550 ℃ for 1 h. The following biomass/$H_3PO_4$ mass ratios were used: | | | | | [268] |
| | | | Biomass/$H_3PO_4$ mass ratio of 1:1.5 | 30 | 1 | 100 | 103.84 | |
| | | | Biomass/$H_3PO_4$ mass ratio of 1:2 | 30 | 1 | 100 | 131.12 | |
| | | | Biomass/$H_3PO_4$ mass ratio of 1:2.5 | 30 | 1 | 100 | 82.74 | |
| | | | Biomass/ $ZnCl_2$ mass ratio of 1:0.75 | 30 | 1 | 100 | 83.60 | |

**Table 6** (continued)

| Feedstock | Pyrolysis temperature (°C) | Type of modification | Activation condition | Adsorption condition | | $CO_2$ concentration (%) | $CO_2$ adsorption capacity (mg/g) | Reference |
|---|---|---|---|---|---|---|---|---|
| | | | | Temperature (°C) | Pressure (bar) | | | |
| | | | Biomass/ $ZnCl_2$ mass ratio of 1:1.5 | 30 | 1 | 100 | 70.84 | |
| | | | Biomass/ $ZnCl_2$ mass ratio of 1:2.5 | 30 | 1 | 100 | 58.96 | |
| | 550 | | The activation step was done with $H_3PO_4$ followed by KOH activation under $N_2$ at 900 °C for 1 h | 30 | 1 | 100 | 180.40 | |
| Walnut shell | 500 | Metalized-biochar | Pristine<br>Impregnation of biochar with 5% metal solution, followed by heat treatment under $N_2$ at 500 °C for 15 min. Following metal solutions were used: | | | | 69.10 | [117] |
| | | | Magnesium nitrate hexahydrate | 30 | 1 | 100 | 80.0 | |
| | | | Aluminium nitrate nanohydrate | 30 | 1 | 100 | ~75.00 | |
| | | | Iron (III) nitrate nanohydrate | 30 | 1 | 100 | ~74.00 | |
| | | | Nickel (II) nitrate hexahydrate | 30 | 1 | 100 | ~70.00 | |
| | | | Calcium nitrate tetrahydrate | 30 | 1 | 100 | ~69.00 | |
| | | | Sodium nitrate | 30 | 1 | 100 | 67.56 | |
| Rambutan peel | 900 | | Pristine<br>Impregnation of biochar with 5% magnesium solution, followed by heat treatment under $N_2$ at 500 °C for 15 min. Following magnesium solutions were used: | 30 | 1 | 100 | 68.74 | [20] |
| | | | Magnesium nitrate hexahydrate | 30 | 1 | 100 | 76.78 | |
| | | | Magnesium sulphate heptahydrate | 30 | 1 | 100 | ~68.00 | |
| | | | Magnesium chloride hexahydrate | 30 | 1 | 100 | ~67.00 | |
| | | | Magnesium acetate tetrahydrate | 30 | 1 | 100 | 68.15 | |
| Tobacco waste | 600 | Metalized-biochar | Pristine<br>Impregnation of biomass with different $AlCl_3$ amounts followed by carbonization under $N_2$ at 600 °C for 3 h. The following biomass/$AlCl_3$ blending ratios were used: | 25 | 1 | 100 | 40.10 | [272] |
| | | | Biomass/$AlCl_3$ blending ratio of 10:0.4 | 25 | 1 | 100 | 59.02 | |
| | | | Biomass/$AlCl_3$ blending ratio of 10:2 | 25 | 1 | 100 | 59.97 | |
| Cottonwood | 600 | Metalized-biochar | Pristine<br>Impregnation of biomass with different metal oxyhydroxide amounts followed by carbonization under $N_2$ at 600 °C for 3 h. The following biomass/metal oxyhydroxide ratios were used: | 25 | 1 | 100 | 57.96 | [228] |
| | | | Biomass/Fe ratio of 1:0.01 | 25 | 1 | 100 | 64.30 | |
| | | | Biomass/Fe ratio of 1:0.05 | 25 | 1 | 100 | 55.61 | |
| | | | Biomass/Fe ratio of 1:0.1 | 25 | 1 | 100 | 66.57 | |
| | | | Biomass/Fe ratio of 1:5 | 25 | 1 | 100 | 60.68 | |
| | | | Biomass/Fe ratio of 1:6 | 25 | 1 | 100 | 65.26 | |
| | | | Biomass/Fe ratio of 1:10 | 25 | 1 | 100 | 53.79 | |

**Table 6** (continued)

| Feedstock | Pyrolysis temperature (°C) | Type of modification | Activation condition | Adsorption condition | | $CO_2$ concentration (%) | $CO_2$ adsorption capacity (mg/g) | Reference |
|---|---|---|---|---|---|---|---|---|
| | | | | Temperature (°C) | Pressure (bar) | | | |
| | | | Biomass/Al ratio of 1:0.03 | 25 | 1 | 100 | 63.87 | |
| | | | Biomass/ Al ratio of 1:0.25 | 25 | 1 | 100 | 62.98 | |
| | | | Biomass/ Al ratio of 1:2.5 | 25 | 1 | 100 | 69.30 | |
| | | | Biomass/ Al ratio of 1:1 | 25 | 1 | 100 | 64.63 | |
| | | | Biomass/ Al ratio of 1:3 | 25 | 1 | 100 | 69.49 | |
| | | | Biomass/ Al ratio of 1:4 | 25 | 1 | 100 | 71.05 | |
| | | | Biomass/ Mg ratio of 1:0.01 | 25 | 1 | 100 | 63.69 | |
| | | | Biomass/ Mg ratio of 1:0.25 | 25 | 1 | 100 | 47.69 | |
| | | | Biomass/ Mg ratio of 1:1 | 25 | 1 | 100 | 35.35 | |
| | | | Biomass/ Mg ratio of 1:3 | 25 | 1 | 100 | 33.83 | |
| | | | Biomass/ Mg ratio of 1:6 | 25 | 1 | 100 | 27.79 | |
| | | | Biomass/ Mg ratio of 1:20 | 25 | 1 | 100 | 35.05 | |
| | | | Biomass/ Mg ratio of 1:40 | 25 | 1 | 100 | 32.33 | |
| Soy bean straw | 500–900 | Amino modification | Heated under $N_2$ until it achieved pre-set temperature (500–900 °C), followed by $NH_3$ ammonification (16%) for 30 min. The following pre-set temperatures were used: | | 1 | | | [200] |
| | | | 500 | 30 | 1 | 10 | ~48 | |
| | | | 500 | 120 | 1 | 10 | ~27 | |
| | | | 600 | 30 | 1 | 10 | ~57 | |
| | | | 600 | 120 | 1 | 10 | ~33 | |
| | | | 700 | 30 | 1 | 10 | ~62 | |
| | | | 700 | 120 | 1 | 10 | ~37 | |
| | | | 800 | 30 | 1 | 10 | ~79 | |
| | | | 800 | 120 | 1 | 10 | ~42 | |
| | | | 900 | 30 | 1 | 10 | ~55 | |
| | | | 900 | 120 | 1 | 10 | ~37 | |
| Sawdust | 600–800 | Amino modification | Impregnation of biochar with urea phosphate for 24 h followed by calcination for 2 h. The following calcination temperatures were used: | | | | | [273] |
| | | | 600 | 30 | 1 | 100 | ~55.88 | |
| | | | 700 | 30 | 1 | 100 | 58.96 | |
| | | | 800 | 30 | 1 | 100 | ~51.92 | |
| Hickory chip | 450 | Amino modification | N-doped (ball milled at 300 rpm for 12 h, mixed with $NH_4OH$ followed by drying in oven at 80 °C for 48 h) | 25 | 1 | 100 | 49.20 | [274] |
| | 600 | | | 25 | 1 | 100 | 52.50 | |
| Sugarcane bagasse | 450 | Amino modification | N-doped (ball milled at 300 rpm for 12 h, mixed with $NH_4OH$ followed by drying in oven at 80 °C for 48 h) | 25 | 1 | 100 | 40.30 | [274] |
| | 600 | | | 25 | 1 | 100 | 48.20 | |

**Table 6** (continued)

| Feedstock | Pyrolysis temperature (°C) | Type of modification | Activation condition | Adsorption condition | | $CO_2$ concentration (%) | $CO_2$ adsorption capacity (mg/g) | Reference |
|---|---|---|---|---|---|---|---|---|
| | | | | Temperature (°C) | Pressure (bar) | | | |
| Chicken manure | 450 | Amino modification | N-doped (treatment using $HNO_3$ solution and $HN_3$ gas at 450 °C for 1 h followed by mixing different amounts of biochar with sodium α-l-gulopyranuronate for 2 h. The following amounts of biochar were used: | | | | | [275] |
| | | | 2.5% biochar | 20 | 1 | 20 | 352.44 | |
| | | | 2.5% biochar | 20 | 1 | 100 | 393.80 | |
| | | | 5% biochar | 20 | 1 | 20 | 361.68 | |
| | | | 5% biochar | 20 | 1 | 100 | 410.08 | |
| | | | 7.5% biochar | 20 | 1 | 20 | 375.32 | |
| | | | 7.5% biochar | 20 | 1 | 100 | 429.44 | |
| | | | 10% biochar | 20 | 1 | 20 | 391.16 | |
| | | | 10% biochar | 20 | 1 | 100 | 446.60 | |

and 900 °C) for 90 min under nitrogen gas. Accordingly, the highest surface area of 569.65 $m^2$/g and micropore volume of 0.201 $cm^3$/g was achieved for biochar prepared at 900 °C. However, after incorporating 5% magnesium nitrate, the surface area and micropore volume reduced to 505.58 $m^2$/g and 0.182 $cm^3$/g, respectively, due to metal deposition and possible pore blocking. It was reported that the $CO_2$ adsorption capacity of biochar impregnated with magnesium nitrate was the highest (76.89 mg/g) among all magnesium-loaded biochar samples. The magnesium oxide and magnesium carbonate formation are demonstrated in Eqs. (13)-(15). Here, the decomposition of magnesium nitrate to its oxide form takes place at the temperature of 400 °C and above [229] (Eqs. (13)-(14)). Then, the further reaction of magnesium oxide with $CO_2$ forms carbonate, as shown in Eq. (15) [20]:

$$Mg(NO_3)_2 6H_2O \rightarrow Mg(NO_3)_2 + 6H_2O \tag{13}$$

$$Mg(NO_3)_2 \rightarrow MgO + 2NO_2 + \frac{1}{2}O_2 \tag{14}$$

$$Mg - O + CO_2 \rightarrow Mg - O \ldots CO_{2(ad)} \tag{15}$$

Finally, after 25 cycles of $CO_2$ adsorption–desorption, magnesium nitrate loaded-biochar showed excellent stability and its adsorption capacity was retained throughout the process. It was also discussed that the $CO_2$ adsorption was predominantly governed by physisorption.

In another study, Lahijani et al. [117] introduced various metals such as Mg, Na, Al, Fe, Ni, and Ca on the surface of walnut shell-derived biochar through impregnation to increase the surface basic sites; this was followed by thermal treatment of metalized-biochar at 500 °C for 15 min. The performance of the metalized-biochar for $CO_2$ adsorption was in the sequence of magnesium > aluminium > iron > nickel > calcium > raw biochar > sodium. It was suggested that anhydrous $Mg(NO_3)_2$ formed at around 110–190°C from the endothermic dehydration reaction of $Mg(NO_3)_2.6H_2O$ as shown in Eq. (13). Next, the thermal decomposition of anhydrous magnesium nitrate to magnesium oxide occurs at a temperature above 400 °C (Eq. (14). The interaction of $CO_2$ with the basic $O^{2-}$ in the $O^{2-}$-$Mg^{2+}$ (MgO) forms carbonate as represented in Eq. (15). Mg-loaded biochar demonstrated the highest $CO_2$ adsorption capacity (80.0 mg/g) compared to the pristine biochar (69.1 mg/g) at 30 °C and 1 bar. It was discussed that after metal deposition on biochar, chemisorption also contributed to the $CO_2$ adsorption through carbonate formation. After metal doping on biochar, the contribution of physisorption reduced due to metal deposition on pore entrance and pore blockage (deduced from the reduction in surface area and porosity), yet the interaction of basic metal oxides with $CO_2$ played an important role in chemisorption. Therefore, the

incorporation of magnesium nitrate into the biochar contributed to a 15.7% enhancement in $CO_2$ adsorption capacity.

Other than that, Creamer et al. [228] investigated the development of various metal oxyhydroxide–biochar composites for carbon dioxide capture. The biochar was prepared using cottonwood and impregnated with three different metal salts (aluminium chloride, iron chloride, and magnesium chloride hexahydrate) at various metal ratios, followed by pyrolysis at 600 ℃ for 3 h. The surface area for the metalized biochar was 289, 367 and 749 $m^2$/g for magnesium-, aluminium- and iron-loaded biochar, respectively. In comparison with the pristine biochar (58 mg/g), the metalized biochar showed higher $CO_2$ adsorption: 63.69 mg/g for Mg-biochar, 71.05 mg/g for Al-biochar and 66.57 mg/g for Fe-biochar. Interestingly, the authors pointed out that Al-biochar exhibited the highest $CO_2$ sorption even though Fe-biochar had the highest surface area. Here, the microporosity was a more influential factor than the surface area; the micropore volume of Al-biochar (0.37 $cm^3$/g) was higher than that of Fe-biochar (0.33 $cm^3$/g). In this case, a high volume of small micropores contributed to a high $CO_2$ uptake.

Apparently, metal loading affects the porosity, surface area, and surface basicity, and the performance of the adsorbents significantly depends on these factors [230]. Therefore, the amount of metal loading should be carefully determined to have the least adverse effect on surface area and microporosity while enhancing the surface basicity for excellent $CO_2$ capture.

#### 6.2.2 Amino-modified biochar

Numerous studies have suggested that basic nitrogen functional groups increase the basicity and nitrogen functionalities on the biochar surface [231, 232]. Among the nitrogen-containing functional groups, amine has been mostly utilized to be functionalized on biochar surfaces, where $CO_2$ molecules selectively bind with amine groups via chemisorptive interactions, thus forming carbamate [233–236]. Although the specific mechanism of this reaction remains unclear, however, some studies discussed that the reaction is in the intermediate formation of zwitterion followed by Brønsted base deprotonation [169, 237]. In $CO_2$ adsorption by primary and secondary amines, the lone pair on the nitrogen atom in the amine molecule attacks $CO_2$ to form zwitterion. Then, further reaction forms carbamate, while the other amine molecule abstracts the proton from the zwitterion intermediate [238].

Recently, Halem et al. [239] reported that the presence of amine in the development of polyvinyl alcohol (PVA)-based biochar nanofibers was important to assist the adsorption of $CO_2$ acidic gas through acid–base attraction. In their study, poultry litter was pyrolyzed at various temperatures of 300 to 600 ℃ for 1 h, followed by nitric acid functionalization using the reflux method. Afterwards, the resulting biochars were treated with diethanolamine (DEA), and the mixtures were then heated at 50 ℃ for 1 h. Biochar was immersed in PVA solution (10 wt%) for 30 min, and finally, the mixtures were converted to nanofibers using electrospinning. It was found that, in comparison with the nanofiber biochar pyrolyzed at 500 ℃ without amine treatment (426 mg/g), the one treated with amine displayed a higher $CO_2$ adsorption capacity of 462 mg/g at 20 ℃. Here, the introduction of amine with basic characteristics was much beneficial for the adsorption of $CO_2$ acidic gas.

Bamdad et al. [240] attempted to tailor the biochar characteristics by thermal and chemical activation of biochar. They developed microporous biochar from sawdust pyrolyzed at 500 ℃ followed by amination using two different functionalization approaches, namely nitration followed by reduction (denoted as AM-SW500), and condensation of aminopropyl triethoxysilane (denoted as AP-SW500). The prepared biochars were then activated in an air-nitrogen mixture at 560 ℃. A significantly higher $CO_2$ adsorption capacity of 145.2 mg/g for AM-SW500-A-560 and 167.2 mg/g for AP-SW500-A-560 was obtained compared to that of pristine biochar (110 mg/g), highlighting the contributing effect of amine in $CO_2$ chemisorption and promotion of the $CO_2$ uptake capacity.

Liu et al. [241] studied a two-step nitrogen-doping and KOH activation method to modify the biochar surface for superior $CO_2$ adsorption capacity. First, the coffee ground was used to prepare the pristine biochar by pyrolyzing it at 400 ℃ under $N_2$ for 1 h. Then, the ammoxidation process was performed via three different methods; (i) dispersion of biochar in 3-Aminopropyltrimethoxysilane (APTES), refluxing at 80 ℃ for 24 h, followed by washing and then drying at 60 ℃ overnight (denoted as SHC), (ii) dispersion of biochar in HCl, then the mixture was treated with poly-condensation of aniline solution by $K_2Cr_2O_7$ in an ice bath for 6 h followed by washing and then drying in a vacuum oven at 60 ℃ (denoted as PHC), and (iii) sonication of biochar in water with the addition of melamine followed by hydrothermal treatment and drying at 60 ℃ (denoted as MHC). Lastly, all prepared biochars were activated by KOH at 400 ℃ for 1 h and then the temperature was further increased to 600 ℃ for the next hour. MHC possessed the highest $CO_2$ adsorption capacity of 37.40 mg/g compared to PHC (~ 22 mg/g) and SHC (18.04 mg/g) at 35 ℃ prior KOH activation. Here, the nitrogen content was the factor that influenced the $CO_2$ adsorption capacity, where the third method developed melamine-modified biochar with the highest nitrogen content (17.4 wt%) compared to the first (4.11 wt%) and second (11.9 wt%) methods. However, the amount of nitrogen content highly decreased in the range of 68–84% after KOH activation due to the decomposition of thermally unstable N species such as nitrile, amide and amine group. It was

discussed that the pyrrolic nitrogen content was the highest (5.1%) in KMHC (after KOH activation for the third route) among all the amination reagents. Therefore, an extreme enhancement in $CO_2$ uptake (117.48 mg/g) at 35 ℃ was obtained. Specifically, in this case, pyrrolic nitrogen was more favourable for $CO_2$ uptake than pyridinic oxide and pyridinic nitrogen.

On the contrary, few studies reported the decrement of $CO_2$ adsorption after functionalizing the amine groups on biochar. Ghani et al. [242] investigated the development of amine-modified biochar derived from coconut shells. The biochar was produced from a lab-scale air blown gasifier operated at 800 ℃ and chemically treated using monoethanolamine (MEA) for 20 min. From the ultimate analysis, the nitrogen content of the biochar increased by 77%, from 0.265 to 1.19 wt%, due to the incorporation of nitrogen components after amine treatment. However, the surface area of the biochar decreased from 171.956 to 10.335 $m^2/g$ after amine functionalization. This reduction in surface area was consistent with a reduction in $CO_2$ adsorption capacity from 46.387 to 45.576 mg/g at 30 ℃. This was due to pore blockage by MEA, inhibiting $CO_2$ adsorption on the biochar surface after the treatment. The authors highlighted that the $CO_2$ capture at 30 ℃ is more physical related to adsorbent and adsorbate attraction formed by the intermolecular electrostatic forces. The pore blockage thus inhibited the intermolecular forces on the biochar surface and led to the decrement of $CO_2$ adsorption. While $CO_2$ capture at 70 ℃ was mostly attributed to chemisorption with the adsorption value of 35.496 mg/g for amine-modified biochar compared to 30.114 mg/g for pristine biochar. Using the similar modification technique, the performance of untreated and amine-treated sawdust was evaluated by Madzaki et al. [85]. The biochar was produced from a lab-scale air blown gasifier reactor at various temperatures (450, 750 and 850 ℃), followed by treatment using MEA for 20 min. The biochar was then subjected to $CO_2$ adsorption at 30 and 70 ℃. It was reported that the pH of amine-treated biochar was in the range of 6.32–6.93, while that of untreated biochar was between 5.09 and 5.57. The biochar surface pH changed from acidic to basic due to incorporating a strong basic component. However, all amine-treated biochar samples (gasified at different temperatures) displayed a lower $CO_2$ adsorption capacity than untreated biochar. The surface area of amine-treated biochars, which were gasified at 450, 750 and 850 ℃, reduced from 8.76 to 0.61 $m^2/g$, 11.36 to 0.15 $m^2/g$ and 182.04 to 3.17 $m^2/g$, respectively. Again, the decrement in $CO_2$ adsorption capacity was mainly caused by pore obstruction by amine, during impregnation of biochar by MEA solution. Furthermore, the quinine functional group that appeared near 1600 $cm^{-1}$ (as observed in FTIR of amine-modified biochars) was likely to be acidic and may result in the decrement of $CO_2$ capture of amine-treated biochar. To conclude, developing a highly microporous and large surface area adsorbent with high nitrogen content and numerous active sites is critically important for high $CO_2$ adsorption capacity.

#### 6.2.3 Alkali-modified biochar

Alkali modification is performed by soaking or mixing either biomass or biochar at a specific alkali concentration for about 6–24 h at a temperature range of 25 to 100 ℃ depending on the used raw materials. Alkali reagents commonly used to activate biochar mainly include sodium hydroxide (NaOH) [194, 243, 244], potassium hydroxide (KOH) [245–248] and potassium carbonate ($K_2CO_3$) [249–251]. Among these reagents, KOH has been widely used as an activating agent for creating small micropores in the carbon skeleton through chemical activation followed by heat treatment [125]. Here, the generation of micro- and meso-porosities results from the separation and degradation of graphitic layers, which is much beneficial for $CO_2$ uptake [207]. During KOH activation, the presence of oxygen-containing functional groups (i.e., carbonyl, quinone, ether and lactone) increases biochar's surface basicity [252, 253]. However, these functional groups decompose at different activation temperatures forming CO and $CO_2$ upon heating. The main products generated for activation temperature below 700 ℃ are $K_2O$, $H_2O$, $H_2$, CO, $CO_2$ and $K_2CO_3$, as presented in Eqs. (16)-(19) [254]. Dehydration of KOH forms potassium oxide ($K_2O$) at 400 ℃, as shown in Eq. (16), while carbon reacts with $H_2O$ to emit hydrogen and carbon monoxide, according to Eq. (17). $CO_2$ is released from the water–gas shift reaction, as shown in (Eq. (18)). Then, potassium carbonate ($K_2CO_3$) is generated as $K_2O$ reacts with $CO_2$ (Eq. (19)). KOH is completely consumed at a temperature above 700 ℃ [255]. For activation temperatures above 700 ℃, the potassium carbonate (Eqs. (19) and (22)) dissociates into $K_2O$ and $CO_2$ and completely disappears when the temperature reaches 800 ℃. The resulting $CO_2$ can further react with carbon to form carbon monoxide at high temperatures (Eq. (23)). In addition, the potassium carbonate can be reduced by carbon and hydrogen to produce metallic potassium at a temperature above 700 ℃, as shown in (Eqs. (24) and (25)) [255]. The intercalation of potassium onto the carbon structure develops new micropores and widens the existing pores [256].

$$2KOH \rightarrow K_2O + H_2O \tag{16}$$

$$C + H_2O \rightarrow H_2 + CO \tag{17}$$

$$CO + H_2O \rightarrow CO_2 + H_2 \tag{18}$$

$$K_2O + CO_2 \rightarrow K_2CO_3 \tag{19}$$

$$C + K_2O \rightarrow 2K + CO \quad (20)$$

$$6KOH + 2C \rightarrow 2K + 3H_2O + 2K_2CO_3 \quad (21)$$

$$K_2CO_3 \rightarrow K_2O + CO_2 \quad (22)$$

$$CO_2 + C \rightarrow 2CO \quad (23)$$

$$K_2CO_3 + 2C \rightarrow 2K + 3CO \quad (24)$$

$$K_2O + H_2 \rightarrow 2K + H_2O \quad (25)$$

Hence, the activation temperature beyond 760 ℃ would expand the carbon atomic layers, as the vaporized metallic potassium can diffuse into the carbon matrix [257]. Accordingly, the activation temperature should exceed the boiling point of potassium which is 760 ℃, to ensure its evaporation and diffusion into carbon layers. Therefore, most studies highlighted that the optimum activation temperature is in the range of 800–850 ℃ [243, 258, 259]. In a recent study conducted by Gomez-Delgado et al. [260], *Prosopis ruscifolia* sawdust was pyrolyzed under $N_2$ at 500 ℃ for 1 h, followed by KOH activation at 800 ℃ and a high $CO_2$ adsorption capacity of 264.4 mg/g was attained. However, the use of lower activation temperature was also reported in the literature. Li et al. [261] investigated different KOH activation temperatures (600, 700 and 800 ℃) for $CO_2$ uptake capacity using mixed sewage sludge and pine sawdust which were initially pyrolyzed at 300 ℃ for 4 h. The KOH-activated biochar at 700 ℃ had the highest surface area and micropore volume of 2623 $m^2$/g and 0.90 $cm^3$/g, respectively, than those activated with KOH at 600 and 800 ℃. It was evident that the high $CO_2$ uptake capacity of KOH-activated biochar at 700 ℃ (182.0 mg/g) compared to other modified biochars (136.7–141.7 mg/g) was due to the largest surface area and micropore volume as the crucial factors for physical adsorption of $CO_2$.

Besides the activation temperature, the amount of used KOH affects the textural properties and the functionalities of the modified biochar [262]. The excessive amount of KOH may disrupt the carbon wall structure, leading to a lower surface area and microporosity of the alkali-modified biochar. Considering that KOH modification results in superior $CO_2$ uptake, in a study carried out by Ding and Liu [262], two different types of seaweed, namely, *Sargassum* and *Enteromorpha*, were used to prepare biochar through single-step carbonization and activation. *Sargassum* and *Enteromorpha* were mixed at different KOH/biomass ratios (0, 1, 2, and 4) and directly calcined at three different temperatures (400, 600 and 800 ℃) in a fixed-bed adsorption system. The *Sargassum* seaweed-based porous biochar prepared at 800 ℃ with KOH/biomass mixing ratio of 1:1 demonstrated the highest $CO_2$ uptake capacity of 46.20 mg/g among the prepared biochars. An excessive activation could disintegrate the carbon wall structure and reduce the surface area. It was noticeable that the total pore volume and surface area of this seaweed-based biochar decreased from 0.16 to 0.07 $cm^3$/g and 60.2 to 16.4 $m^2$/g, respectively, as the KOH/biomass weight ratio increased from 1:1 to 1:4. It was discussed that upon KOH activation, two absorption peaks at 1430 and 1010 $cm^{-1}$ corresponding to carbonyl C = O and carboxylic C-O stretching, respectively, became more intense, as evidenced in FTIR analysis. These oxygen-containing functional groups thus promoted $CO_2$ adsorption on the KOH-modified biochar. Apart from that, the optimum activation temperature of 800 ℃ generated more oxygen-containing functional groups due to the maximum activation roles at high temperatures. After ten cycles of $CO_2$ adsorption–desorption, *Sargassum*-derived KOH-modified biochar exhibited a 13% reduction in its adsorption capacity.

In another study undertaken by Shao et al. [263], microporous carbons were prepared from poplar wood by three different methods. In the first method, poplar wood was mixed with KOH as an activating agent and carbonized at 600 ℃ in one-step activation carbonization. In the second method, residues of poplar wood after bioethanol fermentation were initially mixed with KOH followed by carbonization at 600 ℃. Finally, in the third method, hydrothermal activation was performed on poplar wood. Here, a dried poplar wood was immersed in a sulfuric acid–water mixture and heated up in a stainless-steel autoclave with Teflon lining for 24 h at 160 ℃. The resulting hydrochar was then activated by KOH at different activation temperatures (600, 700 and 800 ℃) and different mass ratios of 1 and 2. Overall, hydrothermal-KOH activated poplar wood at 800 ℃ at a mass ratio of 1:1 displayed the maximum $CO_2$ uptake of 126.10 mg/g at 25 ℃ and 1 bar. In comparison, KOH-activated poplar wood at 600 ℃ presented the lowest $CO_2$ uptake of 48.60 mg/g, while bioethanol-pretreated KOH-activated biochar (at the same temperature of 600 ℃) showed an uptake capacity of 67.90 mg/g. As previously discussed, activation above 760 ℃ results in the formation of new pores as potassium can diffuse into the carbon layers, contributing to a high surface area and micropore volume. Significantly, biochar produced from hydrothermal-KOH activation at 800 ℃ showed the highest BET surface area and micropore volume of 2153 $m^2$/g and 0.85 $cm^3$/g, respectively, compared to the samples obtained from the other two modification methods. The corresponding BET surface area and micropore volume were found to be 511 $m^2$/g and 0.17 $cm^3$/g (for the first method), and 535 $m^2$/g and 0.22 $cm^3$/ (for the second method), respectively. It is important to remember that insufficient activation temperature (< 700 ℃) may result in a lower surface area and microporosity, as KOH is not completely converted to

potassium carbonate in which the intercalation of potassium into the carbon matrix generates new pores and widens the existing pores. Hence, the activation temperature is a key factor when impregnating biochar with KOH and should be carefully determined.

Other than KOH, sodium hydroxide (NaOH) has also been used as the activating agent to develop modified biochar. In this regard, Tan et al. [243] impregnated a commercial coconut shell with NaOH solution. They impregnated the coconut shells with NaOH solution at different concentrations (24–32%) and shook the mix for 1–3 h. It was reported that 32% NaOH concentration and 3 h dwelling time resulted in the maximum BET surface area and micropore area of 378.23 $m^2$/g and 277.42 $m^2$/g, respectively. The highest $CO_2$ uptake capacity of 27.10 mg/g was obtained at 35 ℃ compared to the adsorption temperature of 45 ℃ (24.03 mg/g) and 55 ℃ (16.62 mg/g).

#### 6.2.4 Acid-modified biochar

For developing acid-modified biochar, phosphoric acid ($H_3PO_4$) [264, 265] and zinc chloride ($ZnCl_2$) [266, 267] are the most common activating agents, which serve as dehydration agents. Here, one-step activation is normally adopted, where the activation process is carried out through catalyzed condensation, dehydration and cross-linking reactions. As discussed earlier, the optimum activation temperature for KOH is in the range of 800–850 ℃, whereas $H_3PO_4$ and $ZnCl_2$ require a lower activation temperature between 450 and 500 ℃ [268]. According to Sevilla and Mokaya [269], a lower activation temperature compared to KOH activation is probably due to the difference in the thermal stability of the cross-links formed during the activation process. $H_3PO_4$ is a well-known acid activator, which contributes to the introduction of P-containing functional groups and micropore development on the biochar surface. The pores are formed during the cross-linking reactions, including the cyclization and condensation, where $H_3PO_4$ plays a role as a dehydration agent. Similar to $H_3PO_4$, $ZnCl_2$ is one of the outstanding acid activators and has a boiling point of 732 ℃ [49]. $ZnCl_2$ can penetrate into the carbon structure through the dissolving impact on cellulose, which is beneficial for pore formation. The activation at temperatures below 700 ℃ probably leads to the uniform distribution of $ZnCl_2$ on the biochar surface, as $ZnCl_2$ is still in the liquid state. Thote et al. [270] pre-mixed soybean and $ZnCl_2$ powder at a ratio of 1:1 and pyrolyzed the mixture at 600 ℃ for 2 h. The resultant biochar had a surface area of 811 $m^2$/g and pore volume of 0.33 $cm^3$/g. The $CO_2$ adsorption capacity of the developed biochar was 41.0 mg/g at 30 ℃ and drastically reduced to 22.4 mg/g at high adsorption temperature (70 ℃). Ahmed et al. [271] examined pre-impregnation and post-impregnation methods for developing $ZnCl_2$-activated biochar. In pre-impregnation, slash pine wood was added to $ZnCl_2$ solution and mixed thoroughly for 22 h. Afterwards, the dried mixture was pyrolyzed at 580 ℃ for 2 h. In the second method, slash pine wood was firstly pyrolyzed at 360 ℃ for 2 h; then, the produced biochar was activated with $ZnCl_2$ at 580 ℃ for 2 h. Accordingly, the biochar developed from post-impregnation route showed slightly higher $CO_2$ adsorption capacity of 196.24 mg/g compared to the one developed using pre-impregnation method (190.08 mg/g). They discussed that $CO_2$ adsorption capacities are proportional to the surface area, where large surface area and ultra-micropores (0.57 nm) were beneficial to obtain high $CO_2$ adsorption. In this case, $ZnCl_2$ post-impregnated biochar exhibited a larger surface area of 1093 $m^2$/g than that of pre-impregnated biochar (1081 $m^2$/g). The performance of the biochar activated with different activating agents, such as $H_3PO_4$ and $ZnCl_2$ was assessed by Heidari et al. [268]. In this study, the Eucalyptus wood was immersed into the $H_3PO_4$ (ratios of $H_3PO_4$: Eucalyptus wood = 1.5, 2.0, 2.5:1) or $ZnCl_2$ (ratios of $ZnCl_2$: Eucalyptus wood = 0.75, 1.5, 2.5:1) and then dried overnight. The Eucalyptus wood impregnated with $H_3PO_4$ was then carbonized at 450 ℃ for 1 h, whereas the ones impregnated with $ZnCl_2$ were subjected to the carbonization at 500 ℃ for 2 h. In addition to this, the effect of the multi-step activation using $H_3PO_4$ and KOH was also investigated, where the first activation step was carried out using $H_3PO_4$ followed by KOH activation at 900 ℃ for 1 h. As a result, the $CO_2$ adsorption capacity of the prepared activated biochars was in the following order: $H_3PO_4$ + KOH > $H_3PO_4$ > $ZnCl_2$. The biochar activated with $H_3PO_4$ and KOH exhibited a relatively high adsorption capacity of 180.40 mg/g at 30 ℃ and 1 bar compared to those activated using $H_3PO_4$ (mass ratio of 2.5) and $ZnCl_2$ (mass ratio of 2.5), which resulted in the $CO_2$ capture capacity of 82.72 and 58.96 mg/g, respectively. These findings were in line with the maximum BET surface area (2595 $m^2$/g) and micropore volume (1.236 $cm^3$/g) of the biochar developed using multi-step activation. According to their results, the use of KOH enhanced the $CO_2$ adsorption capacity of biochar by almost 2–3 times compared to those activated by $H_3PO_4$ and $ZnCl_2$ at mass ratio of 2.5. Therefore, the selection of appropriate activating agent, and the determination of optimum biomass/biochar: activating agent ratio is important to achieve a high $CO_2$ uptake capacity.

### 6.3 Physicochemical activation

Physicochemical activation is a combination of physical and chemical treatment. Table 7 shows a summary of physicochemically activated biochars used for $CO_2$ adsorption. Recently, a two-step treatment process, ultrasound irradiation-assisted amine functionalization, has been used as an advanced modification technique to modify biochar's surface area, porosity, and surface chemistry [276, 277]. The oxygen

functional groups (i.e., hydroxyl, carbonyl and epoxy) on the graphene oxide layers of biochar are very significant for $CO_2$ adsorption. However, the graphene oxide layers of pristine biochar remain inaccessible for interaction with $CO_2$ unless the biochar is exfoliated. By applying the ultrasound waves at a certain frequency, the graphitic layers of biochar could be exfoliated. Here, the exfoliated biochar has a higher surface area and availability of oxygen functionalities; therefore, it is more likely to interact with $CO_2$. The waves can also open up the clogged pore and prevents the agglomeration of the graphitic sheet by cleaning the surface of biochar. In addition, the cavitation effect induced by ultrasound leads to the generation of more micropores and, at the same time, reduces the pore blockage by removing the lumps from the biochar structure after pyrolysis [277]. A scheme of the mechanism of action of microwave on biochar and its effect on size reduction is presented in Fig. 13 [278].

In a study conducted by Chatterjee et al. [279] on the effect of ultrasonication as a physical treatment on the $CO_2$ adsorption capacity of biochar, an enhancement in micropore surface area from 312.3 to 354 $m^2/g$ after 30 s of sonication at the frequency of 20 kHz was observed. The authors discussed during cavitation, the formation of microjet impinges on and penetrates through biochar's surface; this phenomenon creates more micropores and removes the pore blockage, thus increasing the micropore surface area. However, prolonging the sonication duration to 1 min reduced the micropore surface area to 268.82 $m^2/g$. It was discussed that the intensity of cavitation increased as the sonication duration increased and disrupted the ordered graphitic layer in biochar, which led to pore-clogging. Advantageously, this treatment can be performed at near room temperature for a short while, less than 1 min, which is beneficial for cost and energy saving compared to $CO_2$ and steam activation methods. Furthermore, ultrasound irradiation can be a techno-economic method applied to large-scale processes without releasing pollutant gases [280].

In an ongoing study, Chatterjee et al. [281] attempted to apply a two-step process to develop biochar with high microporosity and surface area for high $CO_2$ adsorption. Pinewood-derived biochar was first sonicated for 30 s at ambient temperature, named sono-biochar. In the second step, the sono-biochar was functionalized with five different amines: (i) monoethanolamine (MEA), (ii) diethanolamine (DEA), (iii) piperazine (PZ), (iv) polyethylenimine (PEI), and (v) tetraethylenepentamine (TEPA) and their binary (MEA-TEPA), (DEA-TEPA), (DEA-PEI), (TEPA-PEI) and ternary (DEA-TEPA-PEI) mixtures. Here, sono-biochar, after the incorporation of amine, was known sono-aminated biochar. Finally, all the prepared sono-aminated biochars were activated using two activating agents, namely N-(3-dimethylaminopropyl)-N-ethylcarbodiimide hydrochlo-ride-1-hydroxy benzotri-azole (EDC-HOBt) and KOH. Among the single amines, TEPA led to a $CO_2$ sorption capacity of 89.76 mg/g followed by MEA (76.56 mg/g), both activated using EDC-HOBt, which were considerably higher compared to that of raw biochar (13.2 mg/g). It was reported that MEA-functionalized biochar demonstrated a micropore volume of 0.12 $cm^3/g$ and surface area of 374.66 $m^2/g$. However, TEPA-functionalized biochar showed lower micropore volume and surface area of 0.09 $cm^3/g$ and 261.68 $m^2/g$, respectively. Thus, it can be concluded that the synergetic effect of ultrasound-assisted amination was pronounced in the enhancement of $CO_2$ adsorption capacity of TEPA-functionalized biochar, while in the case of MEA-functionalized biochar, physisorption was dominant. Chatterjee et al. [279] proposed a three-step mechanism for TEPA functionalization of biochar, as depicted in Fig. 14. Firstly, the -COOH group of biochar needed to be activated to react with the amine group. Here, EDC as a coupling agent activated the -COOH group and generated O-acylisourea as an intermediate, followed by a nucleophilic reaction from the amino group. This reaction led to amide production and generated iso-urea as a by-product. Besides, the N-acyl urea could be produced during side reaction on O-N migration of the -COOH group. For the second step, selecting suitable additive such as HOBt was necessary to prevent the formation of these by-products and enhance the product yield. Advantageously, urea is soluble in water, and the filtration process could easily separate the unreacted reagent from its product. In the last step (step 3), the epoxy group's interaction with TEPA formed TEPA-functionalized biochar.

In the study of Chatterjee et al. [281], among the blended mixture, the MEA-TEPA-functionalized biochar activated with EDC-HOBt demonstrated the highest $CO_2$ sorption capacity of 84.04 mg/g with a high micropore volume (0.12 $cm^3/g$) and surface area (375.12 $m^2/g$) among the other mixtures. This result was in line with the highest intensity ratio ($I_D/I_G$) of 0.95 obtained from the Raman analysis, confirming that more distortion was introduced to the biochar surface from dual amination using MEA-TEPA, which provided a beneficial combination for $CO_2$ adsorption. For KOH activation, MEA-functionalized biochar exhibited the highest $CO_2$ uptake of 71.68 mg/g. In comparison, the sorption capacity was lower than the corresponding sample activated by EDC-HOBt (76.56 mg/g). Here, the strong base reaction onto the biochar surface reduced the micropore volume from 0.12 to 0.09 $cm^3/g$, and thus reduced the reaction site for $CO_2$ adsorption from surface destruction. Therefore, it is important to use the appropriate amine and activating agent, as both factors contribute to the generation of micropores that influence the efficiency of adsorbent for $CO_2$ uptake.

In another investigation undertaken by Chatterjee et al. [136], various feedstocks, such as miscanthus switchgrass, corn stover and sugarcane bagasse, were subjected to pyrolysis (500, 600, 700 and 800 ℃) and then low-frequency

**Table 7** Effect of physicochemical activation and operating conditions on the $CO_2$ adsorption capacity of biochar

| Feedstock | Pyrolysis temperature (℃) | Type of modification | Activation condition | Activation temperature (℃) | Activation time (min) | Power level (W) | Adsorption condition | | $CO_2$ concentration (%) | $CO_2$ adsorption capacity (mg/g) | Reference |
|---|---|---|---|---|---|---|---|---|---|---|---|
| | | | | | | | Temperature (℃) | Pressure (bar) | | | |
| Pinewood | 550–600 | Ultrasound-assisted amination | Pristine | | | | 70 | 0.15 | 10 | 13.20 | [279] |
| | | | EDC:HOBt (1:1) suspended in TEPA | | 0.5 | 475 | 70 | 0.15 | 10 | 24.20 | |
| | | | | | 1 | 475 | 70 | 0.15 | 10 | 74.36 | |
| | | | | | 3 | 475 | 70 | 0.15 | 10 | 34.32 | |
| | | | | | 0.5 | 700 | 70 | 0.15 | 10 | 30.36 | |
| | | | | | 0.5 | 700 | 25 | 0.15 | 10 | 58.08 | |
| | | | | | 0.5 | 700 | 50 | 0.15 | 10 | 65.12 | |
| | | | | | 0.5 | 700 | 70 | 0.15 | 10 | 89.76 | |
| | | | | | 0.5 | 700 | 70 | 0.15 | 13 | 101.64 | |
| | | | | | 0.5 | 700 | 70 | 0.15 | 15 | 122.76 | |
| | | | | | 0.5 | 700 | 90 | 0.15 | 10 | 48.40 | |
| | | | | | 1 | 700 | 70 | 0.15 | 10 | 76.12 | |
| | | | | | 3 | 700 | 70 | 0.15 | 10 | 69.52 | |
| Pinewood | 550–600 | Ultrasound-assisted amination | EDC:HOBt (1:1) suspended in MEA | | 0.5 | 475 | 70 | 0.1 | 10 | 76.56 | [281] |
| | | | EDC:HOBt (1:1) suspended in PZ | | 0.5 | 475 | 70 | 0.1 | 10 | 44.88 | |
| | | | EDC:HOBt (1:1) suspended in DEA | | 0.5 | 475 | 70 | 0.1 | 10 | 46.20 | |
| | | | EDC:HOBt (1:1) suspended in PEI | | 0.5 | 475 | 70 | 0.1 | 10 | 44.88 | |
| | | | EDC:HOBt (1:1) suspended in MEA-TEPA | | 3 | 700 | 70 | 0.1 | 10 | 84.04 | |
| | | | EDC:HOBt (1:1) suspended in DEA-TEPA | | 0.5 | 475 | 70 | 0.1 | 10 | 47.52 | |
| | | | EDC: OBt (1:1) suspended in DEA-PEI | | 0.5 | 475 | 70 | 0.1 | 10 | 47.52 | |
| | | | EDC:HOBt (1:1) suspended in TEPA-PEI | | 0.5 | 475 | 70 | 0.1 | 10 | 52.80 | |
| | | | EDC:HOBt (1:1) suspended in DEA-TEPA-PEI | | 0.5 | 475 | 70 | 0.1 | 10 | 52.80 | |
| | | | EDC:HOBt (1:1) suspended in MEA | | 0.5 | 475 | 70 | 0.1 | 10 | 71.68 | |

**Table 7** (continued)

| Feedstock | Pyrolysis temperature (℃) | Type of modification | Activation condition | Activation temperature (℃) | Activation time (min) | Power level (W) | Adsorption condition | | $CO_2$ concentration (%) | $CO_2$ adsorption capacity (mg/g) | Reference |
|---|---|---|---|---|---|---|---|---|---|---|---|
| | | | | | | | Temperature (℃) | Pressure (bar) | | | |
| Rice husk | 900 | $CO_2$ activation followed by impregnation with $K_2CO_3$ | 1) $CO_2$ activation<br>2) Refluxed with $K_2CO_3$ solution | 1) 900<br>2) 100 | 60 | | 20 | 1 | 100 | ~154 | [282] |
| | | | | | | | 25 | 1 | 100 | ~136.4 | |
| | | | | | | | 30 | 1 | 100 | ~121 | |
| | | | | | | | 25 | 1 | 20 | ~55 | |
| | | | | | | | 25 | 1 | 50 | ~88 | |
| | | | | | | | 25 | 1 | 100 | ~132 | |
| Soybean straw | 500 | $CO_2$-$NH_3$ mixture | Heated under $N_2$ until it reached the pre-set temperature, followed by activation using $CO_2$-$NH_3$ (20% $CO_2$ and 16% $NH_3$) | 500 | 30 | | 30 | 1 | 10 | ~58 | [200] |
| | | | | 500 | 30 | | 120 | 1 | 10 | ~32 | |
| | | | | 600 | 30 | | 30 | 1 | 10 | ~62 | |
| | | | | 600 | 30 | | 120 | 1 | 10 | ~36 | |
| | | | | 700 | 30 | | 30 | 1 | 10 | ~68 | |
| | | | | 700 | 30 | | 120 | 1 | 10 | ~41 | |
| | | | | 800 | 30 | | 30 | 1 | 10 | ~90 | |
| | | | | 800 | 30 | | 120 | 1 | 10 | ~50 | |
| | | | | 900 | 30 | | 30 | 1 | 10 | ~83 | |
| | | | | 900 | 30 | | 120 | 1 | 10 | ~41 | |
| Wood chips | Gasification | KOH + $CO_2$ activation | 1) Impregnation at KOH/ biomass ratio of 1:1<br>2) $CO_2$ activation | 550 | 60 | | 30 | 1 | 100 | 113.96 | [283] |
| Wood chips + chicken manure | | | | 550 | 60 | | 30 | 1 | 100 | 107.36 | |
| Olive oil waste | Hydrothermal carbonization at 350 ℃ | Mixture of $ZnCl_2$ and pyrrole-2-carboxaldehyde + $CO_2$ activation | 1) Mixing with $ZnCl_2$ and pyrrole-2- carboxaldehyde<br>2) $CO_2$ activation | 700 | 60 | | 0 | 0.1 | 100 | 121.4 | [284] |
| | | | | 700 | 180 | | 0 | 0.1 | 100 | 97.24 | |

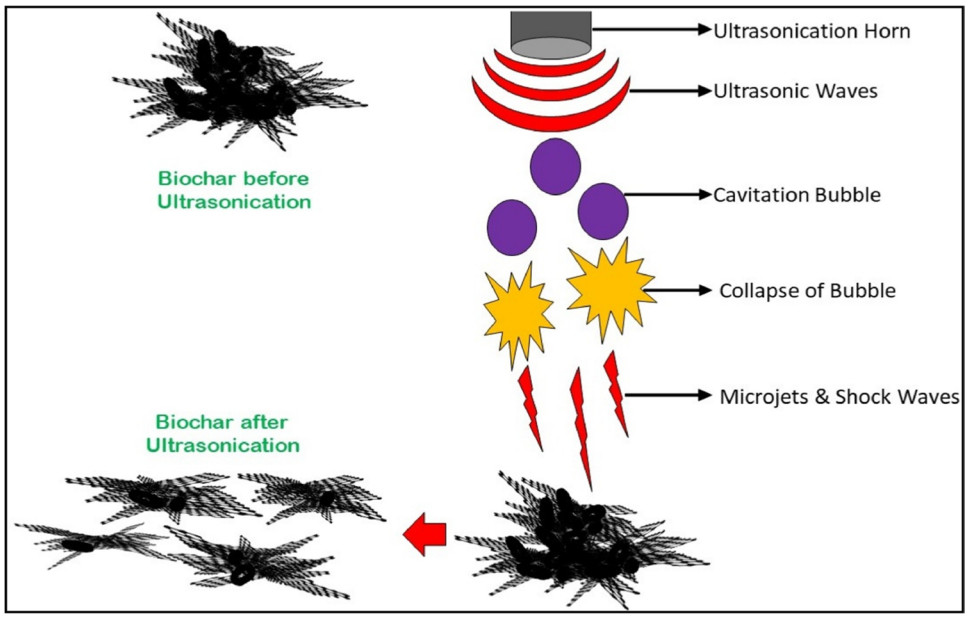


**Fig. 13** Schematic diagram showing the effect of ultrasonication on biochar structure. Adapted with permission from [278]

acoustic treatment and amine functionalization for $CO_2$ adsorption. The SEM images of raw biochar portrayed a non-porous structure, while the creation or opening of new microporous can be observed on sono-activated biochar due to structural degradation (Fig. 15). As can be seen, the structure of all biochars was irregular, rough and bundle like. During pyrolysis at 700 ℃, these structures tend to disrupt and crack, thus releasing volatile matter. In this regard, miscanthus showed the highest micropore volume (0.15 $cm^3/g$) and surface area (324 $m^2/g$) among the prepared biochars pyrolyzed at 700 ℃. Accordingly, the micropore volume and surface area of this biochar increased to 0.21 $cm^3/g$ and 532 $m^2/g$, respectively, after 30 s of ultrasonication. In $CO_2$ adsorption studies, miscanthus-derived biochar synthesised at 700 ℃ and sono-activated biochar presented superior adsorption capacity of 40.92 and 127.16 mg/g, respectively, among the corresponding samples.

In summary, various modification methods affect the physicochemical properties of biochar in their own ways to enhance the $CO_2$ adsorption capacity. In the physical modification, $CO_2$ activation is more likely to generate micropores in biochar, whereas steam activation contributes to developing a wider range of pores, including mesopores and micropores. In the chemical activation, the use of different activating agents introduces various functional groups, such as O- and N-containing functional groups, on the biochar surface to facilitate $CO_2$ adsorption. Most chemical modification techniques aim to produce biochar with basic characteristics favourable for the interaction with $CO_2$ acidic gas. Here, the impregnation of biochar with metal salts solutions such as magnesium, aluminium, iron (III) and calcium increases the surface basicity of biochar, while the introduction of amino groups, especially amine, into biochar increases the N-containing functional groups. Other than that, the introduction of O-containing functional groups on the biochar surface from the alkali modification helps to increase the biochar's surface basicity. Among the alkaline activators, KOH is widely used in the activation process. In the acid modification, $ZnCl_2$ and $H_3PO_4$ play a role as a dehydration agents to initiate pore formation during the cross-linking reaction on the carbon structure. Most recently, the physicochemical activation by ultrasound-assisted amination has gained the attention of researchers to boost the adsorption of $CO_2$. In this method, ultrasound irradiation exfoliates the graphitic layers of biochar, and the following amine-functionalization facilitates $CO_2$ adsorption. Therefore, it is important to apply a suitable modification technique to enhance the $CO_2$ uptake. In modifying the physicochemical properties of biochar, it is also important to consider the cost and environmental impacts so that high-capacity biochar can be developed under optimum process conditions.

## 7 Selectivity towards $CO_2$

Selectivity is one of the indicators in determining the successful development of modified biochar to adsorb $CO_2$. High selectivity highlights the ability of biochar to separate $CO_2$ from gas mixtures. In this context, a suitable modification method should be implemented on the biochar surface to produce biochar with high adsorption capacity and selectivity towards $CO_2$. In the selectivity study conducted by Zubbri et al. [20], the magnesium nitrate loaded-biochar revealed an excellent selectivity towards $CO_2$ compared to other gases with a $CO_2$ uptake of 76.78 mg/g, which

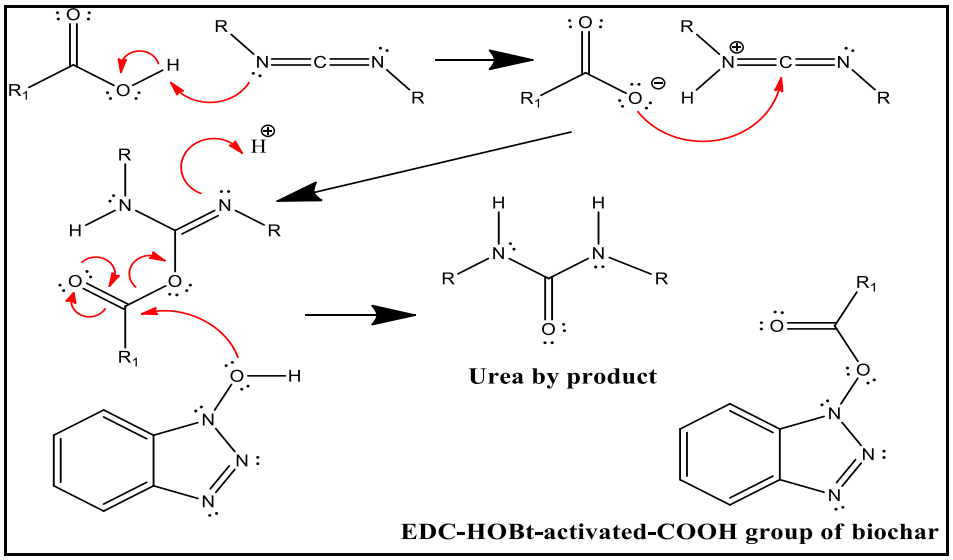


Step 1

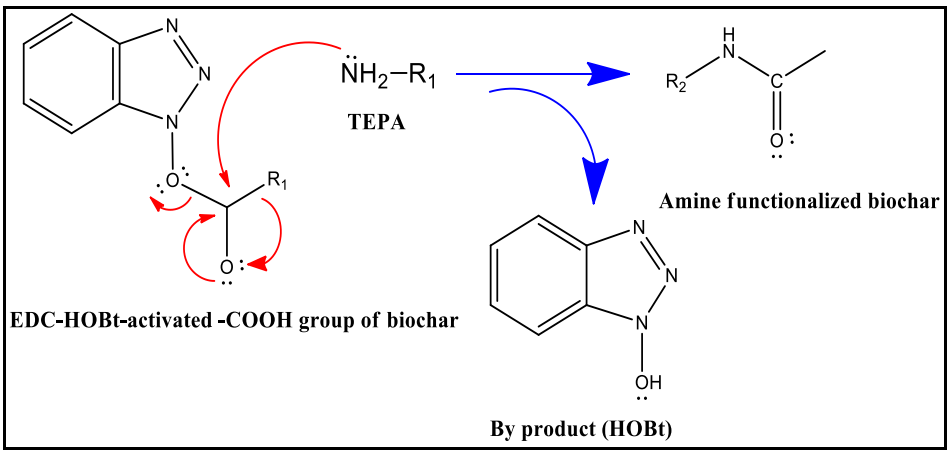


Step 2

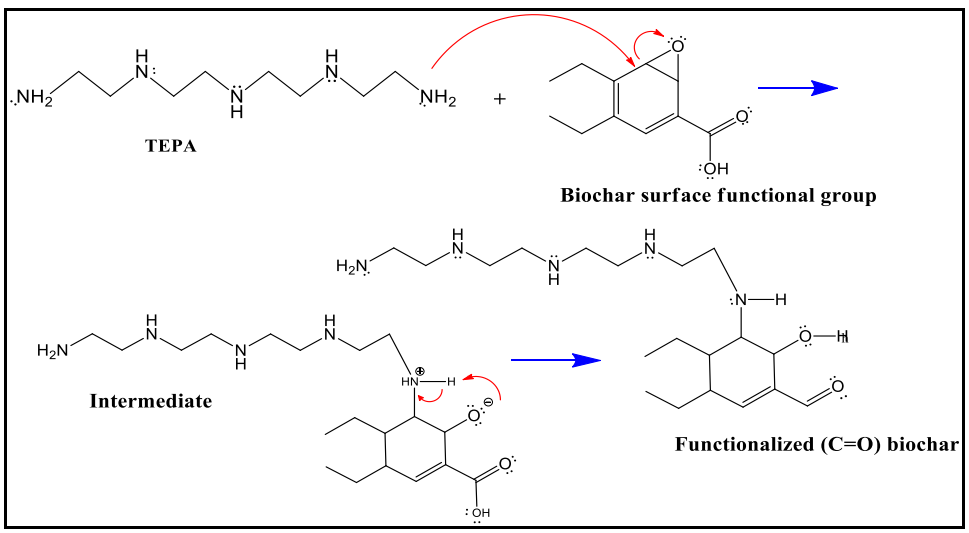


Step 3

**Fig. 14** Overall mechanism of TEPA functionalization of biochar. Adapted with permission from [279]. **Step 1** Mechanism of EDC-HOBt coupling with -COOH group of biochar**. Step 2** Mechanism of TEPA functionalization of the activated carbonyl group of biochar**. Step 3** Mechanism of TEPA functionalization of activated carbonyl group of biochar

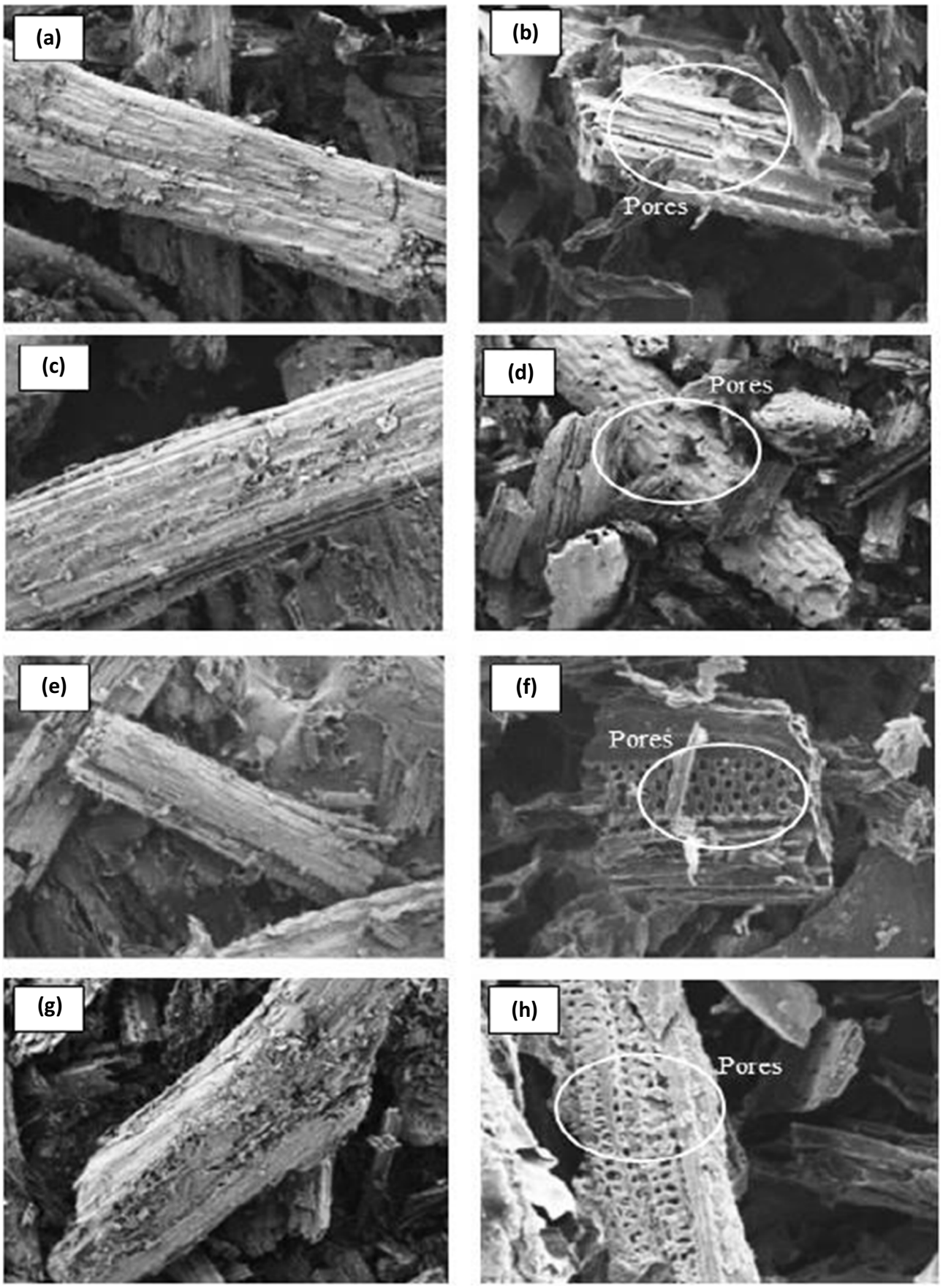
(a)
(b)
Pores
(c)
(d)
Pores
(e)
(f)
Pores
(g)
(h)
Pores

◂**Fig. 15** SEM images of (**a**) raw miscanthus, (**b**) ultrasonicated miscanthus biochar, (**c**) raw switchgrass, (**d**) ultrasonicated switchgrass biochar, (**e**) raw corn stover, (**f**) ultrasonicated corn stover biochar, (**g**) raw sugarcane bagasse and (**h**) ultrasonicated sugarcane bagasse biochar; all biochars were pyrolyzed at 700 °C. Adapted from [136] under the copyright of RSC license (CC-BY 4.0)

was considerably higher than those obtained for other gases such as air (8.11 mg/g), $N_2$ (3.76 mg/g) and $CH_4$ (1.93 mg/g) at 30 ℃ and 1 atm. It was discussed that the selectivity of biochar towards $CO_2$ depends on the polarizability and quadrupole moment of $CO_2$ molecules. $CO_2$ has greater polarizability ($29.1 \times 10^{25}$ $cm^2$) over other gases ($CH_4 = 25.9.1 \times 10^{25}$ $cm^2$, $N_2 = 17.4 \times 10^{25}$ $cm^2$, and $O_2 = 15.8 \times 10^{25}$ $cm^2$) [285, 286], and this greater polarizability of $CO_2$ facilitates the adsorbent-adsorbate interaction. Other than that, the higher quadrupole moment of $CO_2$ molecules ($14.3 \times 10^{-40}$ C $m^2$) compared to other gases such as $CH_4$ (0 C $m^2$), $N_2$ ($4.72 \times 10^{-40}$ C $m^2$) and $O_2$ ($1.03 \times 10^{-40}$ C $m^2$) [287] justifies the stronger affinity of $CO_2$ towards the biochar surface. In another study, Lahijani et al. [117] observed a high selectivity towards $CO_2$ over other gases on walnut shell-derived metal-loaded biochar. Accordingly, the adsorbent exhibited superior adsorption performance towards $CO_2$ (80.0 mg/g) over $CH_4$ (8.75 mg/g), $O_2$ (3.25 mg/g) and $N_2$ (3.24 mg/g). Recently, Zubbri et al. [87] modified hydrochar, obtained from hydrothermal carbonization of biomass using KOH and the resultant biochar showed excellent adsorption performance towards $CO_2$ with a sorption capacity of 122.37 mg/g. However, the sorbent adsorbed the other gases in a small amount with the sequence of air (7.03 mg/g) > $N_2$ (3.09 mg/g) > $CH_4$ (1.93 mg/g).

## 8 Reusability of biochar

Apart from high adsorption ability, an efficient adsorbent must have a good and stable adsorption performance in regeneration. Reusability of biochar in the operations is crucial when selecting a good adsorbent for $CO_2$ capture, especially for large-scale applications. Zubbri et al. [20] showed the stable performance of MgO-loaded rambutan peel-derived biochar after 25 cycles of $CO_2$ adsorption–desorption (30 and 110 ℃, respectively). In another study, Zubbri et al. [87] modified the rambutan peel-derived hydrochar with KOH. The developed adsorbent exhibited stable performance within 10 cycles of adsorption–desorption at previous conditions. Lahijani et al. [117] reported an insignificant loss in $CO_2$ adsorption capacity of Mg-loaded walnut shell-derived biochar after 10 cycles of adsorption at 30 ℃ and desorption at 110 ℃. In a study conducted by Cao et al. [288], it was shown that pine wood, hickory wood, wheat straw, walnut shell, corn stalk, soybean straw and rape straw-derived biochars presented excellent reusability, where all the adsorbents could recover up to 90% of the adsorption capacity within 10 cycles of adsorption–desorption. However, Shahkarami et al. [226] reported that $CO_2$ adsorption capacity of steam activated biochar derived from whitewood started to diminish after 20 cycles, indicating that steam-activated biochar may not preserve a sustainable performance in multi-cycle of $CO_2$ adsorption–desorption.

$CO_2$ adsorption on the pristine biochar surface is physical adsorption involving weak intermolecular forces (van der Waals forces). This physisorption interaction does not require a major change in the electronic orbital arrangement for each species due to the weak intermolecular interactions [289]. Therefore, $CO_2$ (adsorbate) tends to move freely over the adsorbent surface, where a minimal amount of energy is necessary to break the weak interactions. However, in amine-functionalized biochar, where chemisorption takes place, $CO_2$ molecules would be chemically bonded to the amine functionalities on the biochar surface by forming carbamate through a strong covalent bond and occupying the appropriate adsorption sites [289]. Hence, the energy required to desorb $CO_2$ from the amino-modified biochar is higher than that of pristine biochar. During the desorption process, the presence of orbital overlap and charge transfer makes it difficult to remove carbamates from the adsorbent [290, 291]. This condition resulted in a low generation value of amine-functionalized biochar after several cycles of $CO_2$ adsorption–desorption [175, 240, 261]. Yaumi et al. [175] reported a reduction of 8.8% in the $CO_2$ adsorption capacity of melamine-modified biochar developed from rice husk after 12 cycles of $CO_2$ adsorption–desorption at 30 and 110 ℃, respectively. It was discussed that the reduction in the adsorption capacity was due to the fact that the chemically bonded $CO_2$ molecules on the biochar surface were not completely released during the desorption process. This finding was in agreement with the reports of Li et al. [261], who produced biochar from a mixture of sewage sludge and pine sawdust. The resultant biochars were then activated using KOH at different activation temperatures (600,700 and 800 ℃). The biochars activated at 700 and 800 ℃ exhibited slight reductions of 3 and 2%, respectively, after 10 cycles of the cyclic test. Overall, from the technical and economic viewpoints, a stable adsorbent with high $CO_2$ capture capacity and sustainable performance in multi-cycle adsorption–desorption is required to ensure the viability of the adsorption process.

## 9 Challenges in using biochar as $CO_2$ adsorbent

Biochar as a sustainable and relatively low-cost $CO_2$ adsorbent has gained attention for $CO_2$ removal over the past years. However, despite all the claimed advantages, there are still several challenges related to the large-scale application of biochar as the $CO_2$ adsorbent.

First, the regeneration characteristic of $CO_2$ adsorbent after using a few times at a specific adsorption–desorption temperature is important for economic efficiency determination. Therefore, it is necessary to understand the regeneration principles, including the disposal of biochar. Nguyen and Lee [275] experienced a reduction of 12% in $CO_2$ adsorption capacity after 10 cycles for nitrogen-doped biochar. Ding and Liu [262] found that the $CO_2$ adsorption capacity for *Sargassum* and *Enteromorpha* seaweed-derived biochars decreased 15 and 13%, respectively, after 10 cycles. Bamdad et al. [240] showed that the regeneration capacity of nitrogen-functionalized biochar derived from sawmill residue decreased in the range of 4–8% after 5 cycles and by 20% after 10 cycles. Although such regeneration capacity might be reasonable and satisfactory for research studies, biochar's capability as a carbon sequestering material may be rendered by a large reduction in adsorption capacity after several cycles of $CO_2$ uptake and release, especially at large-scale operations. Hence, developing more sustainable and robust biochar-based adsorbents should be considered in future studies.

Secondly, the performance of some developed biochar after certain modifications is still questionable and not fully demonstrated. For sure, high adsorption capacity at ambient temperature is desirable to guarantee the practicability of the proposed modification method in a large-scale application. Nevertheless, some studies reported that their adsorption capacity increased when higher adsorption temperatures (for example 70 °C) were applied [279]. From a large-scale perspective, high adsorption temperature implies huge energy consumption for the desorption process. Hence the modification mechanism and its effect on the adsorbent performance should be fully understood to avoid producing biochar that favours high adsorption temperature.

Thirdly, the availability of biomass feedstocks in huge amounts should be taken into account to produce biochar for large-scale operations. The usage of seasonal crop residues such as paddy straw, paddy husk, wheat straw, etc., might be an issue as these types of feedstocks are not readily available throughout the year. Other than that, several biomass materials might not be suitable for the massive production of biochar. For example, tamarind seeds, orange peels and sunflower seed shells might only be consumed on a small scale at the respective period of time. With the variety of biomass feedstocks throughout the world, selecting a suitable source is important to ensure its availability at a low cost.

## 10 Conclusions

In this review, the adsorption of $CO_2$ on several modified biochars was reviewed and discussed. The literature survey indicates that the $CO_2$ adsorption is significantly affected by biochar's surface area and microporosity and its surface functional groups. In this regard, operating conditions such as pyrolysis temperature, holding time and heating rate play a vital role in developing highly microporous biochar. Additionally, the basicity of the biochar surface has fundamental impacts on the adsorption of acidic $CO_2$ molecules through acid–base interaction. Based on the literature survey, a combination of physical and chemical activation is beneficial in enhancing the $CO_2$ uptake capacity of biochar. This needs a careful determination of the optimum process condition and suitable activating agents. Therefore, future research should focus on the physicochemical treatment methods to obtain microporous biochar with enriched surface functionality to achieve a high $CO_2$ adsorption capacity. In addition, a deep understanding of $CO_2$ adsorption mechanism is crucial in dealing with various modification techniques. Comprehensive studies on the resistance to impurities (such as $H_2S$ as a co-occurring acidic component in biogas), long-term stability as well as cost considerations are required to ensure the successful exploitation of biochar for $CO_2$ adsorption at large-scale operations.

**Acknowledgements** This work has been funded by the Ministry of Education of Malaysia and Universiti Sains Malaysia under FRGS with Project Code: FRGS/1/2019/TK02/USM/01/3. The authors would like to thank Universiti Malaysia Perlis (UniMAP) for the scholarship granted to the first author.

**Authors contributions** Literature review and drafting the original manuscript: Nuradibah Mohd Amer; Critical revision and supervision: Pooya Lahijani; Writing-review and editing: Maedeh Mohammadi; Funding acquisition and review: Abdul Rahman Mohammad.

## Declarations

**Conflict of Interest** The authors declare that they have no conflict of interest.

## References


1. Bose BK (2010) Global warming: Energy, environmental pollution, and the impact of power electronics. IEEE Ind Electron Mag 4:6–17. https://doi.org/10.1109/MIE.2010.935860
2. Vaz S, Paula A, De SR, Eduardo B, Baeta L (2022) Technologies for carbon dioxide capture : A review applied to energy sectors. Clean Eng Technol 8:100456. https://doi.org/10.1016/j.clet.2022.100456
3. (1997) Kyoto Protocol. https://unfccc.int/kyoto_protocol. 13/03/2022. Accessed 13 March 2022.
4. (2015) Paris Agreement. https://unfccc.int/process-and-meetings/the-paris-. 13/03/2022. Accessed 13 March 2022.
5. Gielen D, Boshell F, Saygin D, Bazilian MD, Wagner N, Gorini R (2019) The role of renewable energy in the global energy transformation. Energy Strateg Rev 24:38–50. https://doi.org/10.1016/j.esr.2019.01.006
6. Beiyuan J, Awad YM, Beckers F, Tsang DCW, Ok YS, Rinklebe J (2017) Mobility and phytoavailability of As and Pb in a contaminated soil using pine sawdust biochar under systematic change of redox conditions. Chemosphere 178:110–118. https://doi.org/10.1016/j.chemosphere.2017.03.022
7. Yaumi AL, Bakar MZA, Hameed BH (2017) Recent advances in functionalized composite solid materials for carbon dioxide capture. Energy 124:461–480. https://doi.org/10.1016/j.energy.2017.02.053
8. Lee SY, Park SJ (2015) A review on solid adsorbents for carbon dioxide capture. J Ind Eng Chem 23:1–11. https://doi.org/10.1016/j.jiec.2014.09.001
9. Creamer AE, Gao B (2016) Carbon-based adsorbents for post-combustion $CO_2$ capture: A critical review. Environ Sci Technol 50:7276–7289. https://doi.org/10.1021/acs.est.6b00627
10. Hwang KJ, Choi WS, Jung SH, Kwon YJ, Hong S, Choi C, Lee JW, Shim WG (2018) Synthesis of zeolitic material from basalt rock and its adsorption properties for carbon dioxide. RSC Adv 8:9524–9529. https://doi.org/10.1039/c8ra00788h
11. Ibrahim GH, Al-Meshragi AM (2020) Experimental study of adsorption on activated carbon for $CO_2$ capture. In: L. A. Frazão, A. M. Silva-Olaya & JCS (ed) $CO_2$ Sequestration. IntechOpen, pp 1–20
12. Wang J, Huang H, Wang M, Yao L, Qiao W, Long D, Ling L (2015) Direct capture of low-concentration $CO_2$ on mesoporous carbon-supported solid amine adsorbents at ambient temperature. Ind Eng Chem Res 54:5319–5327. https://doi.org/10.1021/acs.iecr.5b01060
13. Songolzadeh M, Soleimani M, Takht Ravanchi M, Songolzadeh R (2014) Carbon dioxide separation from flue gases: A technological review emphasizing reduction in greenhouse gas emissions. Sci World J 2014:828131. https://doi.org/10.1155/2014/828131
14. Shao J, Zhang J, Zhang X, Feng Y, Zhang H, Zhang S, Chen H (2018) Enhance $SO_2$ adsorption performance of biochar modified by $CO_2$ activation and amine impregnation. Fuel 224:138–146. https://doi.org/10.1016/j.fuel.2018.03.064
15. Pang S (2019) Advances in thermochemical conversion of woody biomass to energy, fuels and chemicals. Biotechnol Adv 37:589–597. https://doi.org/10.1016/j.biotechadv.2018.11.004
16. Lin Y, Ma X, Peng X, Yu Z, Fang S, Lin Y, Fan Y (2016) Combustion, pyrolysis and char $CO_2$-gasification characteristics of hydrothermal carbonization solid fuel from municipal solid wastes. Fuel 181:905–915. https://doi.org/10.1016/j.fuel.2016.05.031
17. Papageorgiou A, Azzi ES, Enell A, Sundberg C (2021) Biochar produced from wood waste for soil remediation in Sweden: Carbon sequestration and other environmental impacts. Sci Total Environ 776:145953. https://doi.org/10.1016/j.scitotenv.2021.145953
18. Han T (2020) Properties of biochar from wood and textile. IOP Conf Ser Earth Environ Sci 546:042060. https://doi.org/10.1088/1755-1315/546/4/042060
19. Manyà JJ, González B, Azuara M, Arner G (2018) Ultra-microporous adsorbents prepared from vine shoots-derived biochar with high $CO_2$ uptake and $CO_2/N_2$ selectivity. Chem Eng J 345:631–639. https://doi.org/10.1016/j.cej.2018.01.092
20. Zubbri NA, Mohamed AR, Kamiuchi N, Mohammadi M (2020) Enhancement of $CO_2$ adsorption on biochar sorbent modified by metal incorporation. Environ Sci Pollut Res 27:11809–11829. https://doi.org/10.1007/s11356-020-07734-3
21. Zhang X, Zhang S, Yang H, Shao J, Chen Y, Feng Y, Wang X, Chen H (2015) Effects of hydrofluoric acid pre-deashing of rice husk on physicochemical properties and $CO_2$ adsorption performance of nitrogen-enriched biochar. Energy 91:903–910. https://doi.org/10.1016/j.energy.2015.08.028
22. Zhang J, Huang B, Chen L, Li Y, Li W, Luo Z (2018) Characteristics of biochar produced from yak manure at different pyrolysis temperatures and its effects on the yield and growth of highland barley. Chem Speciat Bioavailab 30:57–67. https://doi.org/10.1080/09542299.2018.1487774
23. Rehman A, Nawaz S, Alghamdi HA, Alrumman S, Yan W, Nawaz MZ (2020) Effects of manure-based biochar on uptake of nutrients and water holding capacity of different types of soils. Case Stud Chem Environ Eng 2:100036. https://doi.org/10.1016/j.cscee.2020.100036
24. Bong CPC, Lim LY, Lee CT, Ong PY, Klemeš JJ, Li C, Gao Y (2020) Lignocellulosic biomass and food waste for biochar production and application: A review. Chem Eng Trans 81:427–432. https://doi.org/10.3303/CET2081072
25. Igalavithana AD, Choi SW, Dissanayake PD et al (2020) Gasification biochar from biowaste (food waste and wood waste) for effective $CO_2$ adsorption. J Hazard Mater 391:121147. https://doi.org/10.1016/j.jhazmat.2019.121147
26. Yue Y, Cui L, Lin Q, Li G, Zhao X (2017) Efficiency of sewage sludge biochar in improving urban soil properties and promoting grass growth. Chemosphere 173:551–556. https://doi.org/10.1016/j.chemosphere.2017.01.096
27. Racek J, Sevcik J, Chorazy T, Kucerik J, Hlavinek P (2020) Biochar – Recovery material from pyrolysis of sewage sludge: A review. Waste and Biomass Valorization 11:3677–3709. https://doi.org/10.1007/s12649-019-00679-w
28. Huang YF, Te SH, Te CP, Lo SL (2016) Co-torrefaction of sewage sludge and Leucaena by using microwave heating. Energy 116:1–7. https://doi.org/10.1016/j.energy.2016.09.102
29. Islam MS, Kwak JH, Nzediegwu C et al (2021) Biochar heavy metal removal in aqueous solution depends on feedstock type and pyrolysis purging gas. Environ Pollut 281:117094. https://doi.org/10.1016/j.envpol.2021.117094
30. Wang X, Li X, Liu G, He Y, Chen C, Liu X, Li G, Gu Y, Zhao Y (2019) Mixed heavy metal removal from wastewater by using discarded mushroom-stick biochar: Adsorption properties and mechanisms. Environ Sci Process Impacts 21:584–592. https://doi.org/10.1039/c8em00457a
31. Deng Y, Li X, Ni F, Liu Q, Yang Y, Wang M, Ao T, Chen W (2021) Synthesis of magnesium modified biochar for removing copper, lead and cadmium in single and binary systems from aqueous solutions: Adsorption mechanism. Water (Switzerland) 13:599. https://doi.org/10.3390/w13050599
32. Liang M, Lu L, He H, Li J, Zhu Z, Zhu Y (2021) Applications of biochar and modified biochar in heavy metal contaminated soil: A descriptive review. Sustain 13:1–18. https://doi.org/10.3390/su132414041

33. Dai Y, Wang W, Lu L, Yan L, Yu D (2020) Utilization of biochar for the removal of nitrogen and phosphorus. J Clean Prod 257:120573. https://doi.org/10.1016/j.jclepro.2020.120573
34. Anthonysamy SI, Lahijani P, Mohammadi M, Mohamed AR (2021) Alkali-modified biochar as a sustainable adsorbent for the low-temperature uptake of nitric oxide. Int J Environ Sci Technol. https://doi.org/10.1007/s13762-021-03617-3
35. Azwan A, Rahman A, Alias AB, Jaffar NN, Amir MA, Ghani WAWAK (2019) Adsorption of hydrogen sulphide by commercialized Rice Husk Biochar (RHB) & Hydrogel Biochar Composite (RH-HBC). Int J Recent Technol Eng 8:6864–6870. https://doi.org/10.35940/ijrte.d5207.118419
36. Liu WJ, Jiang H, Yu HQ (2019) Emerging applications of biochar-based materials for energy storage and conversion. Energy Environ Sci 12:1751–1779. https://doi.org/10.1039/C9EE00206E
37. Lee J, Kim KH, Kwon EE (2017) Biochar as a Catalyst. Renew Sustain Energy Rev 77:70–79. https://doi.org/10.1016/j.rser.2017.04.002
38. Choi S, Drese JH, Jones CW (2009) Adsorbent materials for carbon dioxide capture from large anthropogenic point sources. Chemsuschem 2:796–854. https://doi.org/10.1002/cssc.200900036
39. Prauchner MJ, da Cunha Oliveira S, Rodríguez-Reinoso F (2020) Tailoring low-cost granular activated carbons intended for $CO_2$ adsorption. Front Chem 8:1–16. https://doi.org/10.3389/fchem.2020.581133
40. Jo K, Baek Y, Lee C, Yoon J (2019) Effect of hydrophilicity of activated carbon electrodes on desalination performance in membrane capacitive deionization. Appl Sci 9:5055. https://doi.org/10.3390/app9235055
41. Abd AA, Naji SZ, Hashim AS, Othman MR (2020) Carbon dioxide removal through physical adsorption using carbonaceous and non-carbonaceous adsorbents: A review. J Environ Chem Eng 8:104142. https://doi.org/10.1016/j.jece.2020.104142
42. Millward AR, Yaghi OM (2005) Metal-organic frameworks with exceptionally high capacity for storage of carbon dioxide at room temperature. J Am Chem Soc 127:17998. https://doi.org/10.1021/ja0570032
43. Yuan Z, Eden MR, Gani R (2016) Toward the development and deployment of large-scale carbon dioxide capture and conversion processes. Ind Eng Chem Res 55:3383–3419. https://doi.org/10.1021/acs.iecr.5b03277
44. Sun H, Wu C, Shen B, Zhang X, Zhang Y, Huang J (2018) Progress in the development and application of CaO-based adsorbents for $CO_2$ capture—a review. Mater Today Sustain 1–2:1–27. https://doi.org/10.1016/j.mtsust.2018.08.001
45. Zhang X, Gao B, Creamer AE, Cao C, Li Y (2017) Adsorption of VOCs onto engineered carbon materials: A review. J Hazard Mater 338:102–123. https://doi.org/10.1016/j.jhazmat.2017.05.013
46. Alhashimi HA, Aktas CB (2017) Life cycle environmental and economic performance of biochar compared with activated carbon: A meta-analysis. Resour Conserv Recycl 118:13–26. https://doi.org/10.1016/j.resconrec.2016.11.016
47. Shafawi AN, Mohamed AR, Lahijani P, Mohammadi M (2021) Recent advances in developing engineered biochar for $CO_2$ capture : An insight into the biochar modification approaches. J Environ Chem Eng 9:106869. https://doi.org/10.1016/j.jece.2021.106869
48. Dulanja P, You S, Deshani A et al (2020) Biochar-based adsorbents for carbon dioxide capture : A critical review. Renew Sustain Energy Rev 119:109582. https://doi.org/10.1016/j.rser.2019.109582
49. Leng L, Xiong Q, Yang L, Li H, Zhou Y, Zhang W, Jiang S, Li H, Huang H (2021) An overview on engineering the surface area and porosity of biochar. Sci Total Environ 763:144204. https://doi.org/10.1016/j.scitotenv.2020.144204
50. US Department of Energy (2015) Carbon dioxide capture for natural gas and industrial applications. Chapter 4: Advancing clean electric power technologies. https://www.energy.gov/sites/default/files/2015/12/f27/QTR2015-4D-Carbon-Dioxide-Capture-for-Natural-Gas-and-Industrial-Applications.pdf. Accessed 22 June 2022
51. United States Department of Energy (2017) Carbon capture opportunities for natural gas fired power systems. Washington DC, USA. https://www.energy.gov/sites/prod/files/2017/01/f34/Carbon%20Capture%20Opportunities%20for%20Natural%20Gas%20Fired%20Power%20Systems_0.pdf. Accessed 22 June 2022
52. Bains P, Psarras P, Wilcox J (2017) $CO_2$ capture from the industry sector. Prog Energy Combust Sci 63:146–172. https://doi.org/10.1016/j.pecs.2017.07.001
53. Kanniche M, Gros-Bonnivard R, Jaud P, Valle-Marcos J, Amann JM, Bouallou C (2010) Pre-combustion, post-combustion and oxy-combustion in thermal power plant for $CO_2$ capture. Appl Therm Eng 30:53–62. https://doi.org/10.1016/j.applthermaleng.2009.05.005
54. Carpenter SM, Long HA (2017) 13-Integration of carbon capture in IGCC systems. In: Wang T, Stiegel G (eds) Integrated Gasification Combined Cycle (IGCC) Technologies. Woodhead Publishing, pp 445–463
55. Blomen E, Hendriks C, Neele F (2009) Capture technologies: Improvements and promising developments. Energy Procedia 1:1505–1512. https://doi.org/10.1016/j.egypro.2009.01.197
56. Spigarelli BP, Kawatra SK (2013) Opportunities and challenges in carbon dioxide capture. J CO2 Util 1:69–87. https://doi.org/10.1016/j.jcou.2013.03.002
57. Padurean A, Cormos CC, Agachi PS (2012) Pre-combustion carbon dioxide capture by gas–liquid absorption for integrated gasification combined cycle power plants. Int J Greenh Gas Control 7:1–11. https://doi.org/10.1016/j.ijggc.2011.12.007
58. Weiss H (1988) Rectisol wash for purification of partial oxidation gases. Gas Sep Purif 2:171–176. https://doi.org/10.1016/0950-4214(88)80002-1
59. Osman AI, Hefny M, Abdel Maksoud MIA, Elgarahy AM, Rooney DW (2021) Recent advances in carbon capture storage and utilisation technologies: A review. Environ Chem Lett 19:797–849. https://doi.org/10.1007/s10311-020-01133-3
60. Chen S, Yu R, Soomro A, Xiang W (2019) Thermodynamic assessment and optimization of a pressurized fluidized bed oxy-fuel combustion power plant with $CO_2$ capture. Energy 175:445–455. https://doi.org/10.1016/j.energy.2019.03.090
61. Pandey, S. Gupta S, Tomar, A. Kumar, A (2010) Post combustion carbon capture technology. Natl Conf Eco Friendly Manuf Sustain Dev. GLA University Mathura, Paper No. 56
62. Moioli S, Nagy T, Langé S, Pellegrini LA, Mizsey P (2017) Simulation model evaluation of $CO_2$ capture by aqueous MEA scrubbing for heat requirement analyses. Energy Procedia 114:1558–1566. https://doi.org/10.1016/j.egypro.2017.03.1286
63. Makertihartha IGBN, Dharmawijaya PT, Zunita M, Wenten IG (2017) Post combustion $CO_2$ capture using zeolite membrane. AIP Conf Proc 1818https://doi.org/10.1063/1.4979941
64. Gonzalez-Garza D, Rivera-Tinoco R, Bouallou C (2009) Comparison of ammonia, monoethanolamine, diethanolamine and methyldiethanolamine solvents to reduce $CO_2$ greenhouse gas emissions. Chem Eng Trans 18:279–284. https://doi.org/10.3303/CET0918044
65. Valluri S, Kawatra SK (2021) Use of frothers to improve the absorption efficiency of dilute sodium carbonate slurry for post combustion $CO_2$ capture. Fuel Process Technol 212:106620. https://doi.org/10.1016/j.fuproc.2020.106620

66 Al-Sudani F (2020) Absorption of carbon dioxide into aqueous ammonia solution using blended promoters (MEA, MEA+PZ, PZ+ArgK, MEA+ArgK). Eng Technol J 38:1359–1372. https://doi.org/10.30684/etj.v38i9a.876

67. Huang HP, Shi Y, Li W, Chang SG (2001) Dual alkali approaches for the capture and separation of $CO_2$. Energy Fuels 15:263–268. https://doi.org/10.1021/ef0002400

68. Knuutila H, Svendsen HF, Anttila M (2009) $CO_2$ capture from coal-fired power plants based on sodium carbonate slurry; a systems feasibility and sensitivity study. Int J Greenh Gas Control 3:143–151. https://doi.org/10.1016/j.ijggc.2008.06.006

69. Zhao R, Zhao L, Wang S, Deng S, Li H, Yu Z (2018) Solar-assisted pressure-temperature swing adsorption for $CO_2$ capture: Effect of adsorbent materials. Sol Energy Mater Sol Cells 185:494–504. https://doi.org/10.1016/j.solmat.2018.06.004

70. Ammendola P, Raganati F, Chirone R, Miccio F (2020) Fixed bed adsorption as affected by thermodynamics and kinetics: Yellow tuff for $CO_2$ capture. Powder Technol 373:446–458. https://doi.org/10.1016/j.powtec.2020.06.075

71. Kishibayev KK, Serafin J, Tokpayev RR, Khavaza TN, Atchabarova AA, Abduakhytova DA, Ibraimov ZT, Sreńscek-Nazzal J (2021) Physical and chemical properties of activated carbon synthesized from plant wastes and shungite for $CO_2$ capture. J Environ Chem Eng 9:106798. https://doi.org/10.1016/j.jece.2021.106798

72. Serafin J, Sre´nscek-Nazzal J, Kami´nska A, Paszkiewicz O, Michalkiewicz B (2022) Management of surgical mask waste to activated carbons for $CO_2$ capture. J CO2 Util 59:101970. https://doi.org/10.1016/j.jcou.2022.101970

73. Voss C (2005) Applications of pressure swing adsorption technology. Adsorption 11:527–529. https://doi.org/10.1007/s10450-005-5979-3

74. Raganati F, Chirone R, Ammendola P (2020) $CO_2$ capture by temperature swing adsorption: Working capacity as affected by temperature and $CO_2$ Partial pressure. Ind Eng Chem Res 59:3593–3605. https://doi.org/10.1021/acs.iecr.9b04901

75. Majchrzak-Kucęba I, Sołtysik M (2020) The potential of biocarbon as $CO_2$ adsorbent in VPSA unit. J Therm Anal Calorim 142:267–273. https://doi.org/10.1007/s10973-020-09858-7

76. Dhoke C, Zaabout A, Cloete S, Amini S (2021) Review on reactor configurations for adsorption-based $CO_2$ capture. Ind Eng Chem Res 60:3779–3798. https://doi.org/10.1021/acs.iecr.0c04547

77. Pires JCM, Martins FG, Alvim-Ferraz MCM, Simões M (2011) Recent developments on carbon capture and storage: An overview. Chem Eng Res Des 89:1446–1460. https://doi.org/10.1016/j.cherd.2011.01.028

78. Lei L, Bai L, Lindbråthen A, Pan F, Zhang X, He X (2020) Carbon membranes for $CO_2$ removal: Status and perspectives from materials to processes. Chem Eng J 401:126084. https://doi.org/10.1016/j.cej.2020.126084

79. Wang Y, Zhao L, Otto A, Robinius M, Stolten D (2017) A review of post-combustion $CO_2$ capture technologies from coal-fired power plants. Energy Procedia 114:650–665. https://doi.org/10.1016/j.egypro.2017.03.1209

80. Karimi M, Shirzad M, Silva JAC, Rodrigues AE (2022) Biomass/Biochar carbon materials for $CO_2$ capture and sequestration by cyclic adsorption processes: A review and prospects for future directions. J $CO_2$ Util 57:. https://doi.org/10.1016/j.jcou.2022.101890

81. Lai JY, Ngu LH (2021) A review of $CO_2$ adsorbents performance for different carbon capture technology processes conditions. Greenh Gas Sci Technol 0:1–41. https://doi.org/10.1002/ghg.2112

82. Ullah R, Salah AH, Saad M, Aparicio S, Atilhan M (2018) Adsorption equilibrium studies of $CO_2$, $CH_4$ and $N_2$on various modified zeolites at high pressures up to 200 bars. Microporous Mesoporous Mater 262:49–58. https://doi.org/10.1016/j.micromeso.2017.11.022

83. Bae JS, Bhatia SK (2006) High-pressure adsorption of methane and carbon dioxide on coal. Energy Fuels 20:2599–2607. https://doi.org/10.1021/ef060318y

84. Ao W, Fu J, Mao X et al (2018) Microwave assisted preparation of activated carbon from biomass: A review. Renew Sustain Energy Rev 92:958–979. https://doi.org/10.1016/j.rser.2018.04.051

85. Madzaki H, Ghani WAWAK, Rebitanim NZ, Alias AB (2016) Carbon Dioxide Adsorption on Sawdust Biochar. Procedia Eng 148:718–725. https://doi.org/10.1016/j.proeng.2016.06.591

86. Gargiulo V, Gomis-Berenguer A, Giudicianni P, Ania CO, Ragucci R, Alfè M (2018) Assessing the potential of biochars prepared by steam-assisted slow pyrolysis for $CO_2$ adsorption and separation. Energy Fuels 32:10218–10227. https://doi.org/10.1021/acs.energyfuels.8b01058

87. Zubbri NA, Mohamed AR, Lahijani P, Mohammadi M (2021) Low temperature $CO_2$ capture on biomass-derived KOH-activated hydrochar established through hydrothermal carbonization with water-soaking pre-treatment. J Environ Chem Eng 9:105074. https://doi.org/10.1016/j.jece.2021.105074

88. Li H, Eddaoudi M, O'Keeffe M, Yaghi OM (1999) Design and synthesis of an exceptionally stable and highly porous metal-organic framework. Nature 402:276–279. https://doi.org/10.1038/46248

89. Abdi J, Hadavimoghaddam F, Hadipoor M, Hemmati-Sarapardeh A (2021) Modeling of $CO_2$ adsorption capacity by porous metal organic frameworks using advanced decision tree-based models. Sci Rep 11:1–14. https://doi.org/10.1038/s41598-021-04168-w

90. Williams JL, Piatrik M, Choi S-K, Stannett V (1977) Postdecrystallization rates of grafted fibers and their effect on fiber elasticity. I. Effect of zinc chloride concentration. J Appl Polym Sci 21:1377–1381. https://doi.org/10.1002/app.1977.070210519

91. Xiang S, He Y, Zhang Z, Wu H, Zhou W, Krishna R, Chen B (2012) Microporous metal-organic framework with potential for carbon dioxide capture at ambient conditions. Nat Commun 3:954–959. https://doi.org/10.1038/ncomms1956

92. Mustafa J, Farhan M, Hussain M (2016) $CO_2$ separation from flue gases using different types of membranes. J Membr Sci Technol 6:153. https://doi.org/10.4172/2155-9589.1000153

93. Shin DW, Hyun SH, Cho CH, Han MH (2005) Synthesis and $CO_2/N_2$ gas permeation characteristics of ZSM-5 zeolite membranes. Microporous Mesoporous Mater 85:313–323. https://doi.org/10.1016/j.micromeso.2005.06.035

94. Brinkmann T, Lillepärg J, Notzke H, Pohlmann J, Shishatskiy S, Wind J, Wolff T (2017) Development of $CO_2$ selective poly(ethylene oxide)-based membranes: From laboratory to pilot plant scale. Engineering 3:485–493. https://doi.org/10.1016/J.ENG.2017.04.004

95. Papari S, Hawboldt K, Helleur R (2015) Pyrolysis: A theoretical and experimental study on the conversion of softwood sawmill residue to biooil. Ind Eng Chem Res 54:605–611. https://doi.org/10.1021/ie5039456

96. Adelawon BO, Latinwo GK, Eboibi BE, Agbede OO, Agarry SE (2021) Comparison of the slow, fast, and flash pyrolysis of recycled maize-cob biomass waste, box-benhken process optimization and characterization studies for the thermal fast pyrolysis production of bio-energy. Chem Eng Commun 0:1–31. https://doi.org/10.1080/00986445.2021.1957851

97. Mazlan MAF, Uemura Y, Osman NB, Yusup S (2015) Characterizations of bio-char from fast pyrolysis of Meranti wood sawdust. J Phys Conf Ser 622:012054. https://doi.org/10.1088/1742-6596/622/1/012054

98. Bruun EW, Ambus P, Egsgaard H, Hauggaard-Nielsen H (2012) Effects of slow and fast pyrolysis biochar on soil C and N turnover dynamics. Soil Biol Biochem 46:73–79. https://doi.org/10.1016/j.soilbio.2011.11.019
99. Brownsort P (2009) Biomass pyrolysis processes: Performance parameters and their influence on biochar system benefits. Dissertation, University of Edinburgh
100. Huang YF, Te CP, Shih CH, Lo SL, Sun L, Zhong Y, Qiu C (2015) Microwave pyrolysis of rice straw to produce biochar as an adsorbent for $CO_2$ capture. Energy 84:75–82. https://doi.org/10.1016/j.energy.2015.02.026
101. Wang J, Wang S (2019) Preparation, modification and environmental application of biochar: A review. J Clean Prod 227:1002–1022. https://doi.org/10.1016/j.jclepro.2019.04.282
102. Nunoura T, Wade SR, Bourke JP, Antal MJ (2006) Studies of the Flash Carbonization Process. 1. Propagation of the Flaming Pyrolysis Reaction and Performance of a Catalytic Afterburner. Ind Eng Chem Res 45:585–599. https://doi.org/10.1021/ie050854y
103. Panwar NL, Pawar A, Salvi BL (2019) Comprehensive review on production and utilization of biochar. SN Appl Sci 1:1–19. https://doi.org/10.1007/s42452-019-0172-6
104. Tian H, Hu Q, Wang J, Chen D, Yang Y, Bridgwater AV (2021) Kinetic study on the $CO_2$ gasification of biochar derived from Miscanthus at different processing conditions. Energy 217:119341. https://doi.org/10.1016/j.energy.2020.119341
105. Brewer CE, Schmidt-Rohr K, Satrio JA, RCB, (2009) Characterization of biochar from fast pyrolysis and gasification systems. Environ Prog Sustain Energy 28:386–396. https://doi.org/10.1002/ep.10378
106. Chen WH, Peng J, Bi XT (2015) A state-of-the-art review of biomass torrefaction, densification and applications. Renew Sustain Energy Rev 44:847–866. https://doi.org/10.1016/j.rser.2014.12.039
107. Demirbas A (2009) Biorefineries: Current activities and future developments. Energy Convers Manag 50:2782–2801. https://doi.org/10.1016/j.enconman.2009.06.035
108. Xie Y, Wang L, Li H, Westholm LJ, Carvalho L, Thorin E, Yu Z, Yu X, Skreiberg Ø (2022) A critical review on production, modification and utilization of biochar. J Anal Appl Pyrolysis 161:105405. https://doi.org/10.1016/j.jaap.2021.105405
109. Wang Y, Qiu L, Zhu M, Sun G, Zhang T, Kang K (2019) Comparative evaluation of hydrothermal carbonization and low temperature pyrolysis of Eucommia ulmoides Oliver for the production of solid biofuel. Sci Rep 9:1–11. https://doi.org/10.1038/s41598-019-38849-4
110. Peng C, Zhai Y, Zhu Y, Wang T, Xu B, Wang T, Li C, Zeng G (2017) Investigation of the structure and reaction pathway of char obtained from sewage sludge with biomass wastes, using hydrothermal treatment. J Clean Prod 166:114–123. https://doi.org/10.1016/j.jclepro.2017.07.108
111. Yan W, Hastings JT, Acharjee TC, Coronella CJ, Vásquez VR (2010) Mass and energy balances of wet torrefaction of lignocellulosic biomass. Energy Fuels 24:4738–4742. https://doi.org/10.1021/ef901273n
112. Reza MT, Lynam JG, Uddin MH, Coronella CJ (2013) Hydrothermal carbonization : Fate of inorganics. Biomass Bioenerg 49:86–94. https://doi.org/10.1016/j.biombioe.2012.12.004
113. Karthik V, Kumar PS, Vo DVN, Sindhu J, Sneka D, Subhashini B, Saravanan K, Jeyanthi J (2021) Hydrothermal production of algal biochar for environmental and fertilizer applications: A review. Environ Chem Lett 19:1025–1042. https://doi.org/10.1007/s10311-020-01139-x
114. Zhang B, Heidari M, Regmi B, Salaudeen S, Arku P, Thimmannagari M, Dutta A (2018) Hydrothermal carbonization of fruit wastes: A promising technique for generating hydrochar. Energies 11:1–14. https://doi.org/10.3390/en11082022
115. Manyà JJ, García-Morcate D, González B (2020) Adsorption performance of physically activated biochars for postcombustion $CO_2$ capture from dry and humid flue gas. Appl Sci 10:1–17. https://doi.org/10.3390/app10010376
116. Creamer AE, Gao B, Zhang M (2014) Carbon dioxide capture using biochar produced from sugarcane bagasse and hickory wood. Chem Eng J 249:174–179. https://doi.org/10.1016/j.cej.2014.03.105
117. Lahijani P, Mohammadi M, Mohamed AR (2018) Metal incorporated biochar as a potential adsorbent for high capacity $CO_2$ capture at ambient condition. J CO2 Util 26:281–293. https://doi.org/10.1016/j.jcou.2018.05.018
118. Mohamed Noor N, Shariff A, Abdullah N, Mohamad Aziz NS (2019) Temperature effect on biochar properties from slow pyrolysis of coconut flesh waste. Malaysian J Fundam Appl Sci 15:153–158. https://doi.org/10.11113/mjfas.v15n2.1015
119. Demirbaş A, Arin G (2002) An overview of biomass pyrolysis. Energy Sources 24:471–482. https://doi.org/10.1080/00908310252889979
120. Shukla N, Sahoo D, Remya N (2019) Biochar from microwave pyrolysis of rice husk for tertiary wastewater treatment and soil nourishment. J Clean Prod 235:1073–1079. https://doi.org/10.1016/j.jclepro.2019.07.042
121. Ng WC, You S, Ling R, Gin KYH, Dai Y, Wang CH (2017) Co-gasification of woody biomass and chicken manure: Syngas production, biochar reutilization, and cost-benefit analysis. Energy 139:732–742. https://doi.org/10.1016/j.energy.2017.07.165
122. Mustaza MNF, Mizan MN, Yoshida H, Izhar S (2021) Torréfaction of mangrove wood by introducing superheated steam for biochar production. IOP Conf Ser Earth Environ Sci 765:012027. https://doi.org/10.1088/1755-1315/765/1/012027
123. Roy P, Dutta A, Gallant J (2018) Hydrothermal carbonization of peat moss and herbaceous biomass (miscanthus): A potential route for bioenergy. Energies 11:2794. https://doi.org/10.3390/en11102794
124. Jindo K, Mizumoto H, Sawada Y, Sanchez-Monedero MA, Sonoki T (2014) Physical and chemical characterization of biochars derived from different agricultural residues. Biogeosciences 11:6613–6621. https://doi.org/10.5194/bg-11-6613-2014
125. Chiang YC, Juang RS (2017) Surface modifications of carbonaceous materials for carbon dioxide adsorption: A review. J Taiwan Inst Chem Eng 71:214–234. https://doi.org/10.1016/j.jtice.2016.12.014
126. Cetin E, Moghtaderi B, Gupta R, Wall TF (2004) Influence of pyrolysis conditions on the structure and gasification reactivity of biomass chars. Fuel 83:2139–2150. https://doi.org/10.1016/j.fuel.2004.05.008
127. Chen D, Li Y, Cen K, Luo M, Li H, Lu B (2016) Pyrolysis polygeneration of poplar wood: Effect of heating rate and pyrolysis temperature. Bioresour Technol 218:780–788. https://doi.org/10.1016/j.biortech.2016.07.049
128. Bagreev A, Bandosz TJ, Locke DC (2001) Pore structure and surface chemistry of adsorbents obtained by pyrolysis of sewage sludge-derived fertilizer. Carbon 39:1971–1979. https://doi.org/10.1016/S0008-622328012900026-4
129. IUPAC (1972) Manual of symbols and terminology, Appendix 2, Part. 1, colloid and surface chemistry. Pure Appl Chem 31:578–638
130. Presser V, McDonough J, Yeon SH, Gogotsi Y (2011) Effect of pore size on carbon dioxide sorption by carbide derived carbon. Energy Environ Sci 4:3059–3066. https://doi.org/10.1039/c1ee01176f
131. Deng S, Wei H, Chen T, Wang B, Huang J, Yu G (2014) Superior $CO_2$ adsorption on pine nut shell-derived activated carbons and

the effective micropores at different temperatures. Chem Eng J 253:46–54. https://doi.org/10.1016/j.cej.2014.04.115
132. Khandaker T, Hossain MS, Dhar PK, Rahman MS, Hossain MA, Ahmed MB (2020) Efficacies of carbon-based adsorbents for carbon dioxide capture. Processes 8:1–32. https://doi.org/10.3390/PR8060654
133. Gao X, Yang S, Hu L, Cai S, Wu L, Kawi S (2022) Carbonaceous materials as adsorbents for $CO_2$ capture: Synthesis and modification. Carbon Capture Sci Technol 3:100039. https://doi.org/10.1016/j.ccst.2022.100039
134. Kloss S, Zehetner F, Dellantonio A, Hamid R, Ottner F, Liedtke V, Schwanninger M, Gerzabek MH, Soja G (2012) Characterization of slow pyrolysis biochars: Effects of feedstocks and pyrolysis temperature on biochar properties. J Environ Qual 41:990–1000. https://doi.org/10.2134/jeq2011.0070
135. Zhang H, Chen C, Gray EM, Boyd SE (2017) Effect of feedstock and pyrolysis temperature on properties of biochar governing end use efficacy. Biomass Bioenerg 105:136–146. https://doi.org/10.1016/j.biombioe.2017.06.024
136. Chatterjee R, Sajjadi B, Chen WY, Mattern DL, Hammer N, Raman V, Dorris A (2020) Effect of pyrolysis temperature on physicochemical properties and acoustic-based amination of biochar for efficient $CO_2$ adsorption. Front Energy Res 8:1–18. https://doi.org/10.3389/fenrg.2020.00085
137. Pallarés J, González-Cencerrado A, Arauzo I (2018) Production and characterization of activated carbon from barley straw by physical activation with carbon dioxide and steam. Biomass Bioenerg 115:64–73. https://doi.org/10.1016/j.biombioe.2018.04.015
138. Zhang P, Sun H, Yu L, Sun T (2013) Adsorption and catalytic hydrolysis of carbaryl and atrazine on pig manure-derived biochars: Impact of structural properties of biochars. J Hazard Mater 244–245:217–224. https://doi.org/10.1016/j.jhazmat.2012.11.046
139. Fu P, Hu S, Sun L, Xiang J, Yang T, Zhang A, Zhang J (2009) Structural evolution of maize stalk/char particles during pyrolysis. Bioresour Technol 100:4877–4883. https://doi.org/10.1016/j.biortech.2009.05.009
140. Keiluweit M, Nico PS, Johnson MG, Kleber M (2010) Dynamic molecular structure of plant biomass-derived black carbon(biochar). Environ Sci Technol 44:1247–1253. https://doi.org/10.1021/es9031419
141. Lua AC, Lau FY, Guo J (2006) Influence of pyrolysis conditions on pore development of oil-palm-shell activated carbons. J Anal Appl Pyrolysis 76:96–102. https://doi.org/10.1016/j.jaap.2005.08.001
142. Elnour AY, Alghyamah AA, Shaikh HM, Poulose AM, Al-Zahrani SM, Anis A, Al-Wabel MI (2019) Effect of pyrolysis temperature on biochar microstructural evolution, physicochemical characteristics, and its influence on biochar/polypropylene composites. Appl Sci 9:7–9. https://doi.org/10.3390/app9061149
143. Gai X, Wang H, Liu J, Zhai L, Liu S, Ren T, Liu H (2014) Effects of feedstock and pyrolysis temperature on biochar adsorption of ammonium and nitrate. PLoS ONE 9:e113888. https://doi.org/10.1371/journal.pone.0113888
144. Selvarajoo A, Oochit D (2020) Effect of pyrolysis temperature on product yields of palm fibre and its biochar characteristics. Mater Sci Energy Technol 3:575–583. https://doi.org/10.1016/j.mset.2020.06.003
145. Titiladunayo IF, McDonald AG, Fapetu OP (2012) Effect of temperature on biochar product yield from selected lignocellulosic biomass in a pyrolysis process. Waste and Biomass Valorization 3:311–318. https://doi.org/10.1007/s12649-012-9118-6
146. Mohd Hasan MH, Bachmann RT, Loh SK, Manroshan S, Ong SK (2019) Effect of pyrolysis temperature and time on properties of palm kernel shell-based biochar. IOP Conf Ser Mater Sci Eng 548:012020. https://doi.org/10.1088/1757-899X/548/1/012020
147. Xu B, Argyle MD, Shi X, Goroncy AK, Rony AH, Tan G, Fan M (2020) Effects of mixture of $CO_2$/$CH_4$ as pyrolysis atmosphere on pine wood pyrolysis products. Renew Energy 162:1243–1254. https://doi.org/10.1016/j.renene.2020.08.069
148. Parvez AM, Afzal MT, Victor Hebb TG, Schmid M (2020) Utilization of $CO_2$ in thermochemical conversion of biomass for enhanced product properties: A review. J CO2 Util 40:101217. https://doi.org/10.1016/j.jcou.2020.101217
149. Mellin P, Yu X, Yang W, Blasiak W (2015) Influence of reaction atmosphere ($H_2O$, $N_2$, $H_2$, $CO_2$, CO) on fluidized-bed fast pyrolysis of biomass using detailed tar vapor chemistry in computational fluid dynamics. Ind Eng Chem Res 54:8344–8355. https://doi.org/10.1021/acs.iecr.5b02164
150. Promraksa A, Rakmak N (2020) Biochar production from palm oil mill residues and application of the biochar to adsorb carbon dioxide. Heliyon 6:e04019. https://doi.org/10.1016/j.heliyon.2020.e04019
151. Fryda L, Visser R (2015) Biochar for soil improvement: Evaluation of biochar from gasification and slow pyrolysis. Agric 5:1076–1115. https://doi.org/10.3390/agriculture5041076
152. Guizani C, Escudero Sanz FJ, Salvador S (2014) Effects of $CO_2$ on biomass fast pyrolysis: Reaction rate, gas yields and char reactive properties. Fuel 116:310–320. https://doi.org/10.1016/j.fuel.2013.07.101
153. Liu R, Liu G, Yousaf B, Abbas Q (2018) Operating conditions-induced changes in product yield and characteristics during thermal-conversion of peanut shell to biochar in relation to economic analysis. J Clean Prod 193:479–490. https://doi.org/10.1016/j.jclepro.2018.05.034
154. Ertaş M, Hakki Alma M (2010) Pyrolysis of laurel (Laurus nobilis L.) extraction residues in a fixed-bed reactor: Characterization of bio-oil and bio-char. J Anal Appl Pyrolysis 88:22–29. https://doi.org/10.1016/j.jaap.2010.02.006
155. Igalavithana AD, Lee SE, Lee YH, Tsang DCW, Rinklebe J, Kwon EE, Ok YS (2017) Heavy metal immobilization and microbial community abundance by vegetable waste and pine cone biochar of agricultural soils. Chemosphere 174:593–603. https://doi.org/10.1016/j.chemosphere.2017.01.148
156. Zhao SX, Ta N, Wang XD (2017) Effect of temperature on the structural and physicochemical properties of biochar with apple tree branches as feedstock material. Energies 10:1293. https://doi.org/10.3390/en10091293
157. Cantrell KB, Hunt PG, Uchimiya M, Novak JM, Ro KS (2012) Impact of pyrolysis temperature and manure source on physicochemical characteristics of biochar. Bioresour Technol 107:419–428. https://doi.org/10.1016/j.biortech.2011.11.084
158. Yang X, Kang K, Qiu L, Zhao L, Sun R (2020) Effects of carbonization conditions on the yield and fixed carbon content of biochar from pruned apple tree branches. Renew Energy 146:1691–1699. https://doi.org/10.1016/j.renene.2019.07.148
159. Zhao B, O'Connor D, Zhang J, Peng T, Shen Z, Tsang DCW, Hou D (2018) Effect of pyrolysis temperature, heating rate, and residence time on rapeseed stem derived biochar. J Clean Prod 174:977–987. https://doi.org/10.1016/j.jclepro.2017.11.013
160. Angin D (2013) Effect of pyrolysis temperature and heating rate on biochar obtained from pyrolysis of safflower seed press cake. Bioresour Technol 128:593–597. https://doi.org/10.1016/j.biortech.2012.10.150
161. Tomczyk A, Sokołowska Z, Boguta P (2020) Biochar physicochemical properties: Pyrolysis temperature and feedstock kind effects. Rev Environ Sci Biotechnol 19:191–215. https://doi.org/10.1007/s11157-020-09523-3
162. Li H, Dong X, da Silva EB, de Oliveira LM, Chen Y, Ma LQ (2017) Mechanisms of metal sorption by biochars: Biochar

characteristics and modifications. Chemosphere 178:466–478. https://doi.org/10.1016/j.chemosphere.2017.03.072
163. Zhang J, Liu J, Liu R (2015) Effects of pyrolysis temperature and heating time on biochar obtained from the pyrolysis of straw and lignosulfonate. Bioresour Technol 176:288–291. https://doi.org/10.1016/j.biortech.2014.11.011
164. Al-wabel MI, Al-omran A, El-naggar AH, Nadeem M, Usman ARA (2013) Pyrolysis temperature induced changes in characteristics and chemical composition of biochar produced from Conocarpus wastes. Bioresour Technol 131:374–379. https://doi.org/10.1016/j.biortech.2012.12.165
165. Yuan JH, Xu RK, Zhang H (2011) The forms of alkalis in the biochar produced from crop residues at different temperatures. Bioresour Technol 102:3488–3497. https://doi.org/10.1016/j.biortech.2010.11.018
166. Gaffar S, Dattamudi S, Baboukani AR, Chanda S, Novak JM, Watts DW, Wang C, Jayachandran K (2021) Physiochemical characterization of biochars from six feedstocks and their effects on the sorption of atrazine in an organic soil. Agronomy 11:716. https://doi.org/10.3390/agronomy11040716
167. Hossain MK, Strezov Vladimir V, Chan KY, Ziolkowski A, Nelson PF (2011) Influence of pyrolysis temperature on production and nutrient properties of wastewater sludge biochar. J Environ Manage 92:223–228. https://doi.org/10.1016/j.jenvman.2010.09.008
168. Chen H, Guo Y, Du Y, Xu X, Su C, Zeng Z, Li L (2021) The synergistic effects of surface functional groups and pore sizes on $CO_2$ adsorption by GCMC and DFT simulations. Chem Eng J 415:128824. https://doi.org/10.1016/j.cej.2021.128824
169. Petrovic B, Gorbounov M, Masoudi Soltani S (2021) Influence of surface modification on selective $CO_2$ adsorption: A technical review on mechanisms and methods. Microporous Mesoporous Mater 312:110751. https://doi.org/10.1016/j.micromeso.2020.110751
170. Boehm HP (1966) Chemical identification of surface groups. Adv Catal 16:179–274. https://doi.org/10.1016/S0360-0564(08)60354-5
171. Montes-Morán MA, Suárez D, Menéndez JA, Fuente E (2004) On the nature of basic sites on carbon surfaces: An overview. Carbon 42:1219–1225. https://doi.org/10.1016/j.carbon.2004.01.023
172. Biniak S, Świątkowski A, Pakuła M (2001) Electrochemical studies of phenomena at active carbon- electrolyte solution interfaces. In: Radovic LR (ed) Chemistry and physics of carbon: A series of advances. Marcel Dekker Inc, New York, pp 126–216
173. Shen W, Fan W (2013) Nitrogen-containing porous carbons: Synthesis and application. J Mater Chem A 1:999–1013. https://doi.org/10.1039/c2ta00028h
174. Guo T, Ma N, Pan Y, Bedane AH, Xiao H, Eić M, Du Y (2018) Characteristics of $CO_2$ adsorption on biochar derived from biomass pyrolysis in molten salt. Can J Chem Eng 96:2352–2360. https://doi.org/10.1002/cjce.23153
175. Yaumi AL, Bakar MZA, Hameed BH (2018) Melamine-nitrogenated mesoporous activated carbon derived from rice husk for carbon dioxide adsorption in fixed-bed. Energy 155:46–55. https://doi.org/10.1016/j.energy.2018.04.183
176. Brewer CE, Unger R, Schmidt-Rohr K, Brown RC (2011) Criteria to select biochars for field studies based on biochar chemical properties. Bioenergy Res 4:312–323. https://doi.org/10.1007/s12155-011-9133-7
177. Zimmerman AR (2010) Abiotic and microbial oxidation of laboratory-produced black carbon (biochar). Environ Sci Technol 44:1295–1301. https://doi.org/10.1021/es903140c
178. Spokas KA (2010) Review of the stability of biochar in soils: Predictability of O: C molar ratios. Carbon Manag 1:289–303. https://doi.org/10.4155/cmt.10.32
179. Enders A, Hanley K, Whitman T, Joseph S, Lehmann J (2012) Characterization of biochars to evaluate recalcitrance and agronomic performance. Bioresour Technol 114:644–653. https://doi.org/10.1016/j.biortech.2012.03.022
180. Shen Y, Linville JL, Ignacio-de Leon PAA, Schoene RP, Urgun-Demirtas M (2016) Towards a sustainable paradigm of waste-to-energy process: Enhanced anaerobic digestion of sludge with woody biochar. J Clean Prod 135:1054–1064. https://doi.org/10.1016/j.jclepro.2016.06.144
181. Chen B, Zhou D, Zhu L (2008) Transitional adsorption and partition of nonpolar and polar aromatic contaminants by biochars of pine needles with different pyrolytic temperatures. Environ Sci Technol 42:5137–5143. https://doi.org/10.1021/es8002684
182. Antal MJ, Grønli M (2003) The art, science, and technology of charcoal production. Ind Eng Chem Res 42:1619–1640. https://doi.org/10.1021/ie0207919
183. Ok YS, Yang JE, Zhang YS, Kim SJ, Chung DY (2007) Heavy metal adsorption by a formulated zeolite-Portland cement mixture. J Hazard Mater 147:91–96. https://doi.org/10.1016/j.jhazmat.2006.12.046
184. Imam T, Capareda S (2012) Characterization of bio-oil, syn-gas and bio-char from switchgrass pyrolysis at various temperatures. J Anal Appl Pyrolysis 93:170–177. https://doi.org/10.1016/j.jaap.2011.11.010
185. Demirbas A (2004) Effects of temperature and particle size on bio-char yield from pyrolysis of agricultural residues. J Anal Appl Pyrolysis 72:243–248. https://doi.org/10.1016/j.jaap.2004.07.003
186. Zhao Z, Wu Q, Nie T, Zhou W (2019) Quantitative evaluation of relationships between adsorption and partition of atrazine in biochar-amended soils with biochar characteristics. RSC Adv 9:4162–4171. https://doi.org/10.1039/C8RA08544G
187. Sun X, Shan R, Li X, Pan J, Liu X, Deng R, Song J (2017) Characterization of 60 types of Chinese biomass waste and resultant biochars in terms of their candidacy for soil application. GCB Bioenergy 9:1423–1435. https://doi.org/10.1111/gcbb.12435
188. Kameyama K, Miyamoto T, Iwata Y (2019) The preliminary study of water-retention related properties of biochar produced from various feedstock at different pyrolysis temperatures. Materials (Basel) 12:1732. https://doi.org/10.3390/ma12111732
189. Bamdad H, Hawboldt K, MacQuarrie S, Papari S (2019) Application of biochar for acid gas removal: experimental and statistical analysis using $CO_2$. Environ Sci Pollut Res 26:10902–10915. https://doi.org/10.1007/s11356-019-04509-3
190. Anthonysamy SI, Lahijani P, Mohammadi M, Mohamed AR (2020) Low temperature adsorption of nitric oxide on cerium impregnated biomass-derived biochar. Korean J Chem Eng 37:130–140. https://doi.org/10.1007/s11814-019-0405-9
191. Dubinin MM (1989) Fundamentals of the theory of adsorption in micropores of carbon adsorbents: Characteristics of their adsorption properties and microporous structures. Carbon 27:457–467. https://doi.org/10.1016/0008-6223(89)90078-X
192. Barrett EP, Joyner LG, Halenda PP (1951) The Determination of pore volume and area distributions in porous substances. I. Computations from nitrogen isotherms. J Am Chem Soc 73:373–380. https://doi.org/10.1021/ja01145a126
193. Mao J, Cao X, Chen N (2013) Characterization of biochars using advanced solid-state 13C nuclear magnetic resonance spectroscopy. In: Lee JW (ed) Advanced Biofuels and Bioproducts. Springer, New York, New York, pp 47–55
194. Tangsathitkulchai C, Naksusuk S, Wongkoblap A, Phadungbut P (2021) Equilibrium and kinetics of $CO_2$ adsorption by coconut shell activated carbon impregnated with sodium hydroxide. Processes 9:1–23. https://doi.org/10.3390/pr9020201
195. Igalavithana AD, Choi SW, Shang J, Hanif A, Dissanayake PD, Tsang DCW, Kwon JH, Lee KB, Ok YS (2020) Carbon dioxide

capture in biochar produced from pine sawdust and paper mill sludge: Effect of porous structure and surface chemistry. Sci Total Environ 739:139845. https://doi.org/10.1016/j.scitotenv.2020.139845
196. Shafeeyan MS, Wan Daud WMA, Houshmand A, Arami-Niya A (2012) The application of response surface methodology to optimize the amination of activated carbon for the preparation of carbon dioxide adsorbents. Fuel 94:465–472. https://doi.org/10.1016/j.fuel.2011.11.035
197. Lim G, Lee KB, Ham HC (2016) Effect of N-containing functional groups on $CO_2$ adsorption of carbonaceous materials: A Density Functional Theory approach. J Phys Chem C 120:8087–8095. https://doi.org/10.1021/acs.jpcc.5b12090
198. Xing W, Liu C, Zhou Z, Zhou J, Wang G, Zhuo S, Xue Q (2014) Oxygen-containing functional group-facilitated $CO_2$ capture by carbide-derived carbons. Nanoscale Res Lett 9:189
199. Liu Y, Wilcox J (2012) Effects of surface heterogeneity on the adsorption of $CO_2$ in microporous carbons. Environ Sci Technol 46:1940–1947. https://doi.org/10.1021/es204071g
200. Zhang X, Wu J, Yang H, Shao J, Wang X, Chen Y, Zhang S, Chen H (2016) Preparation of nitrogen-doped microporous modified biochar by high temperature $CO_2$-$NH_3$ treatment for $CO_2$ adsorption: Effects of temperature. RSC Adv 6:98157–98166. https://doi.org/10.1039/c6ra23748g
201. Liu WJ, Jiang H, Tian K, Ding YW, Yu HQ (2013) Mesoporous carbon stabilized MgO nanoparticles synthesized by pyrolysis of $MgCl_2$ preloaded waste biomass for highly efficient $CO_2$ capture. Environ Sci Technol 47:9397–9403. https://doi.org/10.1021/es401286p
202. Chiang YC, Yeh CY, Weng CH (2019) Carbon dioxide adsorption on porous and functionalized activated carbon fibers. Appl Sci 9:1977. https://doi.org/10.3390/app9101977
203. Fan X, Zhang L, Zhang G, Shu Z, Shi J (2013) Chitosan derived nitrogen-doped microporous carbons for high performance $CO_2$ capture. Carbon 61:423–430. https://doi.org/10.1016/j.carbon.2013.05.026
204. Zhang C, Song W, Sun G et al (2013) $CO_2$ capture with activated carbon grafted by nitrogenous functional groups. Energy Fuels 27:4818–4823. https://doi.org/10.1021/ef400499k
205. Songolzadeh M, Ravanchi MT, Soleimani M (2012) Carbon dioxide capture and storage : A general review on adsorbents. Int J Chem Mol Nucl Mater Metall Eng 6:900–907. https://doi.org/10.5281/zenodo.1076265
206. Igalavithana AD, Mandal S, Niazi NK et al (2017) Advances and future directions of biochar characterization methods and applications. Crit Rev Environ Sci Technol 47:2275–2330. https://doi.org/10.1080/10643389.2017.1421844
207. Sajjadi B, Chen WY, Egiebor NO (2019) A comprehensive review on physical activation of biochar for energy and environmental applications. Rev Chem Eng 35:735–776. https://doi.org/10.1515/revce-2017-0113
208. Dalai AK, Azargohar R (2007) Production of activated carbon from biochar using chemical and physical activation: Mechanism and modeling. ACS Symp Ser 954:463–476. https://doi.org/10.1021/bk-2007-0954.ch029
209. Hagemann N, Spokas K, Schmidt HP, Kägi R, Böhler MA, Bucheli TD (2018) Activated carbon, biochar and charcoal: Linkages and synergies across pyrogenic carbon's ABCs. Water (Switzerland) 10:1–19. https://doi.org/10.3390/w10020182
210. Ahmed MB, Zhou JL, Ngo HH, Guo W, Chen M (2016) Progress in the preparation and application of modified biochar for improved contaminant removal from water and wastewater. Bioresour Technol 214:836–851. https://doi.org/10.1016/j.biortech.2016.05.057
211. Budinova T, Ekinci E, Yardim F, Grimm A, Björnbom E, Minkova V, Goranova M (2006) Characterization and application of activated carbon produced by $H_3PO_4$ and water vapor activation. Fuel Process Technol 87:899–905. https://doi.org/10.1016/j.fuproc.2006.06.005
212. Mestre AS, Pires J, Nogueira JMF, Carvalho AP (2007) Activated carbons for the adsorption of ibuprofen. Carbon 45:1979–1988. https://doi.org/10.1016/j.carbon.2007.06.005
213. Santos RM, Santos AO, Midori E, Nascimento JS, Lima ÁS, Freitas LS (2015) Pyrolysis of Mangaba seed : Production and characterization of bio-oil. Bioresour Technol 196:43–48. https://doi.org/10.1016/j.biortech.2015.07.060
214. Rajapaksha AU, Vithanage M, Ahmad M, Seo DC, Cho JS, Lee SE, Lee SS, Ok YS (2015) Enhanced sulfamethazine removal by steam-activated invasive plant-derived biochar. J Hazard Mater 290:43–50. https://doi.org/10.1016/j.jhazmat.2015.02.046
215. Rodríguez-Reinoso F, Molina-Sabio M, González MT (1995) The use of steam and $CO_2$ as activating agents in the preparation of activated carbons. Carbon 33:15–23. https://doi.org/10.1016/0008-6223(94)00100-E
216. Feng D, Zhang Y, Zhao Y, Sun S, Gao J (2018) Improvement and maintenance of biochar catalytic activity for in-situ biomass tar reforming during pyrolysis and $H_2O$/$CO_2$ gasification. Fuel Process Technol 172:106–114. https://doi.org/10.1016/j.fuproc.2017.12.011
217. Lussier MG, Zhang Z, Miller DJ (1998) Characterizing rate inhibition in steam/hydrogen gasification via analysis of adsorbed hydrogen. Carbon 36:1361–1369. https://doi.org/10.1016/S0008-6223(98)00123-7
218. Aworn A, Thiravetyan P, Nakbanpote W (2008) Preparation and characteristics of agricultural waste activated carbon by physical activation having micro- and mesopores. J Anal Appl Pyrolysis 82:279–285. https://doi.org/10.1016/j.jaap.2008.04.007
219. Maroto-Valer MM, Fauth DJ, Kuchta ME, Zhang Y, Andrésen JM (2005) Activation of magnesium rich minerals as carbonation feedstock materials for $CO_2$ sequestration. Fuel Process Technol 86:1627–1645. https://doi.org/10.1016/j.fuproc.2005.01.017
220. Fan M (2004) Steam activation of chars produced from oat hulls and corn stover. Bioresour Technol 93:103–107. https://doi.org/10.1016/j.biortech.2003.08.016
221. Zhang YJ, Xing ZJ, Duan ZK, Li M, Wang Y (2014) Effects of steam activation on the pore structure and surface chemistry of activated aarbon derived from Bamboo waste. Appl Surf Sci 315:279–286. https://doi.org/10.1016/j.apsusc.2014.07.126
222. Thommes M (2010) Physical adsorption characterization of nanoporous materials. Chem-Ing-Tech 82:1059–1073. https://doi.org/10.1002/cite.201000064
223. Ogungbenro AE, Quang DV, Al-Ali KA, Vega LF, Abu-Zahra MRM (2018) Physical synthesis and characterization of activated carbon from date seeds for $CO_2$ capture. J Environ Chem Eng 6:4245–4252. https://doi.org/10.1016/j.jece.2018.06.030
224. Sevilla M, Al-Jumialy ASM, Fuertes AB, Mokaya R (2018) Optimization of the pore structure of biomass-based carbons in relation to their use for $CO_2$ capture under low- and high-pressure regimes regimes. ACS Appl Mater Interfaces 10:1623–1633. https://doi.org/10.1021/acsami.7b10433
225. Wang J, Nie P, Ding B, Dong S, Hao X, Dou H, Zhang X (2017) Biomass derived carbon for energy storage devices. J Mater Chem A 5:2411–2428. https://doi.org/10.1039/c6ta08742f
226. Shahkarami S, Azargohar R, Dalai AK, Soltan J (2015) Breakthrough $CO_2$ adsorption in bio-based activated carbons. J Environ Sci (China) 34:68–76. https://doi.org/10.1016/j.jes.2015.03.008

227. Wu X, Yu Y, Qin Z, Zhang Z (2014) The advances of post-combustion $CO_2$ capture with chemical solvents: review and guidelines. Energy Procedia 63:1339–1346. https://doi.org/10.1016/j.egypro.2014.11.143
228. Creamer AE, Gao B, Wang S (2016) Carbon dioxide capture using various metal oxyhydroxide–biochar composites. Chem Eng J 283:826–832. https://doi.org/10.1016/j.cej.2015.08.037
229. Mu J, Perlmutter DD (1982) Thermal decomposition of metal nitrates and their hydrates. Thermochim Acta 56:253–260. https://doi.org/10.1016/0040-6031(82)87033-0
230. Guo Y, Tan C, Sun J, Li W, Zhang J, Zhao C (2020) Biomass ash stabilized Mgo adsorbents for $CO_2$ Capture application. Fuel 259:116298. https://doi.org/10.1016/j.fuel.2019.116298
231. Shafeeyan MS, Daud WMAW, Houshmand A, Shamiri A (2010) A review on surface modification of activated carbon for carbon dioxide adsorption. J Anal Appl Pyrolysis 89:143–151. https://doi.org/10.1016/j.jaap.2010.07.006
232. Saha D, Kienbaum MJ (2019) Role of oxygen, nitrogen and sulfur functionalities on the surface of nanoporous carbons in $CO_2$ adsorption: A critical review. Microporous Mesoporous Mater 287:29–55. https://doi.org/10.1016/j.micromeso.2019.05.051
233. Xiong Z, Shihong Z, Haiping Y, Tao S, Yingquan C, Hanping C (2013) Influence of $NH_3/CO_2$ modification on the characteristic of biochar and the $CO_2$ capture. Bioenergy Res 6:1147–1153. https://doi.org/10.1007/s12155-013-9304-9
234. Molavi H, Eskandari A, Shojaei A, Mousavi SA (2018) Enhancing $CO_2/N_2$ adsorption selectivity via post-synthetic modification of $NH_2$-UiO-66(Zr). Microporous Mesoporous Mater 257:193–201. https://doi.org/10.1016/j.micromeso.2017.08.043
235. Sarmah M, Baruah BP, Khare P (2013) A comparison between $CO_2$ capturing capacities of fly ash based composites of MEA/DMA and DEA/DMA. Fuel Process Technol 106:490–497. https://doi.org/10.1016/j.fuproc.2012.09.017
236. Nie L, Mu Y, Jin J, Chen J, Mi J (2018) Recent developments and consideration issues in solid adsorbents for $CO_2$ capture from flue gas. Chinese J Chem Eng 2303–2317https://doi.org/10.1016/j.cjche.2018.07.012
237. Bandosz TJ, Seredych M, Rodríguez-Castellón E, Cheng Y, Daemen LL, Ramírez-Cuesta AJ (2016) Evidence for $CO_2$ Reactive adsorption on nanoporous S- and N-doped carbon at ambient conditions. Carbon 96:856–863. https://doi.org/10.1016/j.carbon.2015.10.007
238. Xie W-H, Li H, Yang M, He L-N, Li H-R (2022) $CO_2$ capture and utilization with solid waste. Green Chem Eng. https://doi.org/10.1016/j.gce.2022.01.002
239. Haleem N, Khattak A, Jamal Y, Sajid M, Shahzad Z, Raza H (2022) Development of poly vinyl alcohol (PVA) based biochar nanofibers for carbon dioxide ($CO_2$) adsorption. Renew Sustain Energy Rev 157:112019. https://doi.org/10.1016/j.rser.2021.112019
240. Bamdad H, Hawboldt K, Macquarrie S (2018) Nitrogen functionalized biochar as a renewable adsorbent for efficient $CO_2$ removal. Energy Fuels 32:11742–11748. https://doi.org/10.1021/acs.energyfuels.8b03056
241. Liu SH, Huang YY (2018) Valorization of coffee grounds to biochar-derived adsorbents for $CO_2$ adsorption. J Clean Prod 175:354–360. https://doi.org/10.1016/j.jclepro.2017.12.076
242. Ghani WAWAK, Rebitanim NZ, Salleh MAM, Alias AB (2015) Carbon Dioxide Adsorption on Coconut Shell Biochar. In: Dincer I, Colpan CO, Kizilkan O, Ezan MA (eds) Progress in Clean Energy, vol 1. Springer International Publishing, Switzerland, pp 683–693
243. Tan YL, Islam A, Asif M, Hameed BH (2014) Adsorption of carbon dioxide by sodium hydroxide-modified granular coconut shell activated carbon in a fixed bed. Energy 77:926–931. https://doi.org/10.1016/j.energy.2014.09.079
244. Islam MA, Ahmed MJ, Khanday WA, Asif M, Hameed BH (2017) Mesoporous activated carbon prepared from NaOH activation of rattan (Lacosperma secundiflorum) hydrochar for methylene blue removal. Ecotoxicol Environ Saf 138:279–285. https://doi.org/10.1016/j.ecoenv.2017.01.010
245. Shen F, Wang Y, Li L, Zhang K, Smith RL, Qi X (2018) Porous carbonaceous materials from hydrothermal carbonization and KOH activation of corn stover for highly efficient $CO_2$ capture. Chem Eng Commun 205:423–431. https://doi.org/10.1080/00986445.2017.1367671
246. Wang R, Wang P, Yan X, Lang J, Peng C, Xue Q (2012) Promising porous carbon derived from celtuce leaves with outstanding supercapacitance and $CO_2$ capture performance. ACS Appl Mater Interfaces 4:5800–5806. https://doi.org/10.1021/am302077c
247. Huang GG, Liu YF, Wu XX, Cai JJ (2019) Activated carbons prepared by the KOH activation of a hydrochar from garlic peel and their $CO_2$ adsorption performance. Xinxing Tan Cailiao/New Carbon Mater 34:247–257. https://doi.org/10.1016/S1872-5805(19)60014-4
248. Serafin J, Ouzzine M, Cruz OF, Sreńscek-Nazzal J, Campello Gómez I, Azar FZ, Rey Mafull CA, Hotza D, Rambo CR (2021) Conversion of fruit waste-derived biomass to highly microporous activated carbon for enhanced $CO_2$ capture. Waste Manag 136:273–282. https://doi.org/10.1016/j.wasman.2021.10.025
249. Yue L, Xia Q, Wang L, Wang L, DaCosta H, Yang J, Hu X (2018) $CO_2$ adsorption at nitrogen-doped carbons prepared by $K_2CO_3$ activation of urea-modified coconut shell. J Colloid Interface Sci 511:259–267. https://doi.org/10.1016/j.jcis.2017.09.040
250. Hu J, Chen Y, Qian K, Yang Z, Yang H, Li Y, Chen H (2017) Evolution of char structure during mengdong coal pyrolysis: influence of temperature and $K_2CO_3$. Fuel Process Technol 159:178–186. https://doi.org/10.1016/j.fuproc.2017.01.042
251. Zhao C, Chen X, Zhao C (2012) $K_2CO_3/Al_2O_3$ for capturing $CO_2$ in flue gas from power plants. part 1: carbonation behaviors of $K_2CO_3/Al_2O_3$. Energy Fuels 26:1401–1405. https://doi.org/10.1021/ef200725z
252. Park SJ, Jung WY (2002) Effect of KOH activation on the formation of oxygen structure in activated carbons synthesized from polymeric precursor. J Colloid Interface Sci 250:93–98. https://doi.org/10.1006/jcis.2002.8309
253. Goel C, Bhunia H, Bajpai PK (2015) Synthesis of nitrogen doped mesoporous carbons for carbon dioxide capture. RSC Adv 5:46568–46582. https://doi.org/10.1039/c5ra05684e
254. Otowa T, Tanibata R, Itoh M (1993) Production and adsorption characteristics of MAXSORB: high-surface-area active carbon. Gas Sep Purif 7:241–245. https://doi.org/10.1016/0950-4214(93)80024-Q
255. Wang J, Kaskel S (2012) KOH activation of carbon-based materials for energy storage. J Mater Chem 22:23710–23725. https://doi.org/10.1039/C2JM34066F
256. Zhang C, Song W, Ma Q, Xie L, Zhang X (2016) Enhancement of $CO_2$ capture on biomass-based carbon from black locust by KOH activation and ammonia modification enhancement of $CO_2$ capture on biomass-based carbon from black locust by KOH activation and ammonia modification. https://doi.org/10.1021/acs.energyfuels.5b02764
257. Rostamian R, Heidarpour M, Mousavi SF, Afyuni M (2015) Characterization and sodium sorption capacity of biochar and activated carbon prepared from rice husk. J Agric Sci Technol 17:1057–1069
258. Mistar EM, Alfatah T, Supardan MD (2020) Synthesis and characterization of activated carbon from Bambusa Vulgaris Striata using two-step KOH activation. J Mater Res Technol 9:6278–6286. https://doi.org/10.1016/j.jmrt.2020.03.041

259. Saad MJ, Chia CH, Zakaria S, Sajab MS, Misran S, Rahman MHA, Chin SX (2019) Physical and chemical properties of the rice straw activated carbon produced from carbonization and KOH activation processes. Sains Malaysiana 48:385–391. https://doi.org/10.17576/jsm-2019-4802-16
260. Gomez-delgado E, Nunell GV, Cukierman AL, Bonelli PR (2022) Influence of the carbonization atmosphere on the development of highly microporous adsorbents tailored to $CO_2$ capture. J Energy Inst 102:184–189. https://doi.org/10.1016/j.joei.2022.03.003
261. Li K, Zhang D, Niu X, Guo H, Yu Y, Tang Z, Lin Z, Fu M (2022) Insights into $CO_2$ adsorption on KOH-activated biochars derived from the mixed sewagesludge and pine sawdust. Sci Total Environ 826:154133. https://doi.org/10.1016/j.scitotenv.2022.154133
262. Ding S, Liu Y (2020) Adsorption of $CO_2$ from flue gas by novel seaweed-based KOH-activated porous biochars. Fuel 260:116382. https://doi.org/10.1016/j.fuel.2019.116382
263. Shao L, Sang Y, Liu N, Liu J, Zhan P, Huang J, Chen J (2020) Selectable microporous carbons derived from poplar wood by three preparation routes for $CO_2$ capture. ACS Omega 5:17450–17462. https://doi.org/10.1021/acsomega.0c01918
264. Kwiatkowski M, Serafin J, Booth AM, Michalkiewicz B (2021) Computer analysis of the effect of activation temperature on the microporous structure development of activated carbon derived from common polypody. Materials (Basel) 14:2951. https://doi.org/10.3390/ma14112951
265. Nowrouzi M, Younesi H, Bahramifar N (2018) Superior $CO_2$ capture performance on biomass-derived carbon/metal oxides nanocomposites from Persian ironwood by $H_3PO_4$ activation. Fuel 223:99–114. https://doi.org/10.1016/j.fuel.2018.03.035
266 Varil T, Bergna D, Lahti R, Romar H, Hu T, Lassi U (2017) Activated carbon production from peat using $ZnCl_2$: Characterization and applications. BioResources 12:8078–8092. https://doi.org/10.15376/biores.12.4.8078-8092
267. Kumar A, Jena HM (2015) High surface area microporous activated carbons prepared from Fox nut ( Euryale ferox ) shell by zinc chloride activation. Appl Surf Sci 356:753–761. https://doi.org/10.1016/j.apsusc.2015.08.074
268. Heidari A, Younesi H, Rashidi A, Ghoreyshi AA (2014) Adsorptive removal of $CO_2$ on highly microporous activated carbons prepared from Eucalyptus camaldulensis wood: Effect of chemical activation. J Taiwan Inst Chem Eng 45:579–588. https://doi.org/10.1016/j.jtice.2013.06.007
269. Sevilla M, Mokaya R (2014) Energy storage applications of activated carbons: Supercapacitors and hydrogen storage. Energy Environ Sci 7:1250–1280. https://doi.org/10.1039/c3ee43525c
270. Thote JA, Iyer KS, Chatti R, Labhsetwar NK, Biniwale RB, Rayalu SS (2010) In situ nitrogen enriched carbon for carbon dioxide capture. Carbon 48:396–402. https://doi.org/10.1016/j.carbon.2009.09.042
271. Ahmed MB, Hasan Johir MA, Zhou JL, Ngo HH, Nghiem LD, Richardson C, Moni MA, Bryant MR (2019) Activated carbon preparation from biomass feedstock: Clean production and carbon dioxide adsorption. J Clean Prod 225:405–413. https://doi.org/10.1016/j.jclepro.2019.03.342
272. Soyler N, SelimCeylan YT (2018) $CO_2$ capture analysis of tobacco biochar-$AlCl_3$ composite. Environ Res Technol 5:34–37
273. Ma Q, Chen W, Jin Z, Chen L, Zhou Q, Jiang X (2021) One-step synthesis of microporous nitrogen-doped biochar for efficient removal of $CO_2$ and $H_2S$. Fuel 289:119932. https://doi.org/10.1016/j.fuel.2020.119932
274. Xu X, Zheng Y, Gao B, Cao X (2019) doped biochar synthesized by a facile ball-milling method for enhanced sorption of $CO_2$ and reactive red. Chem Eng J 368:564–572. https://doi.org/10.1016/j.cej.2019.02.165
275. Nguyen MV, Lee BK (2016) A novel removal of $CO_2$ using nitrogen doped biochar beads as a green adsorbent. Process Saf Environ Prot 104:490–498. https://doi.org/10.1016/j.psep.2016.04.007
276. Liu Y, Sajjadi B, Chen WY, Chatterjee R (2019) Ultrasound-assisted amine functionalized graphene oxide for enhanced $CO_2$ adsorption. Fuel 247:10–18. https://doi.org/10.1016/j.fuel.2019.03.011
277. Sajjadi B, Broome JW, Chen WY, Mattern DL, Egiebor NO, Hammer N, Smith CL (2019) Urea functionalization of ultrasound-treated biochar: A feasible strategy for enhancing heavy metal adsorption capacity. Ultrason Sonochem 51:20–30. https://doi.org/10.1016/j.ultsonch.2018.09.015
278. Mohammed Z, Jeelani S, Rangari V (2022) Effective reinforcement of engineered sustainable biochar carbon for 3D printed polypropylene biocomposites. Compos Part C Open Access 7:100221. https://doi.org/10.1016/J.JCOMC.2021.100221
279. Chatterjee R, Sajjadi B, Mattern DL, Chen WY, Zubatiuk T, Leszczynska D, Leszczynski J, Egiebor NO, Hammer N (2018) Ultrasound cavitation intensified amine functionalization: A feasible strategy for enhancing $CO_2$ capture capacity of biochar. Fuel 225:287–298. https://doi.org/10.1016/j.fuel.2018.03.145
280. Yang H, Li H, Zhai J, Sun L, Yu H (2014) Simple synthesis of graphene oxide using ultrasonic cleaner from expanded graphite. Ind Eng Chem Res 53:17878–17883. https://doi.org/10.1021/ie503586v
281. Chatterjee R, Sajjadi B, Chen W-Y, Mattern DL, Egiebor NO, Hammer N, Raman V (2019) Low frequency ultrasound enhanced dual amination of biochar: A nitrogen-enriched sorbent for $CO_2$ capture. Energy Fuels 33:2366–2380. https://doi.org/10.1021/acs.energyfuels.8b03583
282. Li M, Xiao R (2019) Preparation of a dual pore structure activated carbon from rice husk char as an adsorbent for $CO_2$ capture. Fuel Process Technol 186:35–39. https://doi.org/10.1016/j.fuproc.2018.12.015
283. Dissanayake PD, Choi SW, Igalavithana AD, Yang X, Tsang DCW, Wang CH, Kua HW, Lee KB, Ok YS (2020) Sustainable gasification biochar as a high efficiency adsorbent for $CO_2$ capture: A facile method to designer biochar fabrication. Renew Sustain Energy Rev 124:109785. https://doi.org/10.1016/j.rser.2020.109785
284. González B, Manyà JJ (2020) Activated olive mill waste-based hydrochars as selective adsorbents for $CO_2$ capture under post-combustion conditions. Chem Eng Process - Process Intensif 149:107830. https://doi.org/10.1016/j.cep.2020.107830
285. Younas M, Sohail M, Kong LL, Bashir MJK, Sethupathi S (2016) Erratum to: Feasibility of $CO_2$ adsorption by solid adsorbents: A review on low-temperature systems. Int J Environ Sci Technol 13:1839–1860. https://doi.org/10.1007/s13762-016-1008-1
286. Cheung O, Hedin N (2014) Zeolites and related sorbents with narrow pores for $CO_2$ separation from flue gas. RSC Adv 4:14480–14494. https://doi.org/10.1039/c3ra48052f
287. Choi HS, Suh MP (2009) Highly selective $CO_2$ capture in flexible 3d coordination polymer networks. Angew Chemie - Int Ed 48:6865–6869. https://doi.org/10.1002/anie.200902836
288. Cao L, Zhang X, Xu Y, Xiang W, Wang R, Ding F, Hong P, Gao B (2022) Straw and wood based biochar for $CO_2$ capture: Adsorption performance and governing mechanisms. Sep Purif Technol 287:120592. https://doi.org/10.1016/j.seppur.2022.120592
289. Kamarudin KSN, Zaini N, Khairuddin NEA (2018) $CO_2$ removal using amine-functionalized kenaf in pressure swing adsorption system. J Environ Chem Eng 6:549–559. https://doi.org/10.1016/j.jece.2017.12.040

290. Abdullah MO, Tan IAW, Lim LS (2011) Automobile adsorption air-conditioning system using oil palm biomass-based activated carbon: A review. Renew Sustain Energy Rev 15:2061–2072. https://doi.org/10.1016/j.rser.2011.01.012
291. Lee CS, Ong YL, Aroua MK, Daud WMAW (2013) Impregnation of palm shell-based activated carbon with sterically hindered amines for $CO_2$ adsorption. Chem Eng J 219:558–564. https://doi.org/10.1016/j.cej.2012.10.064
292. Benson SM, Franklin M, Orr J (2008) Carbon dioxide capture and storage. MRS Bull 33:303–305
293. Figueiredo JL, Pereira MFR, Freitas MMA, Órfão JJM (1999) Modification of the surface chemistry of activated carbons. Carbon 37:1379–1389. https://doi.org/10.1016/S0008-6223(98)00333-9